Design and Optimisation of the Limaçon Rotary Compressor

Kui Lu

Submitted in total fulfilment of the requirements for the degree

of

Doctor of Philosophy

Federation University Australia

PO Box 663
University Drive, Mount Helen
Victoria 3353
Australia

September 2022

Abstract

The limaçon positive displacement machine is characterised by its internal geometry and unique mechanical motion; both based on a mathematical curve known as the limaçon of Pascal. The limaçon technology offers many advantages, such as compact size and double-acting functionality, and its great potential for fluid processing applications has been proven by a number of patents and innovative designs in engines, expanders, and pumps. However, no commercial application of the limaçon technology in the field of positive displacement compressors has been reported in the literature. This could be attributed to the fact that the potential of the limaçon technology for gas compression has not been established as yet. The process of establishing potential is necessary before funds and resources are dedicated to investing in prototyping and testing. This process entails a considerable amount of modelling, coding and analysis as one must ensure the embodiment is geometrically capable of delivering suction and compression strokes, ports can be arranged to support the workings of these strokes, a number of measurable parameters can be identified as impacting compressor performance and it is possible to calculate a set of parameters which optimise this performance. To achieve this objective, a comprehensive mathematical model of a limaçon machine, implemented as a compressor, was first developed. The model, which is multi-physical in nature, spans such domains as kinematics, fluid dynamics, characteristics of the port flow, internal leakage due to seal vibration, dynamics of the discharge valve, and thermodynamics. Subsequently, the simulation of the model has been performed to numerically study the operational characteristics of the limaçon compressor and to investigate the effect of various parameters on the compressor performance. It was found that the increase in the operating speed and

pressure ratio would lead to negative effects on machine performance, especially on volumetric efficiency. Additionally, the results of simulations indicated that the level of fluid over-compression is influenced by the characteristics of the discharge valve.

To ensure the suitability of limaçon technology for use in positive displacement compressors, a study was undertaken to determine whether such an embodiment lent itself to optimisation efforts. For this purpose, the thorough mathematical model which has been developed to simulate compressor workings was then used for optimisation purposes whereby a Bayesian optimisation procedure was applied. The optimisation procedure was conducted in a two-stage fashion where the first stage optimises the machine dimensions to meet volumetric requirements specified by the designer; and the second stage focuses on revealing the optimum combination of port geometries that improves machine performance. A numerical illustration was presented to prove the validity of the presented approach, and the results show that considerable improvements in the isentropic and volumetric efficiencies can be attained. Moreover, the optimised design was tested under different operating speeds and pressure ratios to investigate its robustness. It was found that the optimised design can exhibit relatively stable performance when the working conditions vary within a small bandwidth around that used in the optimisation procedure.

The limaçon technology has three embodiments, namely the limaçon-to-limaçon (L2L), the limaçon-to-circular, and the circolimaçon. The circolimaçon embodiment features using circular arcs, rather than limaçon curves, to develop profiles for the rotor and housing. This embodiment simplifies the manufacturing process and reduces the production cost associated with producing a limaçon technology. A feasibility study of the circolimaçon

embodiment was conducted by comparing its performance with that of the L2L type device. The machine dimensions and port geometries obtained from the optimisation procedure were used in the comparative study. A nonlinear three-degree of freedom model was presented to describe the dynamic behaviour of the apex seal during the machine operation. Additionally, the leakage through the seal-housing gap was formulated by considering the inertia and viscous effects of the flow. The results from the case study suggest that the circolimaçon embodiment exhibits comparable performance to the L2L-type machine, despite having more significant seal vibrations. Moreover, it was also discovered that the circolimaçon compressor with a small capacity undergoes a lower level of seal dynamics, indicating better machine reliability.

Acknowledgements

First of all, I would like to take this opportunity to express my sincere gratitude to my supervisors, Associate Professor Ibrahim A. K. Sultan and Dr. Truong H. Phung, for their patient guidance and continuous support throughout this research project. Additionally, I am grateful for the life wisdom they shared with me during my PhD journey, which allowed me to gain more than just academic achievements.

Thanks to the Federation University Australia, the Institute of Innovation, Sciences and Sustainability, and the Graduate Research School for providing me with the opportunity and support to pursue the PhD degree. In addition, I would also express my deepest thanks to the International Student Advisory, the Federation University Australia Foundation, and the Graduate Research School for their invaluable assistance to many international students including me through the stressful COVID-19 pandemic.

Thanks to you, dad and mom. I could not have done this PhD without your unconditional love, care, and support over the past 30 years. Also, thank you to my beloved wife, Shanshan Jia, for your love and constant support, for putting up with me, for encouraging and helping me through frustrations, for taking care of the whole family, for bringing our dearest daughter, Xinyi, into this world, and for the cherished moments of love and joy over the past 8 years.

Kui Lu was supported by Findlay Engineering & Federation University Co-Funded Scholarship (FedUni Research Project (No. G2037)).

Declaration of authorship and originality

Except where explicit reference is made in the text of the thesis, this thesis contains no material published elsewhere or extracted in whole or in part from a thesis by which I have qualified for or been awarded another degree or diploma. No other person's work has been relied upon or used without due acknowledgment in the main text and the list of references of the thesis. No editorial assistance has been received in the production of the thesis without due acknowledgment. Except where duly referred to, the thesis does not include material with copyright provisions or requiring copyright approvals.

Signature of Candidate:

Print name: Kui Lu

Date: 2nd September 2022

Contents

LIST OF FIGURES X

LIST OF TABLES XIII

PUBLICATIONS DURING CANDIDATURE XIV

Publications included in the thesis xiv

Additional publications by the candidate relevant to the thesis but not forming part of it xiv

CONTRIBUTION TO PUBLICATIONS INCLUDED IN THE THESIS XV

CHAPTER 1. INTRODUCTION 1-1

1.1. Background 1-1

1.2. Problem statement and research questions 1-7

1.3. Literature review 1-9

1.3.1. Influencing factors of compressor performance 1-9

1.3.2. Recent innovative modelling in compressor research 1-29

1.3.3. Challenges and opportunities for future studies 1-35

1.4. Structure of the thesis 1-38

1.5. References 1-39

CHAPTER 2. MATHEMATICAL MODELLING AND PARAMETRIC STUDY OF THE LIMAÇON ROTARY COMPRESSOR 2-1

2.1. Abstract 2-1

2.2. Introduction 2-2

2.3. Mathematical models of the limaçon compressor 2-6

2.3.1. The kinematic model 2-6

2.3.2. Mass flow rate through the port 2-7

2.3.3. Mass flow rate through the discharge valve 2-11

2.3.4. The leakage model 2-14

2.3.5. The thermodynamic model 2-16

2.4. Numerical illustration 2-20

2.5. The effect of various parameters on the performance 2-24

2.5.1. Effects of operating speed 2-25

2.5.2. Effects of pressure ratio 2-26

2.5.3. Effects of the diameter of the valve 2-28

2.6. Conclusion 2-29

2.7. References 2-30

CHAPTER 3. ON THE DESIGN OF A CLASS OF ROTARY COMPRESSORS USING BAYESIAN OPTIMISATION 3-1

3.1. Abstract 3-1

3.2. Introduction 3-2

3.3. Geometric Characteristics of the Limaçon Compressor 3-4

3.4. Optimization Process 3-10

3.4.1. Bayesian Optimization Method 3-10

3.4.2. Two-Stage Optimization 3-13

3.1. Numerical Illustration 3-15

3.2. Conclusions 3-23

3.3. References 3-23

CHAPTER 4. A COMPARATIVE STUDY OF TWO EMBODIMENTS OF THE LIMAÇON ROTARY COMPRESSOR BASED ON THEORETICAL MODELLING OF APEX SEAL DYNAMICS AND LEAKAGE. 4-1

4.1. Abstract 4-1

4.2. Introduction 4-2

4.3. Background on the limaçon technology 4-5

4.3.1. Geometric characteristics 4-5

4.3.2. The circolimaçon machine 4-8

4.4. Dynamic model of apex seal 4-10

4.5. Leakage through the seal-housing gap 4-17

4.5.1. Conservation of momentum 4-18

4.5.2. Continuity equation 4-19

4.5.3. Conservation of energy 4-20

4.6. Comparative analysis 4-22

4.6.1. Comparison of seal dynamics 4-23

4.6.2. Comparison of machine performance 4-27

4.6.3. Effects of limaçon aspect ratio on seal dynamics 4-29

4.7. Conclusion 4-31

4.8. References 4-32

CHAPTER 5. CONCLUSION AND RECOMMENDATIONS FOR FUTURE WORK 5-1

REFERENCES 5-4

List of figures

Fig. 1-1 Common mechanisms of positive displacement compressors. (a) Reciprocating piston; (b) Vane-type; (c) Screw-type; (d) Rolling piston type. 1-2

Fig. 1-2. The limaçon rotary compressor. 1-6

Fig. 1-3. An illustration of the workings of positive displacement compressors..... 1-10

Fig. 1-4. Theoretical P-V diagram. 1-10

Fig. 1-5. Structure of the reed-type valve..... 1-25

Fig. 1-6. Schematic diagram of ANN applied in positive displacement compressors. .. 1-30

Fig. 1-7. A schematic diagram of GA..... 1-33

Fig. 1-8. Process of Bayesian optimisation applied in positive displacement compressor. 1-34

Fig. 2-1. (a) The limaçon compressor; (b) Illustration of the working process (suction is blue and discharge is red). 2-4

Fig. 2-2. Sectional view of the discharge valve. 2-12

Fig. 2-3. Schematic view of the motion of the discharge valve. 2-13

Fig. 2-4. Path of the leakage: (a) Side leakage, (b) Apex leakage..... 2-15

Fig. 2-5. Variation of the working chamber volume. 2-22

Fig. 2-6. Variation of chamber pressure. 2-22

Fig. 2-7. Variation of valve chamber pressure and valve displacement..... 2-23

Fig. 2-8. Variation of the fluid mass in the working chamber, m_c, and valve chamber, m_{vc}. 2-23

Fig. 2-9. Variation of the torque, τ. 2-24

Fig. 2-10. The P-V diagram. 2-24

Fig. 2-11. Performance at different operating speeds. 2-26

Fig. 2-12. Valve displacement at three specific operating speeds. 2-26

Fig. 2-13. Performance at different pressure ratios. 2-27

Fig. 2-14. Effect of the diameter of the valve on the variation of chamber pressure. .. 2-28

Fig. 3-1. (a) The limaçon compressor; (b) illustration of the working process (suction is blue and delivery is red). 3-6

Fig. 3-2. The rotor-housing clearance. 3-8

Fig. 3-3. Illustration of the two-stage optimization process. 3-16

Fig. 3-4. Result of the first stage: (a) distribution of E_{o1}; and distribution of first stage design variables: (b) half chord length; (c) aspect ratio; (d) rotor clearance. 3-18

Fig. 3-5. Distribution of E_{o2}. 3-19

Fig. 3-6. Distribution of second stage design variables: (a) leading edge of inlet port; (b) leading edge of outlet port; (c) inlet port angular width; (d) outlet port angular width; (e) inlet port length; (f) outlet port length 3-20

Fig. 3-7. Performance of the optimized compressor under different speeds (at P_o = 300 kPa). 3-21

Fig. 3-8. Performance of the optimized compressor under different outlet pressure (at 1400 rpm) 3-22

Fig. 4-1. A limaçon-to-limaçon machine. 4-6

Fig. 4-2. Limaçon curves based on different limaçon aspect ratios. 4-7

Fig. 4-3. An illustration of the circolimaçon machine. 4-9

Fig. 4-4. Kinematics of the apex seal. 4-12

Fig. 4-5. Dynamics of the apex seal. 4-13

Fig. 4-6. Schematic diagram of leakage path: (a) actual flow path, (b) approximated flow path..... 4-18

Fig. 4-7. Sample results of the leakage model..... 4-22

Fig. 4-8. Flowchart of the simulation process..... 4-24

Fig. 4-9. Pressure of the upper and lower chambers of the circolimaçon compressor……. 4-25

Fig. 4-10. Comparison of seal dynamics between the circolimaçon and L2L compressors. 4-26

Fig. 4-11. Seal movement to cover the apex-housing gap in the circolimaçon machine…. 4-26

Fig. 4-12. Forces acting on different points of the apex seal..... 4-27

Fig. 4-13. Volumetric efficiency under different pressure ratios and operating speeds…. 4-28

Fig. 4-14. Isentropic efficiency under different pressure ratios and operating speeds. 4-29

Fig. 4-15. Fluid mass inside the working chamber..... 4-29

Fig. 4-16. Comparison of seal vibrations under different limaçon aspect ratios. 4-30

List of tables

Table 1-1. Summary of various mechanisms of positive displacement compressors 1-3

Table 1-2. Recently proposed design of positive displacement compressors 1-5

Table 1-3. Leakage flow models 1-16

Table 1-4. Empirical correlations proposed in different literature 1-19

Table 1-5. Comparison of different capacity control methods 1-28

Table 1-6. Summary of machine learning methods applied in positive displacement compressors 1-35

Table 2-1. Dimensions of the limaçon compressor 2-20

Table 3-1. Assumptions of optimisation process 3-16

Table 3-2. Searching domain of each design variable 3-17

Table 3-3. Comparison of obtained result and required result 3-18

Table 3-4. Performance comparison of other types of rotary compressors 3-22

Table 4-1. Dimensions of the circolimaçon compressor 4-22

Table 4-2. Maximum magnitudes of each force under different limaçon aspect ratios..... 4-31

Publications during candidature

Publications included in the thesis

1. **Lu, K.,** Phung, T. H., and Sultan, I. A. (2021). On the Design of a Class of Rotary Compressors Using Bayesian Optimization. *Machines*, *9*(10), 219. https://doi.org/10.3390/machines9100219

2. **Lu, K,** Sultan, I. A., and Phung, T. H., (2022) "Mathematical modeling and parametric study of the limaçon rotary compressor". *International Journal of Refrigeration*, *134*, 219-231.https://doi.org/10.1016/j.ijrefrig.2021.11.014

3. **Lu, K,** Sultan, I. A., and Phung, T. H., (2022) " A comparative study of two embodiments of the limaçon rotary compressor based on theoretical modelling of apex seal dynamics and leakage". *International Journal of Refrigeration.* https://doi.org/10.1016/j.ijrefrig.2022.10.004

4. **Lu, K,** Sultan, I. A., and Phung, T. H., (under review) " A literature review of the positive displacement compressor research: current challenges and future opportunities"

Additional publications by the candidate relevant to the thesis but not forming part of it

1. **Lu, K.,** Sultan, I. A. and Phung, T. H. (2021) "A study on the use of machine learning methods to improve reciprocating compressor reliability via torque tailoring", Int. Conf. on Maintenance and Intelligent Asset Manag. (ICMIAM2021), Dec. 12-15, 2021, Ballarat, Australia. doi: 10.1109/ICMIAM54662.2021.9715205

2. **Lu, K.,** Sultan, I. A. and Phung, T. H. (accepted and under production) "Geometric Design of The Limaçon Rotary Compressor Using Bayesian Optimization", The 3rd Int. Conf. on Energy and Power (ICEP2021)., Nov 18-20, Chiang Mai, Thailand.

3. Belfiore, C., **Lu, K.,** Phung, T. H. and Sultan, I. A. (accepted and under production) " Designs and Applications of the Rotary Limaçon Compressors and Expanders – A review", The 3rd Int. Conf. on Energy and Power (ICEP2021)., Nov 18-20, Chiang Mai, Thailand.

Contribution to publications included in the thesis

Chapter	Publication title	Status	Contribution of candidate
1	A literature review of the positive dis-placement compressor research: current challenges and future opportunities	Under review	85%
2	Mathematical modelling and parametric study of the limaçon rotary compressor	Published	85%
3	On the Design of a Class of Rotary Compressors Using Bayesian Optimization	Published	85%
4	A comparative study of two embodiments of the limaçon rotary compressor based on theoretical modelling of apex seal dynamics and leakage	Published	85%

Chapter 1. Introduction[*] [†]

1.1. Background

Often energy available in natural sources needs to be transformed (via the use of fluid machines) into forms that can be used for domestic or industrial purposes. The compressor is one fluid machine that converts the mechanical energy into the internal or kinetic energy of the gaseous working fluid. Generally, compressors are divided into two categories, namely rotodynamic compressors and positive displacement compressors. Rotodynamic compressors require the interaction between a continuously flowing fluid and a set of blades (aka impeller) to execute the exchange of energy by means of fluid dynamic action. The centrifugal compressor is a typical embodiment of the rotodynamic compressor. For positive displacement compressors, the characteristic mode of operation is that the volume of the working chamber periodically changes due to the mechanical motion of the displacer (i.e., piston or rotor). With the volume reducing, the fluid entrapped in the working chamber is compressed until the designated pressure is reached.

Positive displacement compressors can be further classified into two groups based on the motion of the displacer. The first group is the reciprocating compressor, in which the piston executes linear motion inside the working chamber. This type of compressor has a superior sealing performance and presents low susceptibility to variations in the working condition (Stouffs et al., 2001). Especially the ability to attain high delivery pressure at low

[*] Section 1.1 and 1.3 of this chapter have been combined as a review paper and submitted to International Journal of Refrigeration for publication.

[†] A review of applications of the limaçon technology in positive displacement machine has been presented at 3rd ICEP conference (Nov 18-20, Ching Mai, Thailand): Belfiore, C., Lu, K., Phung, T. H. and Sultan, I. A. (2021) " Designs and Applications of the Rotary Limaçon Compressors and Expanders – A review", The 3rd Int. Conf. on Energy and Power (ICEP2021)., Nov 18-20, Chiang Mai, Thailand.

flow rates makes the reciprocating compressor popular in such industries as petrochemical plants and gas transmission (Sultan and Phung, 2019). Another subset of the positive displacement compressor is the rotary compressor, whose rotor implements circular or nearly circular motion in the working chamber. Rotary compressors embody such successful technologies as screw, rolling piston, and vane devices. One noticeable aspect of the rotary group over reciprocating devices is that fewer components are involved in the design, especially the removal of the connecting rod. This generally facilitates the simplicity of the machine structure and leads to a lower weight to displacement ratio (Spark and Lu, 2019). Fig. 1-1 depicts some examples of the positive displacement compressor. Table 1-1 presents a summary of various types of positive displacement compressors.

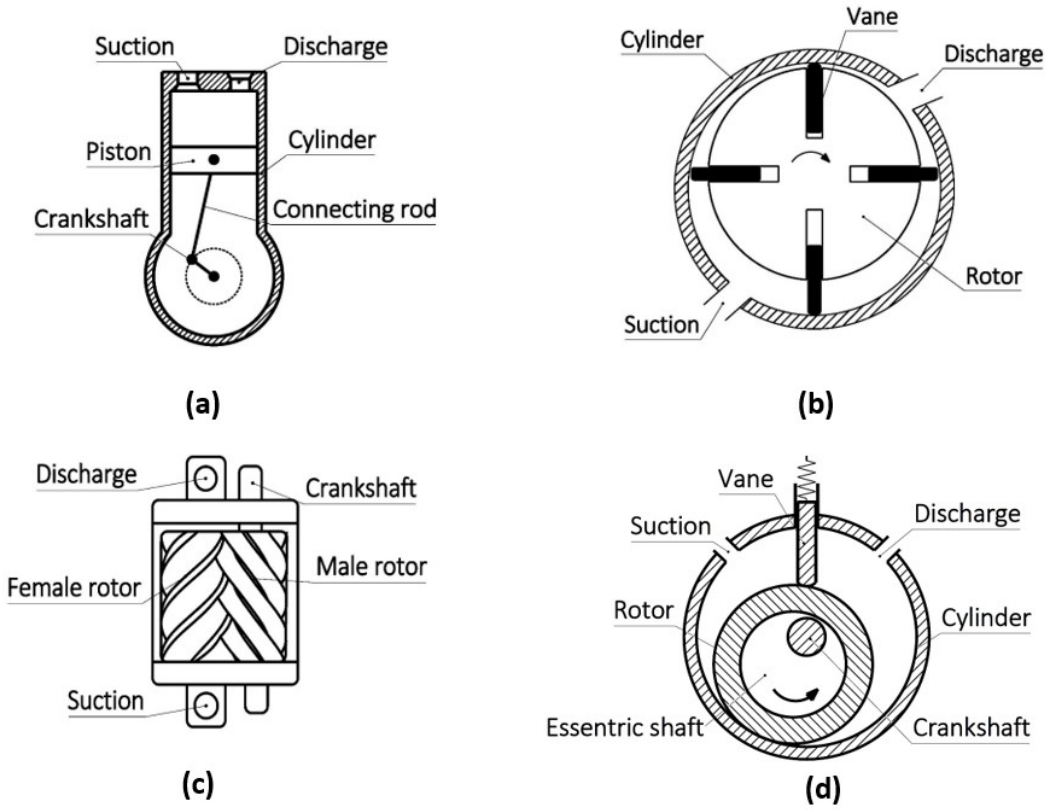

Fig. 1-1 Common mechanisms of positive displacement compressors. (a) Reciprocating piston; (b) Vane-type; (c) Screw-type; (d) Rolling piston type.

Table 1-1. Summary of various mechanisms of positive displacement compressors

Type	Operating features	Mechanism	Pros and cons
Reciprocating	Displacing element moves reciprocally and linearly	Piston	Pros: • High pressure-ratio functionality • Flexibility to working conditions • Low maintenance cost Cons: • Vibration issues • Pressure pulsation
		Diaphragm	Pros: • Low level of component wear • Prevent contamination of fluid flow • Safe to work with toxic and explosive fluids Cons: • Low life cycle of displacing element and low flow rate of discharge (Li et al., 2014)
		Linear	Pros: • Removal of crank mechanism improves efficiency • Oil-free compression • Quiet operation Cons: • Require accurate sensing and control methods for piston motion (Liang, 2017)
Rotary	Displacing element features circular or near-circular motion	Rolling piston	Pros: • Simple operation and easy installation • Low maintenance cost Cons: • Relatively low efficiency • Friction issues between rotor and vane (Yanagisawa et al., 1982)

Table 1-1. Summary of various mechanisms of positive displacement compressors (Continued)

Type	Operating features	Mechanism	Pros and cons
Rotary	Displacing element features circular or near-circular motion	Vane	Pros: • Simple operation and easy installation • Low maintenance cost Cons: • A proper sealing scheme is needed to address internal leakage issues
		Screw	Pros: • Ability to maintain desirable performance at high speed and long service life (Stosic et al., 2011) • Less vibration • Ability to handle two-phase flows Cons: • High initial investment as well as maintenance cost.
		Scroll	Pros: • Compact size and light weight • Quiet operation Cons: • Low capacity • High discharge temperature

Over the years, positive displacement compressors have possessed particular popularity in many industries. In the automobile industry, by way of example, reciprocating compressors are employed for tyre inflation or to actuate pneumatic brake systems. Also, in refrigeration systems, various types of positive displacement compressors are utilised to compress the refrigerant for the workings of the thermodynamic cycles featured in these systems. In recent market research, the global compressor market was reported at 39.9 billion USD in 2019, and it is expected to reach 48.5 billion USD by 2030, with the

majority of the market share contributed by positive displacement compressors (Prescient and Strategic Intelligence, 2020). However, it is worth mentioning that compressed gas is regarded as one of the most expensive energy forms (Silva et al., 2017). It was reported that nearly 20% of energy consumption in industries is attributed to the production of compressed gas (Vittorini and Cipollone, 2016), whereas less than 30% of the compressed gas can be efficiently used (Saidur et al., 2010). In this context, the performance improvement of positive displacement compressors has become a popular topic of research in both academia and industry. It is therefore unsurprising that many emerging compressor technologies with significant energy-efficient potential have appeared in recent years. Table 1-2 lists recently proposed designs.

Table 1-2. Recently proposed design of positive displacement compressors

Authors	Type	Main features of the design
Heidari et al. (2017)	Reciprocating	• Two sets of concentric fins are used as piston • Heat transfer increased by 32 times compared to the conventional design • Exergetic efficiency increased by 23.3%
Hu et al. (2019)	Rotary	• Rotating cylinder design • Noticeable improvement in volumetric efficiency at the low operating frequency
Shin et al. (2019)	Rotary	• Dual cylinder design in which the additional cylinder utilises the inner space of the rotor • Cooling capacity improved by up to 37.99% • Mechanical losses reduced by 36.43%
Shakya and Ooi (2020)	Rotary	• A pair of vanes coupled together and cut through the rotor diametrically • No geometrical constraints for rotor size, allowing the structure to be extremely compact
Gao and Liu (2021)	Reciprocating	• Continuously self-air-cooling. • Performance increased significantly at high output pressure and long working time

The limaçon technology is featured by the utilisation of the limaçon of Pascal which is a member of the epitrochoidal curves family. Due to its special mathematical characteristics, the limaçon curve possesses great potential for use in rotary fluid processing machines. Fig. 1-2 illustrates a compressor that employs limaçon technology. The rotor chord produces the limaçon motion by rotating about its midpoint, whose path falls on the base circle, and sliding at the limaçon pole, and the limaçon profile of the machine housing is the trajectory of the apices of the rotor chord. Subsequently, the lenticular profile of the rotor is developed from the lower portion of the housing and mirrored about the rotor chord.

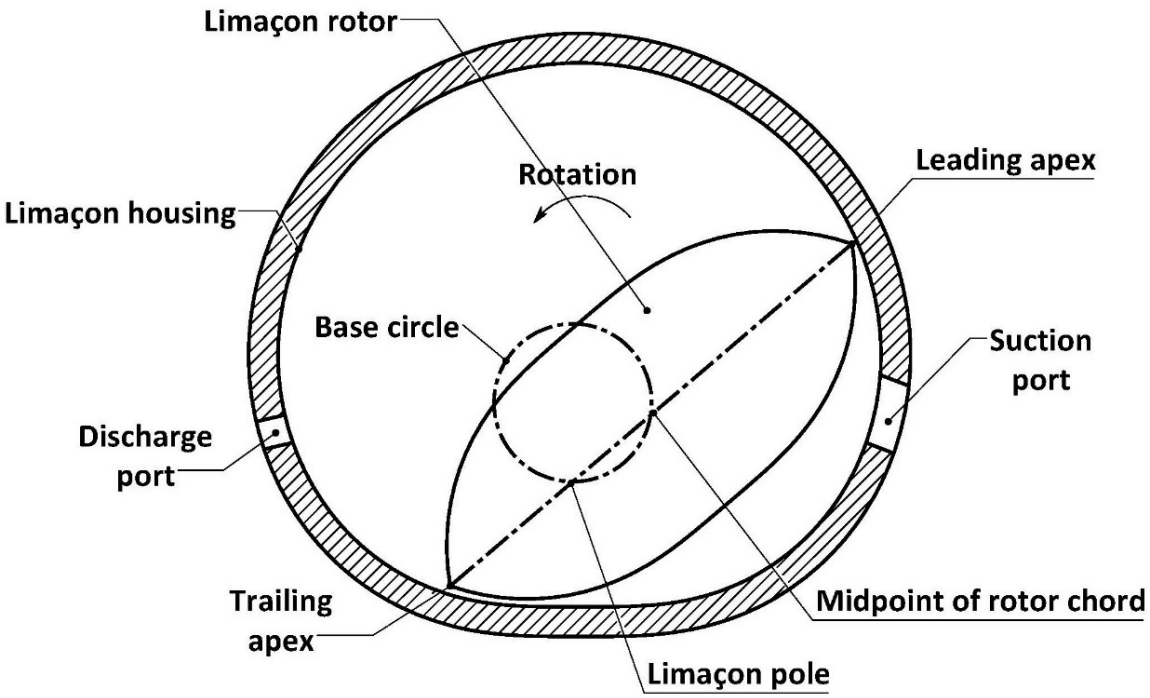

Fig. 1-2. The limaçon rotary compressor.

Compared to other compressor designs, the limaçon technology is more compact in size and possesses low-speed functionality, enabling the machine to be used in applications requiring low mass flow rates. Additionally, the arrangement between the rotor and housing implies the double-acting nature of the machine, which can implement two com-

pression strokes in one complete working cycle. More importantly, the most distinguishing feature of the limaçon technology is the ability to achieve larger capacity within a small machine size (explained in Section 2.3.1). Despite all the advantages offered by this technology, engineers and researchers are keen on investigating such well-established technologies as reciprocating, screw, and vane type devices. The limaçon technology, on the other hand, has not yet received enough attention from either academia or industrial communities. This can be attributed to the lack of adequate explanation for the mathematical characteristics of the limaçon technology. Moreover, the inappropriate use of circular profiles for the machine housing leads to the hoped-for performance that did not occur in the early prototypes.

1.2. Problem statement and research questions

In order to spark commercial-scale interest in such a promising technology, it is necessary to undertake a comprehensive study (which spans a number of fields of enquiry) to establish the potential of the limaçon construct for use as a rotary positive displacement compressor. For the limaçon technology to be suitable for compressor implementation, it must fulfil the characteristics which are listed below along with their corresponding fields of enquiry shown in italics,

i. Geometric capability of delivering suction and compression strokes (*Machine design)*
ii. Possibility of placing the inlet and discharge ports in a manner which supports the suction and compression processes (*Machine design and mathematical modelling)*

iii. Existence of measurable parameters that impact performance in manners which are possible to comprehend via simulations (*Machine design, thermodynamics, and fluid dynamics)*

iv. Ability to set these parameters with the objective of optimising performance (*Mathematical modelling and optimisation*)

In order to accomplish the objectives of this research project, the work scope is presented in sequential order as follows:

(1). Developing a comprehensive mathematical model to describe the geometric and thermodynamic workings of a proposed limaçon compressor embodiment (*Detailed in Chapter 2*)

(2). Analysing how variations in different design variables impact the volumetric and thermodynamic performance of the proposed compressor (*Detailed in Chapter 2*)

(3). Exploring suitable machine learning methods to develop an optimisation procedure which can optimise such a complex and comprehensive mathematical model built to describe the performance of the compressor (*Detailed in Chapter 3*)

(4). Optimising the compressor performance via proper settings of a design vector which encompasses such parameters as machine dimensions, profiles of housing and rotor, and locations of ports, to obtain satisfactory performance (*Detailed in Chapter 3*)

(5). Investigating the apex seal vibration in different embodiments (namely L2L and circolimaçon) of the limaçon compressor (*Detailed in Chapter 4*)

Based on the discussion presented above, the project research questions can be listed as follows:

- Does the limaçon technology have the potential to be utilised in positive displacement compressors?
- How will the design variables, i.e., operating and geometrical parameters, affect the compressor performance? and is it possible to set these variables in a fashion that optimises the performance?
- Can machine learning methods be utilised to develop the optimisation procedure for the limaçon compressor?
- How will the dynamics of the apex seal affect the machine performance for different embodiments?

1.3. Literature review

This section is intended to provide a review of earlier and recent literature on various topics of positive displacement compressors. The structure of the literature review is outlined as follows. Section 1.3.1 reviews the previous research on influencing factors of compressor performance, including leakage, heat transfer, friction and lubrication, valve and port characteristics, and capacity control methods. In Section 1.3.2, the current status of the application of machine learning algorithms in positive displacement compressors is discussed. Existing challenges and opportunities for future research are proposed in Section 1.3.3.

1.3.1. Influencing factors of compressor performance

1.3.1.1. Basic equations for positive displacement compressors

Fig. 1-3 is employed here as a good example of positive displacement compressors where the working fluid is admitted into a compression chamber of volume, V, through a

suction valve with the help of the vacuum created by a moving machine member which controls the volume, V. This moving machine member is the reciprocating piston shown in Fig. 1-3, but it can also be a rotating component in other designs as depicted in Fig. 1-1.

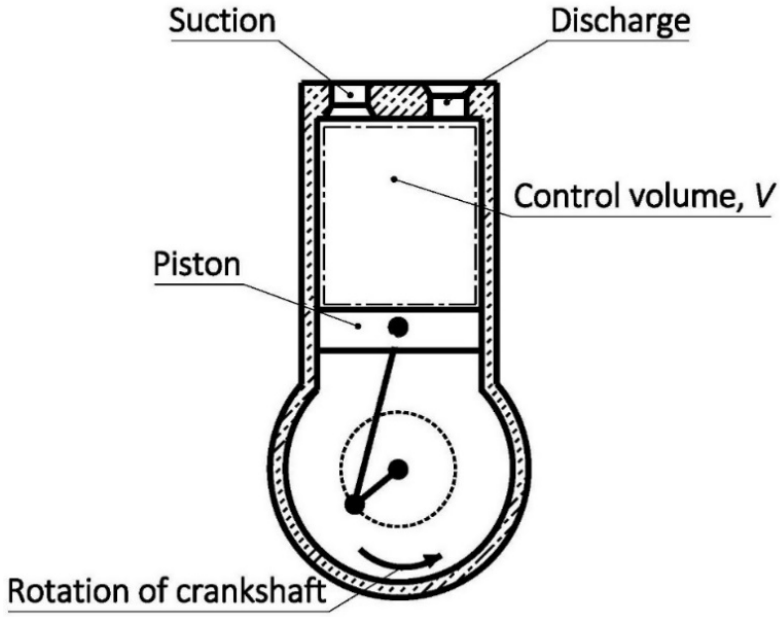

Fig. 1-3. An illustration of the workings of positive displacement compressors.

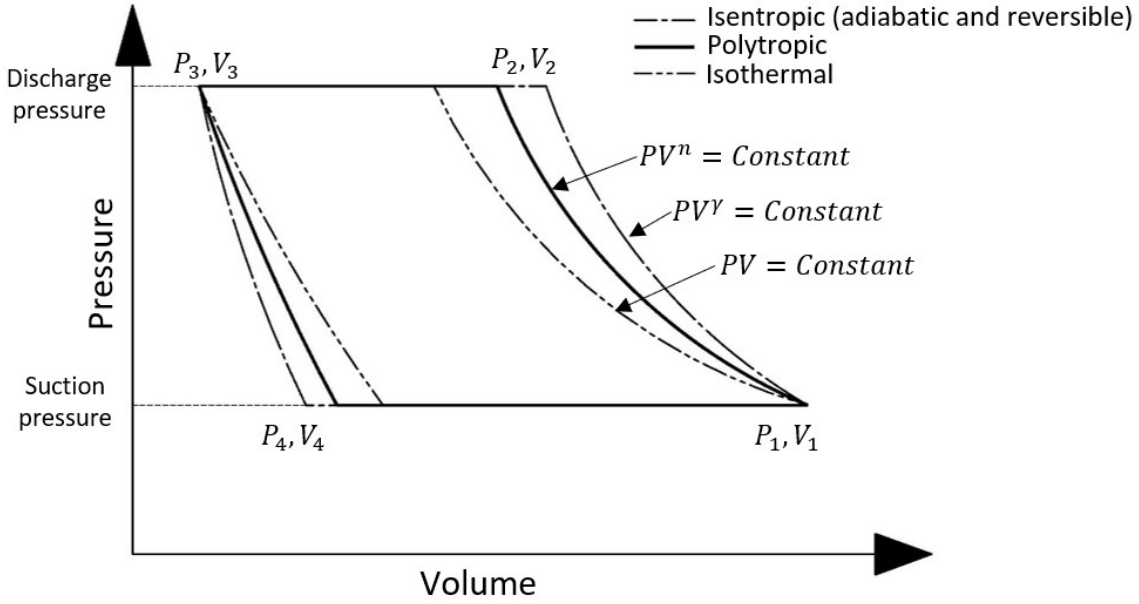

Fig. 1-4. Theoretical P-V diagram.

Irrespective of the geometry of the specific positive displacement compressor under study, they all share the same constituents which impact their volumetric and work performance. Fig. 1-4 shows a theoretical pressure-volume (P-V) diagram that characterises the thermodynamic states of the working fluid in a compression cycle. As shown in Fig. 1-4, the compression stroke occurs from state 1 to state 2, during which the working fluid is compressed from suction pressure, P_1, to the discharge pressure, P_2. As the compressed fluid is discharged, the volume of the compression chamber decreases to V_3 (aka the clearance volume). Subsequently, the volume is slightly increased to V_4 due to the expansion of the fluid trapped in the clearance. The suction stroke takes place from state 4 to state 1, and the theoretical volume, V_i, of the fresh charge, or the free air delivery (FAD), and the swept volume, V_s, are theoretically expressed as follows,

$$V_i = V_1 - V_4 \tag{1-1}$$

and

$$V_s = V_1 - V_3 \tag{1-2}$$

The ratio between the volumes given by equations (1-1) and (1-2) is the volumetric efficiency, which is expressed by the equation below,

$$\eta_v = \frac{V_i}{V_s} = \frac{V_1 - V_4}{V_1 - V_3} \tag{1-3}$$

The volumetric efficiency is an important parameter to quantify the volumetric performance of positive displacement compressors. Often, the measured volumetric efficiency figures are lower than the ideal theoretical values due to the effects of leakage and valve dynamics. Another performance index is the compression efficiency, which is defined as the ratio of the theoretical and actual work needed per cycle. Depending on the theoretical process of choice, the compression efficiency is expressed as follows,

$$\eta_{isen} = \frac{W_{isen}}{W_{actual}}, \qquad \text{Isentropic efficiency}$$
$$\eta_{p} = \frac{W_{p}}{W_{actual}}, \qquad \text{Polytropic efficiency} \tag{1-4}$$
$$\eta_{iso} = \frac{W_{iso}}{W_{actual}}, \qquad \text{Isothermal efficiency}$$

where the theoretical work for each case can be calculated as follows (Ueno et al., 2003),

$$W_{isen} = \frac{\gamma P_1 V_i}{\gamma - 1}\left[\left(\frac{P_2}{P_1}\right)^{\frac{\gamma-1}{\gamma}} - 1\right], \qquad \text{Isentropic work}$$
$$W_{p} = \frac{n P_1 V_i}{n - 1}\left[\left(\frac{P_2}{P_1}\right)^{\frac{n-1}{n}} - 1\right], \qquad \text{Polytropic work} \tag{1-5}$$
$$W_{iso} = P_1 V_i \ln\left(\frac{P_2}{P_1}\right), \qquad \text{Isothermal work}$$

where γ is the ratio of specific heats, n is the polytropic index.

It is worth mentioning that the compression work, owing to the losses (e.g., friction), is always less than the mechanical work, W_s, measured at the crankshaft. Therefore, the mechanical efficiency, η_m, is used to quantify how efficiently mechanical work can be converted into compression work,

$$\eta_m = \frac{W_{actual}}{W_s} \tag{1-6}$$

In addition to the efficiency terms described above, the Coefficient of Performance (COP) is often used to indicate the performance of a vapour compression refrigeration system (VCR). The COP is defined as the ratio of the cooling or heating capacity, Q, to the energy required, W_R, which is expressed as,

$$COP_{cooling/heating} = \frac{Q_{cooling/heating}}{W_R} \tag{1-7}$$

The compressor is the most energy-consuming unit in the VCR system, and therefore, equation (1-7) can also be used to indicate the compressor performance of the VCR system to a certain extent.

The performance indices mentioned above are affected by various factors. For example, internal leakages and gas superheating can result in a decrease in volumetric efficiency. The following sections will review the studies that investigate the effect of influencing factors on the performance of positive displacement compressors.

1.3.1.2. Leakage

Leakage is one of the main factors affecting the performance of positive displacement compressors. Compressed gas escapes through clearances due to the pressure difference that exists between the various fluid compartments in a machine. Published literature suggests that various methods have been proposed to analyse the leakage occurring in positive displacement compressors. The main difference amongst these methods is the assumptions made to characterise the leakage flow. The most used method is the isentropic flow model, which assumes the leakage flow to be isentropic and compressible flowing through an orifice or a convergent nozzle. For example, Cho et al. (2000) suggest these equations to calculate the mass flow rate, $\dot{m}$, of the leakage,

$$\dot{m} = \begin{cases} CAP_u \sqrt{\dfrac{2\gamma}{(\gamma-1)RT_u}\left[\left(\dfrac{P_d}{P_u}\right)^{\frac{2}{\gamma}} - \left(\dfrac{P_d}{P_u}\right)^{\frac{\gamma+1}{\gamma}}\right]}, & \dfrac{P_d}{P_u} \geq \left(\dfrac{2}{\gamma+1}\right)^{\frac{\gamma}{\gamma-1}} \\ CAP_u \sqrt{\dfrac{\gamma}{RT_u}\left(\dfrac{2}{\gamma+1}\right)^{\frac{\gamma+1}{\gamma-1}}}, & \dfrac{P_d}{P_u} < \left(\dfrac{2}{\gamma+1}\right)^{\frac{\gamma}{\gamma-1}} \end{cases} \tag{1-8}$$

where C is discharge coefficient, A_L is the flow area of the leakage, R is the ideal gas constant of the fluid, T and P are temperature and pressure, respectively, and the subscripts u and d denote the upstream and downstream of the leakage path, respectively.

The results presented by Yuan et al. (1992) suggest that the orifice assumption produces conservative estimates of leakage values in comparison to more accurate differential models which take gas viscosity and inertia into account. The graphs featured in the work by Yuan et al. (1992) suggest that a carefully selected discharge coefficient can bring the results of the orifice assumption to be almost identical to the results of the more sophisticated and computationally costly model. Kim et al. (2017) utilised Computational Fluid Dynamics (CFD) to determine the flow coefficient with respect to the change in upstream pressure and the width of radial clearance. It was found that the flow coefficient ranges from 0.17 to 0.85 for the radial clearance width of 10 to 60 μm under an upstream pressure of 30 bar. In a recent study, Pereira and Deschamps (2020) used various dimensionless parameters to illustrate the effect of working gas types, operating conditions, and geometric characteristics on the overall leakage. The results show that the model could accurately predict the radial and tangential leakages, with average errors of 2.4% and 7.9%, respectively.

Another method is the Fanno flow model, which treats the leakage as an adiabatic flow by considering the viscous effect of the fluid over the path that has a constant cross-sectional area. Yanagisawa and Shimizu (1985) adopted such a model to investigate the leakage in a rolling piston compressor. The authors found that the eccentric assembly of the main bearing can minimise the effect of dynamic behaviours of bearings on the radial clearance, reducing the leakage flow considerably. Rodgers and Nieter (1996) and Kang et al. (2002) compared the Fanno flow model with the isentropic flow model and found that the Fanno flow model provided more realistic predictions than the isentropic nozzle model, especially with a larger clearance. Teh and Ooi (2009a) discovered that the shorter

rotor-cylinder configuration could reduce the leakage flow, achieving a volumetric efficiency of more than 95%. However, the longer configuration is usually preferable for minimising the frictional loss. The authors suggested using the eccentric cylinder to balance the impacts on the performance caused by leakage loss and frictional loss. Silva and Deschamps (2015) analysed the leakage through the valve by using the Fanno flow leakage model. It was found that the leakage flow through the discharge valve was more significant than the suction valve leakage. Additionally, the authors reported reductions of volumetric and isentropic efficiencies of 2.7% and 4.4%, respectively, per 1 μm increment of the valve clearance. Recently, Aw and Ooi (2020) combined the Fanno flow model with CFD to determine the empirical correlations for the equivalent channel width for various factors, including pressure ratios and rotation angles. According to the result, this model can predict the leakage flow within the discrepancy of ±15%.

It is worth mentioning that both the isentropic and Fanno flow models consider the leakage compressible. The work of Ferreira and Lilie (1984) chose a different method in which the leakage flow is assumed to be turbulent and incompressible. Predictions provided by this method agree well with experimental measurements in the small clearance region, but the discrepancy gradually becomes more evident as the clearance increases. This might attribute to the inertial force that this model neglects. The work of Ishii et al. (1996) is another example that employs the incompressible leakage model. It has been found that the results obtained from the incompressible flow model are more accurate than that of the model based on more complicated compressible formulations. Hence, the authors suggested that the incompressible model is adequate to analyse the leakage flow, while the compressible flow model is not necessarily useful. This contradicts the opinion proposed by Lohn and Pereira (2014), who pointed out that the incompressible

model cannot sufficiently describe the complexity of the leakage flow and generates more uncertainties. Table 1-3 below summarises different leakage models.

Table 1-3. Leakage flow models

Leakage model	Features
Isentropic flow model	• Simplest approach • Isentropic and compressible flow through a leakage path that can be regarded as an orifice or a convergent nozzle. • The viscous effect is described by the empirical flow coefficient, which requires extra computational and experimental work.
Fanno flow model	• Adiabatic and compressible flow • Constant cross-sectional area of the flow path • Long but narrow flow path • Viscous effect is included by using the friction factor
Incompressible flow model	• Leakage flow is assumed to be turbulent and incompressible • The viscous effect is considered • The influence of inertial force needs to be included when the clearance and pressure exceed a certain level

1.3.1.3. Heat transfer

Heat transfer describes a process that the heat transfers from one object to another via three mechanisms, i.e., convection, conduction, and radiation. For positive displacement compressors, heat is generated during the compression process and directly affects the temperature of the working fluid and machine components. This can lead to undesirable consequences, affecting the machine performance as well as reliability. Thus, compressors are generally designed such that some of this heat is transferred to the gas surroundings via convection and conduction. These are the major mechanisms of heat transfer realised in positive displacement compressors, while the effect of radiation is relatively insignificant. Hence, this section will focus on previous studies that investigate convection and conduction occurring in positive displacement compressors.

1.3.1.3.1. Convection

Convection is one of the modes of heat transfer that involves the movement of fluid and temperature gradients. Theoretically, the rate, $\dot{Q}_{cov}$, of convective heat transfer can be calculated by the equation below,

$$\dot{Q}_{cov} = hA\Delta T \tag{1-9}$$

where A is the heat transfer area, ΔT is the temperature difference. The term h in equation (1-9) is the convective heat transfer coefficient, and it is determined from the empirical Nusselt number correlation, Nu, by using the following equations,

$$h = Nu\frac{k}{D_h} \tag{1-10}$$

and

$$Nu = cRe^{a}Pr^{b} \tag{1-11}$$

where k is the thermal conductivity of the fluid, D_h is the hydraulic diameter,Re is the Reynolds number, Pr is the Prandtl number, and a, b, and c are the empirical constants.

Before the 1970s, the Nu correlations were mainly developed for investigating heat transfer in internal combustion (IC) engines, e.g., Annand (1963). The work of Adair et al. (1972) was among the first that proposed a Nusselt correlation for the reciprocating compressor. Later, Liu and Zhou (1984) further developed the correlation by modifying the expression of swirl velocity, which considers the effect of lubricating oil. These two correlations (Adair's and Liu's) were compared by Tan and Ooi (2011), who investigated the heat transfer in the revolving-vane compressor. The authors modified the characteristic velocity to cater for the geometric characteristics of the machine, and the result showed that Liu's correlation could produce relatively accurate predictions, with a maximum error of less than 2%.

In another study of heat transfer in the reciprocating compressor, Hsieh and Wu (1996) pointed out that the fluid velocity changed rapidly at the beginning of the discharge process, and consequently, the average piston velocity was inadequate to represent the fluid velocity inside the cylinder. As such, they suggested the normalised viscosity term to replace the Prandtl number and introduced an additional Reynolds number. Based on the experiment, a set of correlations was determined for different processes of the working cycle, and the comparison between the numerical result obtained by proposed correlations agreed well with the experimental data. However, as reported by the authors, this correlation is not suitable for dealing with phase-changing cases. Disconzi et al. (2012) pointed out that the recirculating flow, caused by valve dynamics during the suction and discharge process, strongly affected the effective area of heat transfer. The authors suggested relating the characteristic velocity of the Reynolds number to the mass flow rate through valves, proposing different correlations specifically for each process during the cycle.

Ooi and Zhu (2004) revealed that existing correlations were inadequate for the scroll compressor due to the geometry complexity. The authors presented a 2D model that brought the effect of geometry on flow characteristics into consideration, and a comparison was made between the proposed model and earlier models. The result showed that predictions of the amount of heat transfer calculated by the proposed model were significantly higher, and this is mainly due to the effect of recirculating flow and the geometry deformation on the fluid velocity in the late compression period. Another study on the scroll compressor was conducted by Jang and Jeong (2006) who take into account the effect of orbiting scroll oscillation on heat transfer occurring in the scroll wrap. Based on the experimental result, the authors proposed a modified Nusselt correlation, which could

provide more accurate predictions of the discharge temperature. Recently, Rak and Pietrowicz (2020) proposed a correlation for scroll compressors by curve-fitting the data of the CFD simulation. It was found that this correlation could bring the error to less than 15% compared to results from 2D numerical models. Table 1-4 shows correlations proposed in different literature for positive displacement compressors.

Table 1-4. Empirical correlations proposed in different literature

Authors	**Nusselt number correlation**		**Application**
Adair et al. (1972)	$Nu = 0.053Re^{0.8}Pr^{0.6}$		Reciprocating compressor
Liu and Zhou (1984)	$Nu = 0.75Re^{0.8}Pr^{0.6}$		Reciprocating compressor
Hsieh and Wu (1996)	Pure compression	$Nu = 0.163Re^{1.093}\left(\frac{\mu}{\mu_o}\right)^{0.484}$	Reciprocating compressor
	Compression with discharge	$Nu = (-1.64Re_d + 0.382Re^{1.166})\left(\frac{\mu}{\mu_o}\right)^{0.15}$ where Re_d is the Reynolds number based on the velocity at the beginning of the discharge process	
	Pure expansion	$Nu = 0.0488Re^{1.093}\left(\frac{\mu}{\mu_o}\right)^{0.484}$	
	Expansion with suction	$Nu = 0.296Re^{1.093}\left(\frac{\mu}{\mu_o}\right)^{0.484}$	
Jang and Jeong (2006)	$Nu = \left(1 + 3.5\frac{D_h}{D_c}\right)[1 + 8.48(1 - \mathrm{e}^{-5.35St})]Nu_b$ where D_c is the diameter of the curvature, respectively, St is the Strouhal number, and Nu_b is the Dittus-Bolter equation.		Scroll compressor
Disconzi et al. (2012)	Suction	$Nu = 0.08Re^{0.9}Pr^{0.6}$	Reciprocating compressor
	Compression	$Nu = 0.08Re^{0.8}Pr^{0.6}$	
	Discharge	$Nu = 0.08Re^{0.8}Pr^{0.6}$	
	Expansion	$Nu = 0.12Re^{0.8}Pr^{0.6}$	

1.3.1.3.2. Conduction

Conduction, which takes place between the adjacent components, is another major mechanism of heat transfer for positive displacement compressors. Proper analysis of conduction can improve the machine reliability as it provides insight into the temperature distribution and thermal loading of compressor components.

Padhy and Dwivedi (1994) proposed a lumped model in which the rolling piston compressor was separated into 22 elements. The results show good agreement between the estimates and the measured data; it has been found that the largest discrepancy was 3.37 $^{\circ}C$ for the temperature of the fluid inside the cylinder. This lumped model was later adopted for the reciprocating compressor by Ooi (2003), who reported the discrepancy between predictions and measures below 10%. Another application of the lumped method was detailed by Sanvezzo and Deschamps (2012); the authors investigated conductive heat transfer in the reciprocating compressor. The numerical results are in reasonable agreement with the experimental data, with the maximum discrepancy of 14.4$^{\circ}C$ (located on the cylinder surface). Dutra and Deschamps (2013) conducted an experiment to investigate the conductive heat transfer in a reciprocating compressor. Temperatures of 11 locations were acquired under 3 operating conditions and the thermal conductance at each tested location was determined accordingly. Patil et al. (2019) discovered that the rate of heat transfer increased as the result of fast compression, whereas the overall heat transfer coefficient decreased at the beginning of the compression and eventually stabilised between 8 to 12 W/m^2K. Additionally, an isothermal efficiency of 84-86% was reported at the compression ratio of 2.05-2.35. In another study, Stosic (2015) utilised the quasi-one-dimensional model to obtain the fluid temperature and calculate the heat transfer by convection and conduction. The author reported that the result agreed with

records of the visualisation experiment; and it was found that the temperature was linearly distributed along the rotor axis and the maximum temperature of the rotor could be reduced from 700K to 350K, thus improving the machine reliability at high pressure ratios.

1.3.1.4. Friction and lubrication

In mechanical systems, undesirable friction is primarily responsible for the decrease in mechanical efficiency. More importantly, severe wear and component failure generally occur at contact regions between moving components, as such deteriorating machine durability.

Available literature shows that the reduction of friction loss in positive displacement compressors is mainly achieved by two approaches. The first method is through the geometric optimisation of the machine. Yanagisawa and Shimizu (1985c) investigated friction losses of the rolling piston compressor. They concluded that the vane-tip friction is mainly affected by the absolute sliding velocity of the vane-tip, whereas the tangential force strongly influences the vane side friction. Additionally, the total frictional loss has been found to be more sensitive to the change in the rotor radius rather than the cylinder length. Later, Ooi (2005) found that a narrower but taller cylinder could reduce the friction loss occurring in the rolling piston compressor. This leads to an increase in mechanical efficiency of up to 14%. Teh and Ooi (2009b) then introduced a revolving vane mechanism, in which the rotor and the cylinder rotate concentrically. Compared to the traditional rolling piston compressor, the proposed design minimises relative motions between the contacting surfaces in the cylinder, and consequently, the total friction loss was reduced by 19.7%, bringing about the mechanical efficiency to 94.1%.

Liu et al. (2010) developed an optimisation procedure to reduce friction losses among bearing components of the scroll compressor, including the thrust bearing, the crank bearing, and the upper and lower bearings. The authors found that friction loss could be reduced from 11.4% to 38.1% by introducing smaller diameters to the four bearings. Yang et al. (2013) reported that friction losses at the bearings of the reciprocating compressor decreased with the stroke-to-bore ratio, whereas the friction between the piston and cylinder wall exhibited an opposite trend due to the increase in piston mean velocity. In sliding vane compressors, Bianchi and Cipollone (2015) discovered that lighter vane blades and a slower operating speed could achieve a significant reduction in friction losses. Recently, Gu et al. (2021) proposed a new variant of the sliding vane compressor, which features a rotating cylinder. Under the same working condition, it was found that the proposed design could reduce friction losses by up to 10% compared with the conventional design.

Another method to reduce friction losses is to apply lubricants. Kim and Lancey (2003) modelled the lubrication system of a rolling piston compressor to predict the lubricating oil flow rate. Compared with the measured data, predicted values obtained by the model presented acceptable accuracy, with a difference of 5.8%. Afshari et al. (2017) investigated the effect of the oil viscosity on the energy consumption of a reciprocating compressor used for air-water heat pumps. Wu et al. (2017) proposed a comprehensive network model to describe the circulation of lubricating oil throughout the screw compressor. Based on their experiment, it was found that the overall performance of the machine could be improved by injecting low-temperature lubricating oil from the discharge end bearing to the working chamber. In recent research conducted by Ozsipahi et al. (2019), the lubrication system of a compact inverter reciprocating compressor was numerically

modelled by using two CFD methods, namely the Sliding Mesh and the Moving Reference Frame.

Apart from the common role in reducing friction loss, lubricants can be used to address losses caused by other factors, such as leakage and gas superheating. Valenti et al. (2013) conducted research on the effect of lubricating oil on the performance of a mid-size vane compressor. The results revealed that the lubricating oil (with the size of 100μm) could effectively reduce the fluid temperature to as low as 60 °C, allowing the compression work to decrease by 23-28%. Later, Pizarro-Recabarren and Barbosa (2016) investigated the cooling effect of the lubricating oil in the reciprocating refrigeration compressor. It was reported that the lubricating oil could slightly increase the cooling capacity and indicated COP by 2.3% and 9%, respectively.

1.3.1.5. Valve dynamic and port characteristics

Valve is an essential component of a positive displacement compressor in controlling the fluid flow during the suction and discharge stages. A suction valve is used to adjust the amount of fresh charge, while a discharge valve is used to prevent the backflowing of compressed fluid.

Reciprocating compressors are generally equipped with both suction and discharge valves; studies on the valve dynamic of reciprocating compressors can be sought in a large body of literature. Some typical examples are as follows. Nagata et al. (2010) analysed the effect of the compressor operating speed on the suction valve. The authors found that low operational speed could result in severe vibration of the valve over the suction port, causing the volumetric efficiency to fluctuate periodically. As the speed increased, the viscous effect of the lubricant on the valve could be reduced, which increases the maxi-

mum displacement. On conducting an experimental study on the trans-critical CO_2 compressor, Ma et al. (2012) suggested that a reasonable low discharge pressure and a smaller size of valve lift are preferable for valve life due to lower stress from the rebound process. The results of the investigation of the effect of various factors on the impact load acting on the ring valve done by Wang et al. (2013) have suggested that the valve inclination became more severe during the closing of the discharge valve, and the inclining angle of the discharge valve became unpredictable when the pressure ratio exceeded 2.55. Additionally, the impact velocity of the valve was mainly affected by the variation of the piston velocity and the volume of the compression chamber. An important topic is valve failure; on this topic, Mu et al. (2019) have proposed a dynamic model to analyse the factor that causes such failures. The proposed model considered the relationship between the valve displacement and various factors, including the effective length, the elastic force, the mass of the valve reed, and the viscous stiction. In a recent study, Egger et al. (2020) introduced a mechanical support mechanism to the conventional valve. They reported that the proposed design could increase the cooling capacity by 22% and considerably reduce the impact stress during the suction process, while the improvement of COP was quite limited due to the additional friction losses caused by the support mechanism.

In rotary compressors, the suction valve is not necessarily required as the suction and discharge ports are physically separated by the rotor. In contrast, the discharge valve plays an important role in ensuring the fluid is delivered at the designated pressure and avoiding the high-pressure backflow. Generally, the reed-type valve, as shown in Fig. 1-5, is commonly used in various rotary compressors. Huang and Xie (2008) presented a dynamic analysis to investigate the influence of the retainer on the reliability of the valve. The simulation results show that the pressure pulsation became more severe during the discharge

process when the size of the retainer was reduced. Teh et al. (2009) modelled a rotating valve that is employed in the revolving vane compressor. Compared to the conventional design, the rotating valve was found to possess better reliability due to the softening effect of the centrifugal force. However, the author suggested that the dimensions of the valve should be chosen following the operating speed to avoid valve loss due to centrifugal overloading and resonance.

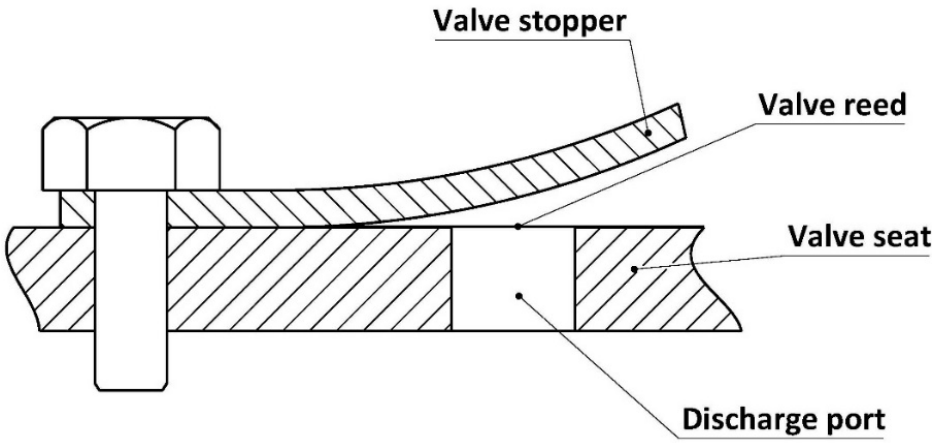

Fig. 1-5. Structure of the reed-type valve.

Yu et al. (2018) applied the fluid-structure interaction (FSI) to analyse the effect of the torsional movement. They reported that the maximum impact stress was found to increase with the torsional movement, and the level of the torsional movement was significantly affected by the geometry of the discharge port and the mounting method of the valve reed. Later, Min et al. (2018) proposed an empirical correlation of the discharge coefficient to calculate the effective area. This correlation was derived based on the CFD simulation that considers the influence of geometric parameters, including the valve lift, the valve size, and the port dimensions. Compared to the experimental result, the proposed correlation was found to predict cooling capacity and input power with an error band of 10%.

During the suction and discharge processes, the mass flow rate of the fluid is not only affected by the dynamic behaviour of the valve, but also by the port characteristics, including, position, geometry, and size. Kim et al. (2004) studied the performance of the twin rotary compressor, and their result showed that the adiabatic efficiency could be increased when either the port diameter or porting angle were increased. Mujic et al. (2008) found that the shape and size of the discharge port were the dominant parameters that affect the gas pulsation occurring in the screw compressor. In a study of the limaçon positive displacement machine, Sultan and Schaller (2011) utilised the stochastic optimisation technique to find the port geometry that can produce the best performance for given machine dimensions. Lim et al. (2017) reported that the increase in the size of the port led to a higher suction loss but a lower discharge loss. In another study, Zhao et al. (2020) proposed a new design of the discharge port to alleviate the severe pressure difference between the up- and down-side chambers of the scroll compressor. The results showed that a 2.4% of improvement in the isentropic efficiency and a 50% of reduction in pressure difference could be achieved by applying the proposed discharge port. Recently, Gu et al. (2021) analysed the influence of the port configuration employed in their proposed sliding vane compressor with a rotating cylinder. The authors concluded that the machine performance was more sensitive to the variation of the coverage angle.

1.3.1.6. Capacity control

Capacity control is referred to as the method that assists the compressor to adjust the machine capacity as per the working load on demand. In the compressor system, capacity control methods can ensure the machine operates efficiently and protect the system from damage. In the open literature, stepless control and variable speed control are the two commonly used methods in positive displacement compressors.

The principle of stepless control is to delay the closing time of the suction vale via the supply of the external force (usually hydraulic force), allowing excess fluid to escape from the working chamber (Hong et al., 2009). As a result, the amount of fluid that is compressed matches the working load. Stepless control was proposed by the work of Tuymer (1974), and it has been mainly used in reciprocating compressors. In the past decade, the research interest in stepless control has focused on theoretical modelling and performance analysis (Hong et al., 2009; Bin et al., 2013; Wang et al., 2018), dynamics of the suction valve (Jin and Hong, 2012; Tang et al., 2014; Liu et al., 2016), and the optimisation of the actuator (Jiang et al., 2020; Zhang et al., 2020; Sun et al., 2021).

Another frequently used capacity control method is speed control, in which the operating speed is regulated by a variable speed drive to respond to the variation of the working load. In practice, speed control is widely employed for domestic refrigeration and air-conditioning systems (Li, 2013). Tassou and Qureshi (1996) assessed the performance of three compressors with speed control. The result showed that the volumetric efficiency of all tested compressors increased with the speed, while the isentropic efficiency exhibited an opposite trend. Additionally, the authors also reported that speed control provided an energy-saving up to 9.6%, 23.7%, and 9.8% for the rotary compressor, and the open-type and semi-hermetic reciprocating compressors, respectively. In another study, Aprea et al. (2006) found that an average energy saving of 20% could be achieved if speed capacity control is introduced to the scroll compressor. Wang et al. (2017) compared the variable speed method with sliding valve control, and it was noticed that the variable-speed control could provide an adiabatic efficiency of 72.8% at a 25% load condition, which is better than the 42.5% obtained from the sliding valve mechanism.

Capacity control of fluid compression systems can also be realised in some other ways. Bypass/recycling is the simplest way to adjust the compressor capacity, which directs the redundant fluid in the discharge side back into the suction side via a bypass pipe (Yaqub and Zubair, 2000). However, the compression work of the bypassed fluid is wasted, making this method an inefficient form of capacity control. The work by Jeong et al. (2014) reported that the compressor performance with speed control was 5 times better than that with gas bypass at part load. However, the work by Wang et al. (2012) pointed out that the COP and energy efficiency of the scroll compressor could be improved up to 34% and 42%, respectively, if the gas was bypassed at the suction instead of after compression stroke.

Other capacity control methods include clearance pocket and suction throttling (Holdack-Janssen and Kruse, 1984; Yaqub and Zubair, 1996; Wang et al., 2015; Hollingsworth et al., 2019), but the literature available on these topics is limited. Table 1-5 presents a comparison of different capacity control methods.

Table 1-5. Comparison of different capacity control methods

Methods	Principle	Pros and cons
Stepless control	The closing of the suction valve is delayed by an external force, allowing excess fluid to flow out of the working chamber	Pros: • Theoretically, capacity adjustment ranges from 0 to 100% Cons: • Fatigue and wear consequences on the suction valve due to the reverse flow
Speed control	Operating speed is regulated to match the working load	Pros: • Most energy-efficient Cons: • High cost of variable speed drives for large-scale applications • Difficult to ensure reliable valve operation • Mechanical resonance, pulsation, and torsional-related issues might occur

Table 1 5. Comparison of different capacity control methods (Continued)

Methods	Principle	Pros and cons
Bypass	Compressed fluid is by-passed to the suction line before delivering, thus reducing the capacity	Pros: • The simplest way to apply Cons: • Compression work on the bypassed fluid is wasted • Usually requires a heat exchanger to cool the bypassed fluid
Clearance pocket	The additional clearance volume is introduced to the working chamber	Pros: • Compression work on the fluid in the clearance area can be recovered Cons: • Less efficient with low compression ratios
Suction throttling	Reduce the suction pressure by throttling the fresh charge via the control valve at the suction	Pros: • Least costly and easy to apply Cons: • High discharge temperature • Worst performance

1.3.2. Recent innovative modelling in compressor research

In the design phase, mathematical modelling is the most practical and economical method to simulate the thermodynamic processes implemented by the machine and predict the performance of the system. The published literature shows that most of the mathematical model is derived by using physical and thermodynamic laws together with the description of machine dimensions and geometries. For example, Ooi and Wong (1997) proposed a mathematical model of the rolling piston compressor, which considers geometric, thermodynamic, dynamics and frictional effects.

However, the process executed by the compressor is rather intricate, causing the mathematical relationship underlying such a process is not readily obtainable (Sultan, 2007). As such, the conventional modelling method is usually insufficient to describe the workings of the compressor under the actual condition. Recently, there has been a trend

of using machine learning methods for mathematically impractical applications. One remarkable benefit is that such a method is trained by a small number of actual measurements to explore the hidden function that relates inputs and outputs, meaning the mathematical relationship between parameters is unnecessary. This section will provide an overview of several machine learning methods that have been applied to the modelling and optimisation process of positive displacement compressors.

1.3.2.1. Artificial Neural Network

Artificial neural network (ANN) is a method inspired by biological neural networks to solve complex problems in a variety of disciplines (Jain et al., 1996). A typical structure of ANN has three layers, namely input, hidden (can be multiple), and output layers. In practice, each input data, x, is multiplied by a weighting factor, w, and then connected to the output via the hidden layer, which contains an added bias, b, the summation function, $\sum$, and activation function, f. Fig. 1-6 depicts the schematic diagram of the ANN workflow.

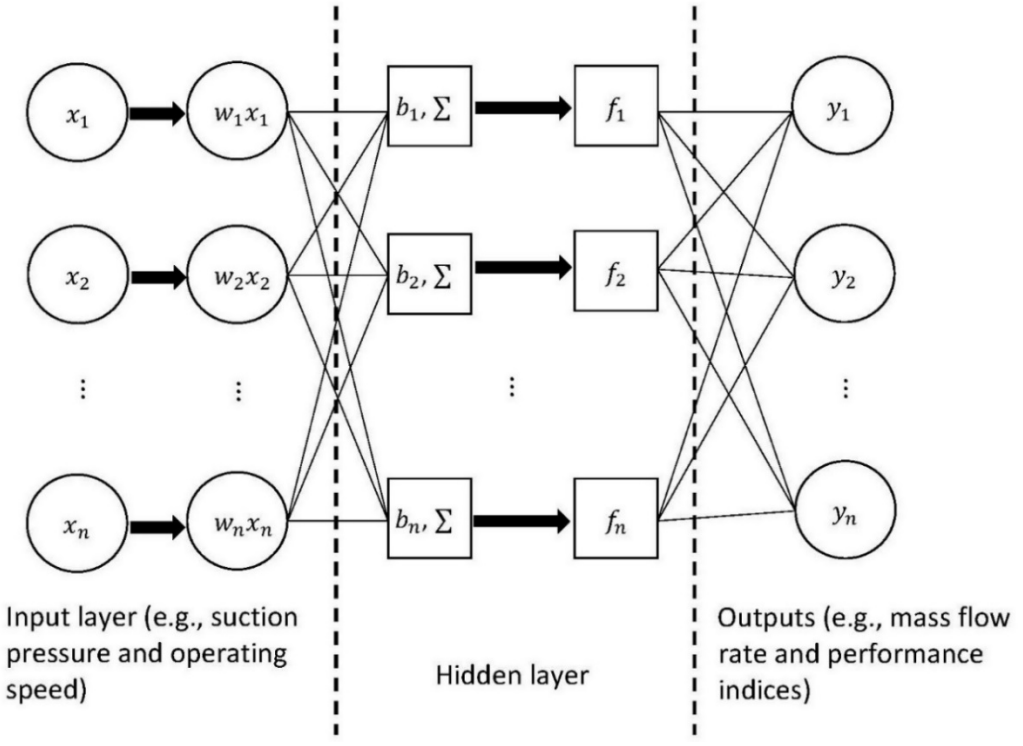

Fig. 1-6. Schematic diagram of ANN applied in positive displacement compressors.

In positive displacement compressors, ANN is a popular method for mathematical modelling and performance prediction. Namdeo et al. (2008) applied ANN to analyse the leakage through the valve so that the valve failure can be detected at an early stage. Sanaye et al. (2011) modelled the rotary vane compressor by using the ANN method. The predictions from the ANN model agreed well with the experimental data, showing the largest mean relative error (MREs) of 7.36%. In a later study, Belman-Flores et al. (2015) further demonstrated the accuracy of the ANN model and compared it with the physical model in terms of modelling a reciprocating compressor. Tian et al. (2015) proposed a hybrid model, which combines Partial Least Squares (PLS) regression with ANN, to predict the thermodynamic performance of the scroll compressor. Compared to the model using only ANN or PLS, the hybrid model produced relatively accurate results, in which the largest MREs was 1.96% and the correlation coefficients ranged from 0.9703 to 0.9999. In another study, Zendehboudi et al. (2017) compared the reliability of two modelling methods, i.e., ANN and Adaptive Neuro-Fuzzy Inference System (ANFIS), in modelling a scroll compressor that has a vapour injection mechanism. The authors found that both modelling techniques showed comparable performance in terms of predictions of the discharge flow rate and power consumption, with the largest difference of less than 0.7%.

1.3.2.2. Genetic Algorithm Optimisation

Genetic algorithm (GA) is another machine learning method used in the optimisation of many engineering problems. It is inspired by the principle of natural selection and evolution to find design solutions from a large search space based on fitness/objective values (Whitley, 1994). A classic GA is comprised of five phases, including encoding, fitness/objective evaluation, reproduction, crossover, and mutation. Fig. 1-7 presents a detailed process of GA.

The work of Huang and Tsay (2009) is an example that used the GA method to optimise the mechanical efficiency of the sliding vane compressor. Chen and Ooi (2021) developed an optimisation procedure for the coupled vane compressor based on the Non-dominated Sorting Genetic Algorithm II (NSGA-II). From the optimisation result, the authors found that a larger working chamber while a smaller rotor could improve the compressor performance with respect to the same cylinder size. The NSGA-II was also adopted by studies of reciprocating compressors aimed at optimising the actuator for the stepless control system (Jiang et a., 2020; Zhang et al., 2020). In a recent study, Silva and Dutra (2021) applied GA to optimise the piston trajectory of the reciprocating compressor. The authors reported that the optimum piston trajectory could increase the thermodynamic efficiency from 88.3% to 92.1% and the volumetric efficiency from 70.9% to 72%. In addition, the proposed optimum design was found to be more efficient and less affected by the pressure ratio under the working condition other than the baseline.

1.3.2.1. Other methods

There are some other machine learning methods applied in the modelling and optimisation of positive displacement compressors, albeit to a limited level. Lu et al. (2021) used the Bayesian optimisation method to optimise the port geometries of the limaçon rotary compressor. According to the results, the authors discovered that most of the obtained outcomes fell into the desired region, and the average isentropic and volumetric efficiencies obtained from the optimisation were 93.81% and 83.62%, respectively. In addition, the authors also reported that the obtained optimum design exhibited a certain level of robustness when the operating condition fluctuated within a small percentage around that used in the optimisation. Fig. 1-8 shows the process of the Bayesian optimisation method applied in positive displacement compressors.

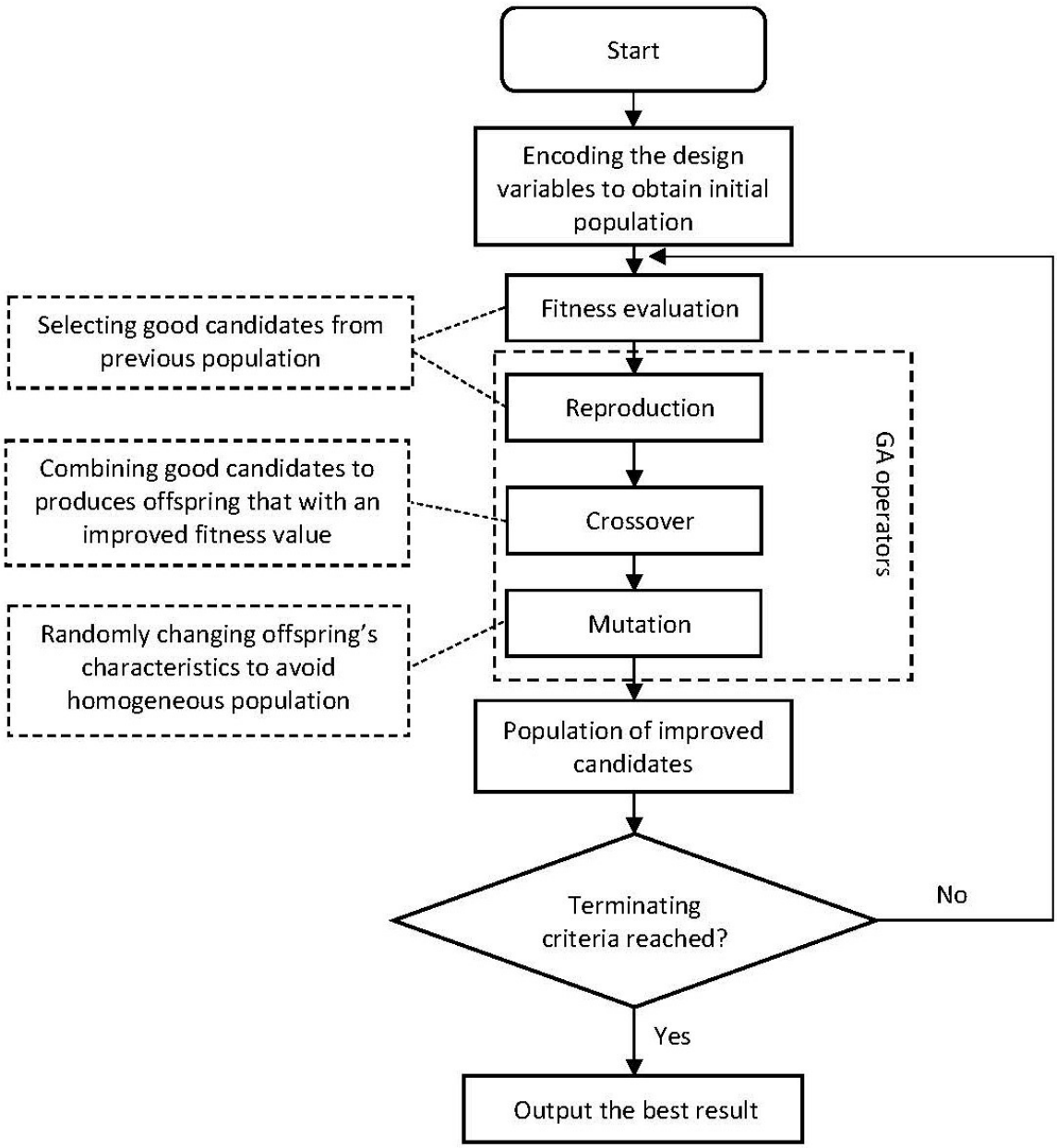

Fig. 1-7. A schematic diagram of GA.

Sultan and Kalim (2011) presented a two-level hybrid optimisation, which incorporates the simultaneous perturbation stochastic approximation (SPSA), to find the best piston trajectory of the reciprocating compressor driven by the geared five-bar mechanism. Later, Phung and Sultan (2021) also employed the SPSA method to optimise dimensions of the limaçon positive displacement machine for given operating conditions. Qi et al. (2018) employed Principal Component Analysis (PCA) to denoise the large-scale data, and

the denoised data was then used by the Support Vector Machine (SVM) classifier to obtain the sparse coefficient for the fault-diagnosis model. The authors reported that the proposed model was robust to the change in working conditions, with an accuracy rate of 80% for detecting potential faults. Recently, Lu et al. (2021) adopted PCA to optimise the heat transfer and torque patterns to improve the reliability of the reciprocating compressor. Table 1-6 summarises the application of various machine learning methods in positive displacement compressors.

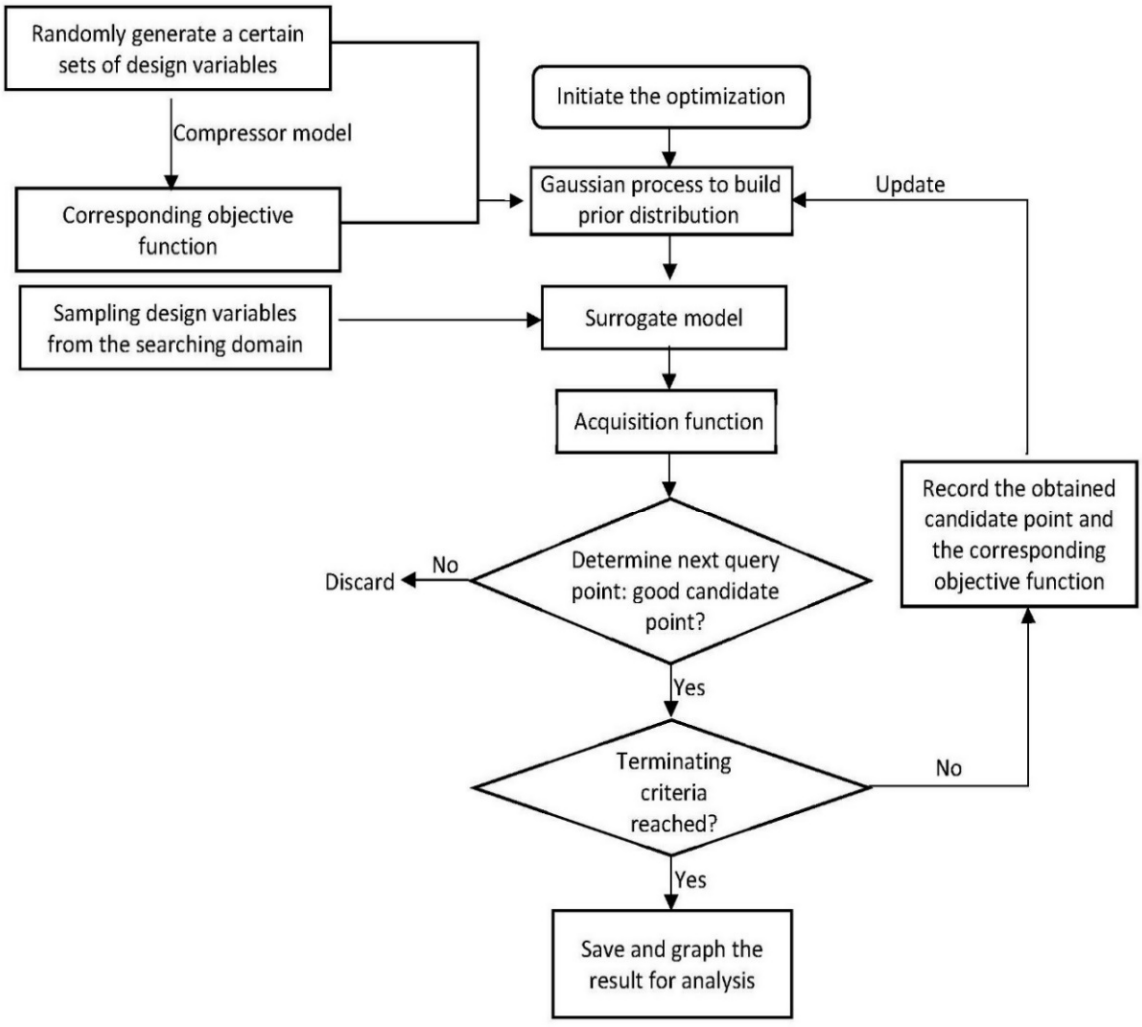

Fig. 1-8. Process of Bayesian optimisation applied in positive displacement compressor.

Table 1-6. Summary of machine learning methods applied in positive displacement compressors

Methods	Type of compressor	Applications	Main reference
ANN	Sliding vane	Detection of valve failure	Sanaye et al. (2011)
	Reciprocating	Mathematical modelling	Namdeo et al. (2008)
ANN	Scroll	Performance prediction	Tian et al. (2015)
GA	Sliding vane	Improvement of mechanical efficiency	Huang and Tsay (2009)
	Coupled vane	Optimisation of rotor-chamber configuration	Chen and Ooi (2021)
	Reciprocating	Optimisation of valve actuator and piston trajectory	Silva and Dutra (2021)
Bayesian optimisation	Limaçon (rotary)	Optimisation of port geometry	Lu et al. (2021)
SPSA	Reciprocating	Optimisation of piston trajectory	Sultan and Kalim (2011)
	Limaçon (rotary)	Machine geometric design	Phung and Sultan (2021)
PCA	Reciprocating	Fault diagnosis	Qi et al. (2018)
		Reliability improvement	Lu et al. (2021)

1.3.3. Challenges and opportunities for future studies

Although numerous research works have been dedicated to various aspects of positive displacement compressors, further investigations are needed to address some key issues that are listed as follows:

(1). In practice, the compressor performance and working characteristics reported in the literature may be insufficient to guide the selection process, as most studies were conducted under specific working conditions. More experimental studies

are needed to provide more detailed information on positive displacement compressors, especially the new technologies.

(2). It is worth mentioning here that compressor performance maps are useful tools to guide the machine selection process as per the demand of the application. However, performance mapping of positive displacement compressors was rarely discussed in the available literature (Ma et al., 2020), and more importantly, the current standard (AHRI Standard 540-2020) of the mapping approach applies only to a limited range of applications (AHRI, 2020). Therefore, it is also recommended that more research efforts should be conducted on this topic.

(3). The application of lubricating oil has many positive effects on machine performance (Afshari et al., 2016). However, the extreme condition (i.e., high temperature and pressure) at the compressor discharge and the presence of the fluid-oil mixture significantly affects the viscosity of the oil and deteriorates the lubricating performance. Hence, further study on lubrication systems is required. In fact, one solution to such an issue is by applying materials, such as nanoparticle additives, that have extreme condition functionality (Karnaz et al., 2017), this may need interdisciplinary collaborations between mechanical and material engineering.

(4). Although research interest in the two-phase flow has increased significantly, the discontinuity of properties of the two-phase flow is still a challenging issue and further development of two-phase flow modelling is necessary.

(5). With the aid of advanced simulation resources, compressor models based on CFD have become more accessible, offering more insights into complicated phenomena such as heat transfer. However, the difficulties in solving problems that require multiphysics modelling still exist, and the balance between model accuracy and computational cost also remains a challenge.

(6). Machine learning methods have become increasingly popular in the modelling and optimisation of positive displacement compressors. The major benefit of using machine learning methods is that the mathematical relationship between parameters is not necessarily required. Therefore, it could be expected that future work on modelling and optimisation will be more effective if machine learning methods are widely adopted.

(7). The exergy and thermoeconomic analysis are effective methods to identify the irreversibility and their associated costs in the system. The research effort, especially from the industry, should pay more attention to such a method, as it can provide useful information about potential improvements and capital savings for the compressor and its system.

(8). Waste heat recovery is a promising method to recycle the thermal energy produced in the fluid-compression. One noticeable advantage of this method is the improvement in energy utilisation due to the recovery of waste heat. However, the current challenge with this method is the cost and technology to be utilised to recover low-grade waste heat, which makes this method less attractive to small-scale applications, such as domestic refrigeration. Therefore, future research to address this issue would be beneficial for improving the energy efficiency and sustainability of compressor systems.

Due to their essential role in many engineering systems, positive displacement compressors have received particular attention from the research sector. Many studies have been dedicated to better understanding the intricate workings of the compressor and bringing about improvements in machine performance. This paper presents a review of the published literature available on different topics of positive displacement compressors, including modelling of internal leakage and heat transfer, methods and design improvements to reduce friction, the effect of valve dynamics and port geometry, and capacity control strategies.

Machine learning methods have been demonstrated to be accurate and computationally cost-effective in solving complex problems. In positive displacement compressors, ANN is one of the most used machine learning methods to model the operation and predict the machine performance. In the past decade, other machine learning techniques, such as Bayesian optimisation, have been adopted in the design and optimisation phase, albeit to a limited level.

As research and development progressed, the performance of existing compressor technologies has been improved, and many innovative designs with significant potential for further performance improvements have been conceptualised and even commercialised. However, more studies are still needed for the current challenging issues; these are also the directions of research on positive displacement compressors in the future.

1.4. Structure of the thesis

The thesis presented here endeavours to demonstrate a new positive displacement compressor technology via creating a multi-physical model which encompasses the various aspects encountered in the positive displacement domain; namely, kinematics, ther-

modynamics, fluid dynamics and vibration analysis. The resulting model will then be utilised to assess the suitability of the technology and identify the set of parameters which govern the performance of the investigated compressor. Consequently, an optimisation technique will be employed to estimate the best values of these parameters which ensure optimum performance for given operating conditions.

The thesis consists of five chapters and its structure is outlined as follows. Chapter 1 starts with the introduction of the background information and motivations of the project, which also establishes the research objectives and presents a review of the relevant literature. In Chapter 2, the mathematical model of the proposed limaçon rotary compressor is formulated, and the effect of various operating parameters on the compressor performance is investigated. Chapter 3 presents an optimisation process based on the Bayesian optimisation method to optimise the geometrical parameters and port locations for the best volumetric and thermodynamic performance. Chapter 4 investigates the effect of the apex seal vibration on the performance of two embodiments, i.e., circolimaçon and limaçon-to-limaçon. This chapter also details a comparative study discussing the viability of the circolimaçon embodiment. Finally, the findings produced by this research project and recommendations for future works on the limaçon rotary compressor are presented in Chapter 5.

1.5. References

Stouffs, P., Tazerout, M., & Wauters, P. (2001). Thermodynamic analysis of reciprocating compressors. *International Journal of Thermal Sciences, 40*(1), 52-66.

Sultan, I. A., & Phung, T. H. (Eds.). (2019). Positive Displacement Machines: Modern Design Innovations and Tools. Academic Press.

Spark, I. J., & Lu, K. (2019). The orbital displacer: Implications and applications. In I. A. Sultan & T. H. Phung (Eds.), *Positive Displacement Machines* (pp. 3-34): Academic Press.

Li, J., Jia, X., Wu, Z., & Peng, X. (2014). The cavity profile of a diaphragm compressor for a hydrogen refueling station. *International journal of hydrogen energy*, *39*(8), 3926-3935.

Liang, K. (2017). A review of linear compressors for refrigeration. *International Journal of Refrigeration*, *84*, 253-273.

Yanagisawa, T., Shimizu, T., Chu, I., & Ishijima, K. (1982). Motion analysis of rolling piston in rotary compressor. In *International Compressor Engineering Conference*; Purdue e-Pubs: West Lafayette, IN, USA.

Stosic, N., Smith, I. K., & Kovacevic, A. (2011). Numerical and experimental research in heat transfer to screw compressor rotors. In *ASME/JSME Thermal Engineering Joint Conference* (Vol. 38921, p. T20050).

Chen, Y., Halm, N. P., Groll, E. A., & Braun, J. E. (2002). Mathematical modeling of scroll compressors—part I: compression process modeling. *International Journal of Refrigeration*, *25*(6), 731-750.

Prescient & Strategic Intelligence. (2020). *Compressor market research report (2020-2030).* Retrieved from https://www.psmarketresearch.com/market-analysis/compressor-market

Silva, W. L. V., Souza, L. C. O., Bortolaia, L. A., Paula, M. R. D., & Leal, E. M. (2017). Study of the electricity consumption reduction of a compressed air system: the case of a steelmaking company. *REM-International Engineering Journal*, *70*(4), 421-428.

Vittorini, D., & Cipollone, R. (2016). Energy saving potential in existing industrial compressors. *Energy*, *102*, 502-515.

Saidur, R., Rahim, N. A., & Hasanuzzaman, M. (2010). A review on compressed-air energy use and energy savings. *Renewable and sustainable energy reviews*, *14*(4), 1135-1153.

Sultan, I. A. (2005). The limaçon of Pascal: mechanical generation and utilization for fluid processing. *Proceedings of the Institution of Mechanical Engineers, Part C: Journal of Mechanical Engineering Science*, *219*(8), 813-822.

Heidari, M., Mortazavi, M., & Rufer, A. (2017). Design, modeling and experimental validation of a novel finned reciprocating compressor for Isothermal Compressed Air Energy Storage applications. *Energy*, *140*, 1252-1266.

Hu, Y. S., Wei, H. J., Xu, J., Du, Z. C., Yang, S., & Ren, L. P. (2019). The Theoretical and Experimental Research of a Novel Rotary Cylinder Compressor. In *IOP Conference Series: Materials Science and Engineering* (Vol. 604, No. 1, p. 012073). IOP Publishing.

Shin, M., Na, S., Lee, J., Min, B., & Choi, G. (2019). Model analysis of a novel compressor with a dual chamber for high-efficiency systems. *Applied Thermal Engineering*, *158*, 113717.

Shakya, P., & Ooi, K. T. (2020). Introduction to Coupled Vane compressor: Mathematical modelling with validation. *International Journal of Refrigeration*, *117*, 23-32.

Gao, X., & Liu, Y. (2021). Design, modeling and characteristics research of a novel self-air-cooling reciprocating compressor. *International Journal of Refrigeration*, *128*, 62-70.

Lu, K., Sultan, I. A., & Phung, T. H. (2021). Mathematical modeling and parametric study of the limaçon rotary compressor. *International Journal of Refrigeration*.

Ueno, K., Bye, R.E., Hunter, K.S. (2003) *Compressor Efficiency Definitions*. Retrieved from http://vairex.com/resources/VAIREX_Compressor_Efficiency_Def_12May03.pdf

Cho, N. K., Youn, Y., Lee, B. C., & Min, M. K. (2000). The characteristics of tangential leakage in scroll compressors for air-conditioners. In *International Compressor Engineering Conference*; Purdue e-Pubs: West Lafayette, IN, USA.

Yuan, X., Chen, Z., & Fan, Z. (1992). Calculating model and experimental investigation of gas leakage. In *International Compressor Engineering Conference*; Purdue e-Pubs: West Lafayette, IN, USA.

Kim, G., Min, B., Na, S., Choi, G., & Kim, D. (2017). Estimation of leakage through radial clearance during compression process of a rolling piston rotary compressor. *Journal of Mechanical Science and Technology*, *31*(12), 6033-6040.

Pereira, E. L., & Deschamps, C. J. (2020). Numerical analysis and correlations for radial and tangential leakage of gas in scroll compressors. *International Journal of Refrigeration*, *110*, 239-247.

Yanagisawa, T., & Shimizu, T. (1985a). Leakage losses with a rolling piston type rotary compressor. I. Radical clearance on the rolling piston. *International Journal of Refrigeration*, 8(2), 75-84.

Yanagisawa, T., & Shimizu, T. (1985b). Leakage losses with a rolling piston type rotary compressor. II. Leakage losses through clearances on rolling piston faces. *International journal of refrigeration*, 8(3), 152-158.

Rodgers, R. J., & Nieter, J. J. (1996). Comprehensive analysis of leakage in rotary compressors. In *International Compressor Engineering Conference*; Purdue e-Pubs: West Lafayette, IN, USA.

Kang, D. J., Kim, J. W., & Sohn, C. B. (2002). Effects of leakage flow model on the thermodynamic performance of a scroll compressor. In *International Compressor Engineering Conference*; Purdue e-Pubs: West Lafayette, IN, USA.

Teh, Y. L., & Ooi, K. T. (2009). Theoretical study of a novel refrigeration compressor-Part III: Leakage loss of the revolving vane (RV) compressor and a comparison with that of the rolling piston type. *International journal of refrigeration*, *32*(5), 945-952.

Silva, L. R., & Deschamps, C. J. (2015). Modeling of gas leakage through compressor valves. *International journal of refrigeration*, *53*, 195-205.

AW, K. T., & Ooi, K. T. (2020). Leakage study of a Lubricant-free Revolving Vane Compressor. *International Journal of Refrigeration*. doi: https://doi.org/10.1016/j.ijrefrig.2020.12.017

Ferreira, R. T. S., & Lilie, D. E. B. (1984). Evaluation of the leakage through the clearance between piston and cylinder in hermetic compressors. In *International Compressor Engineering Conference*; Purdue e-Pubs: West Lafayette, IN, USA.

Ishii, N., Bird, K., Sano, K., Oono, M., Iwamura, S., & Otokura, T. (1996). Refrigerant leakage flow evaluation for scroll compressors. In *International Compressor Engineering Conference*; Purdue e-Pubs: West Lafayette, IN, USA.

Lohn, S. K., & Pereira, E. L. L. (2014). Numerical investigation of the gas leakage through the piston-cylinder clearance of reciprocating compressors. In *International Compressor Engineering Conference*; Purdue e-Pubs: West Lafayette, IN, USA.

Annand, W. J. D., & Thermodynamics and Fluid Mechanics Group (1963). Heat transfer in the cylinders of reciprocating internal combustion engines. *Proceedings of the Institution of Mechanical Engineers*, *177*(1), 973-996.

Adair, R. P., Qvale, E. B., & Pearson, J. T. (1972). Instantaneous heat transfer to the cylinder wall in reciprocating compressors. In *International Compressor Engineering Conference*; Purdue e-Pubs: West Lafayette, IN, USA.

Liu, R., & Zhou, Z. (1984). Heat transfer between gas and cylinder wall of refrigerating reciprocating compressor. In *International Compressor Engineering Conference*; Purdue e-Pubs: West Lafayette, IN, USA.

Tan, K. M., & Ooi, K. T. (2011). Heat transfer in compression chamber of a revolving vane (RV) compressor. *Applied thermal engineering*, *31*(8-9), 1519-1526.

Hsieh, W. H., & Wu, T. T. (1996). Experimental investigation of heat transfer in a high-pressure reciprocating gas compressor. *Experimental thermal and fluid science*, *13*(1), 44-54.

Disconzi, F. P., Deschamps, C. J., & Pereira, E. L. (2012). Development of an in-cylinder heat transfer correlation for reciprocating compressors. In *International Compressor Engineering Conference*; Purdue e-Pubs: West Lafayette, IN, USA.

Ooi, K. T., & Zhu, J. (2004). Convective heat transfer in a scroll compressor chamber: a 2-D simulation. *International Journal of Thermal Sciences*, *43*(7), 677-688.

Jang, K., & Jeong, S. (2006). Experimental investigation on convective heat transfer mechanism in a scroll compressor. *International Journal of Refrigeration*, *29*(5), 744-753.

Rak, J., & Pietrowicz, S. (2020). Internal flow field and heat transfer investigation inside the working chamber of a scroll compressor. *Energy*, *202*, 117700.

Padhy, S. K., & Dwivedi, S. N. (1994). Heat transfer analysis of a rolling-piston rotary compressor. *International journal of refrigeration*, *17*(6), 400-410.

Ooi, K. T. (2003). Heat transfer study of a hermetic refrigeration compressor. *Applied thermal engineering*, *23*(15), 1931-1945.

Sanvezzo Jr, J., & Deschamps, C. J. (2012). A heat transfer model combining differential and integral formulations for thermal analysis of reciprocating compressors. In *International Compressor Engineering Conference*; Purdue e-Pubs: West Lafayette, IN, USA.

Dutra, T., & Deschamps, C. J. (2013). Experimental characterization of heat transfer in the components of a small hermetic reciprocating compressor. *Applied thermal engineering*, *58*(1-2), 499-510.

Patil, V. C., Acharya, P., & Ro, P. I. (2019). Experimental investigation of heat transfer in liquid piston compressor. *Applied Thermal Engineering*, *146*, 169-179.

Stosic, N. (2015). On heat transfer in screw compressors. *International journal of heat and fluid flow*, *51*, 285-297.

Yanagisawa, T., & Shimizu, T. (1985c). Friction losses in rolling piston type rotary compressors. III. *International journal of refrigeration*, *8*(3), 159-165.

Ooi, K. T. (2005). Design optimization of a rolling piston compressor for refrigerators. *Applied thermal engineering*, *25*(5-6), 813-829.

Teh, Y. L., & Ooi, K. T. (2009b). Theoretical study of a novel refrigeration compressor–Part I: Design of the revolving vane (RV) compressor and its frictional losses. *International journal of refrigeration*, *32*(5), 1092-1102.

Liu, Y., Hung, C., & Chang, Y. (2010). Design optimization of scroll compressor applied for frictional losses evaluation. *International journal of refrigeration*, *33*(3), 615-624.

Yang, B., Bradshaw, C. R., & Groll, E. A. (2013). Modeling of a semi-hermetic CO2 reciprocating compressor including lubrication submodels for piston rings and bearings. *International journal of refrigeration*, *36*(7), 1925-1937.

Bianchi, G., & Cipollone, R. (2015). Friction power modeling and measurements in sliding vane rotary compressors. *Applied Thermal Engineering*, *84*, 276-285.

Gu, H., Zhou, X., Chen, Y., Wu, J., Wu, Z., Jiang, Y., & Sundén, B. (2021). Analysis, modeling and simulations of an innovative sliding vane rotary compressor with a rotating cylinder. *Energy Conversion and Management*, *230*, 113822.

Kim, H. J., & Lancey, T. W. (2003). Numerical study on the lubrication oil distribution in a refrigeration rotary compressor. *International journal of refrigeration*, *26*(7), 800-808.

Afshari, F., Comakli, O., Lesani, A., & Karagoz, S. (2017). Characterization of lubricating oil effects on the performance of reciprocating compressors in air–water heat pumps. *International Journal of Refrigeration*, *74*, 505-516.

Wu, X., Xing, Z., He, Z., Wang, X., & Chen, W. (2017). Effects of lubricating oil on the performance of a semi-hermetic twin screw refrigeration compressor. *Applied thermal engineering*, *112*, 340-351.

Ozsipahi, M., Kose, H. A., Cadirci, S., Kerpicci, H., & Gunes, H. (2019). Experimental and numerical investigation of lubrication system for reciprocating compressor. *International Journal of Refrigeration*, *108*, 224-233.

Valenti, G., Colombo, L., Murgia, S., Lucchini, A., Sampietro, A., Capoferri, A., & Araneo, L. (2013). Thermal effect of lubricating oil in positive-displacement air compressors. *Applied Thermal Engineering*, *51*(1-2), 1055-1066.

Pizarro-Recabarren, R. A., & Barbosa, J. R. (2016). The effect of the lubricating oil on heat transfer in a hermetic reciprocating compressor. *Journal of the Brazilian Society of Mechanical Sciences and Engineering*, *38*(1), 189-208.

Nagata, S., Nozaki, T., & Akizawa, T. (2010). Analysis of dynamic behavior of suction valve using strain gauge in reciprocating compressor. In *International Compressor Engineering Conference*; Purdue e-Pubs: West Lafayette, IN, USA.

Ma, Y., He, Z., Peng, X., & Xing, Z. (2012). Experimental investigation of the discharge valve dynamics in a reciprocating compressor for trans-critical CO2 refrigeration cycle. *Applied Thermal Engineering*, *32*, 13-21.

Wang, Y., Xue, C., Feng, J., & Peng, X. (2013). Experimental investigation on valve impact velocity and inclining motion of a reciprocating compressor. *Applied Thermal Engineering*, *61*(2), 149-156.

Mu, G., Wang, F., Mi, X., & Gao, G. (2019). Dynamic modeling and analysis of compressor reed valve based on movement characteristics. *Applied Thermal Engineering*, *150*, 522-531.

Egger, A., Almbauer, R., Dür, L., Hopfgartner, J., & Lang, M. (2020). Multi-Response optimization applied to a mechanically assisted reed valve of a hermetic reciprocating compressor. *International Journal of Refrigeration*, *119*, 119-130.

Huang, B., & Xie, F. (2008). Dynamic analysis of the discharge valve of the rotary compressor. In *International Compressor Engineering Conference*; Purdue e-Pubs: West Lafayette, IN, USA.

Teh, Y. L., Ooi, K. T., & Djamari, D. W. (2009). Theoretical study of a novel refrigeration compressor–Part II: Performance of a rotating discharge valve in the revolving vane (RV) compressor. *International Journal of Refrigeration*, *32*(5), 1103-1111.

Yu, X., Ren, Y., Tan, Q., Lu, Z., Jia, X., & Wang, X. (2018). Study on the torsional movement of a reed valve in a rotary compressor. *Advances in Mechanical Engineering*, *10*(6), 1687814018778402.

Min, B., Na, S., Yang, J., & Choi, G. (2018). Geometric correlation of discharge coefficients for discharge valve system in rolling piston rotary compressor. *Journal of Mechanical Science and Technology*, *32*(8), 3943-3954.

Kim, H. J., Ahn, J. M., Hwang, S. W., & Kiem, M. K. (2004). Performance analysis of a twin rotary compressor. In *International Compressor Engineering Conference*; Purdue e-Pubs: West Lafayette, IN, USA.

Mujic, E., Kovacevic, A., Stosic, N., & Smith, I. K. (2008). The influence of port shape on gas pulsations in a screw compressor discharge chamber. *Proceedings of the Institution of Mechanical Engineers, Part E: Journal of Process Mechanical Engineering*, *222*(4), 211-223.

Sultan, I. A., & Schaller, C. G. (2011). Optimum positioning of ports in the limaçon gas expanders. *Journal of engineering for gas turbines and power*, *133*(10).

Lim, Y. D., Lin, M., & Ooi, K. T. (2017). Simulation study of multi-chamber rotary compressor. In *IOP Conference Series: Materials Science and Engineering* (Vol. 232, No. 1, p. 012064). IOP Publishing.

Zhao, R., Li, W., & Zhuge, W. (2020). Unsteady characteristic and flow mechanism of a scroll compressor with novel discharge port for electric vehicle air conditioning. *International Journal of Refrigeration*, *118*, 403-414.

Gu, H., Chen, Y., Wu, J., Jiang, Y., & Sundén, B. (2021). Impact of discharge port configurations on the performance of sliding vane rotary compressors with a rotating cylinder. *Applied Thermal Engineering*, *186*, 116526.

Hong, W., Jin, J., Wu, R., & Zhang, B. (2009). Theoretical analysis and realization of stepless capacity regulation for reciprocating compressors. *Proceedings of the Institution of Mechanical Engineers, Part E: Journal of Process Mechanical Engineering*, *223*(4), 205-213.

Tuymer, W. J. (1974). Stepless variable capacity control. In *International Compressor Engineering Conference*; Purdue e-Pubs: West Lafayette, IN, USA.

Bin, T., Yuanyang, Z., Liansheng, L., Guangbin, L., Le, W., Qichao, Y., Haiping, X., Feng, Z., & Wenhui, M. (2013). Thermal performance analysis of reciprocating compressor with stepless capacity control system. *Applied thermal engineering*, *54*(2), 380-386.

Wang, Y., Jiang, Z., Zhang, J., Zhou, C., & Liu, W. (2018). Performance analysis and optimization of reciprocating compressor with stepless capacity control system under variable load conditions. *International Journal of Refrigeration*, *94*, 174-185.

Jin, J., & Hong, W. (2012). Valve dynamic and thermal cycle model in stepless capacity regulation for reciprocating compressor. *Chinese journal of mechanical engineering*, *25*(6), 1151-1160.

Tang, B., Zhao, Y., Li, L., Wang, L., Liu, G., Yang, Q., Xu, H., Zhu, F., & Meng, W. (2014). Dynamic characteristics of suction valves for reciprocating compressor with stepless capacity control system. *Proceedings of the Institution of Mechanical Engineers, Part E: Journal of Process Mechanical Engineering*, *228*(2), 104-114.

Liu, G., Zhao, Y., Tang, B., & Li, L. (2016). Dynamic performance of suction valve in stepless capacity regulation system for large-scale reciprocating compressor. *Applied Thermal Engineering*, *96*, 167-177.

Jiang, Z., Zhou, C., Wang, Y., Zhang, J., Liu, W., & Sun, X. (2020). Optimization Design of Actuator Parameters in Multistage Reciprocating Compressor Stepless Capacity Control System Based on NSGA-II. *Mathematical Problems in Engineering*, *2020*.

Zhang, J., Zhou, C., Jiang, Z., Wang, Y., & Sun, X. (2020). Optimization Design of Actuator Parameters with Stepless Capacity Control System Considering the Effect of Backflow Clearance. *Applied Sciences*, *10*(8), 2703.

Sun, X., Zhang, J., Wang, Y., Wang, J., & Qi, Z. (2021). Optimization of capacity control of reciprocating compressor using multi-system coupling model. *Applied Thermal Engineering*, *195*, 117175.

Li, W. (2013). Simplified steady-state modeling for variable speed compressor. *Applied thermal engineering*, *50*(1), 318-326.

Qureshi, T. Q., & Tassou, S. A. (1996). Variable-speed capacity control in refrigeration systems. *Applied Thermal Engineering*, *16*(2), 103-113.

Aprea, C., Mastrullo, R., & Renno, C. (2006). Experimental analysis of the scroll compressor performances varying its speed. *Applied thermal engineering*, *26*(10), 983-992.

Wang, Z., Wang, Z., Wang, J., Jiang, W., & Feng, Q. (2017). Research of thermal dynamic characteristics for variable load single screw refrigeration compressor with different capacity control mechanism. *Applied Thermal Engineering*, *110*, 1172-1182.

Yaqub, M., & Zubair, S. M. (2000). Performance evaluation of hot-gas by-pass capacity control schemes for refrigeration and air-conditioning systems. *Energy*, *25*(6), 543-561.

Jeong, S. K., Lee, D. B., & Hong, K. H. (2014). Comparison of system performance on hot-gas bypass and variable speed compressor in an oil cooler for machine tools. *Journal of Mechanical Science and Technology*, *28*(2), 721-727.

Wang, B., Han, L., Shi, W., & Li, X. (2012). Modulation method of scroll compressor based on suction gas bypass. *Applied Thermal Engineering*, *37*, 183-189.

Hollingsworth, J., Phillippi, G., Hinchliff, M., Kulhanek, C., Rimpel, A. M., & Maywald, F. (2019). Reciprocating Compressors. In *Compression Machinery for Oil and Gas* (pp. 167-252). Gulf Professional Publishing.

Wang, L., Liu, G. B., Zhao, Y. Y., & Li, L. L. (2015). Performance comparison of capacity control methods for reciprocating compressors. In *IOP Conference Series: Materials Science and Engineering* (Vol. 90, No. 1, p. 012029). IOP Publishing.

Yaqub, M., & Zubair, S. M. (1996). Thermodynamic analysis of capacity-control schemes for refrigeration and air-conditioning systems. *Energy*, *21*(6), 463-472.

Holdack-Janssen, H., & Kruse, H. (1984). Continuous and discontinuous capacity control for high speed refrigeration compressors. In *International Compressor Engineering Conference*; Purdue e-Pubs: West Lafayette, IN, USA.

Ooi, K. T., & Wong, T. N. (1997). A computer simulation of a rotary compressor for household refrigerators. *Applied thermal engineering*, *17*(1), 65-78.

Sultan, I. A. (2007). A surrogate model for interference prevention in the limaçon-to-limaçon machines. *Engineering Computations*.

Jain, A. K., Mao, J., & Mohiuddin, K. M. (1996). Artificial neural networks: A tutorial. *Computer*, *29*(3), 31-44.

Sanaye, S., Dehghandokht, M., Mohammadbeigi, H., & Bahrami, S. (2011). Modeling of rotary vane compressor applying artificial neural network. *International journal of refrigeration*, *34*(3), 764-772.

Namdeo, R., Manepatil, S., & Saraswat, S. (2008). Detection of valve leakage in reciprocating compressor using artificial neural network (ANN). In International Compressor Engineering Conference; Purdue e-Pubs: West Lafayette, IN, USA.

Belman-Flores, J. M., Ledesma, S., Barroso-Maldonado, J. M., & Navarro-Esbrí, J. (2015). A comparison between the modeling of a reciprocating compressor using artificial neural network and physical model. *International Journal of Refrigeration*, *59*, 144-156.

Tian, Z., Gu, B., Yang, L., & Lu, Y. (2015). Hybrid ANN–PLS approach to scroll compressor thermodynamic performance prediction. *Applied Thermal Engineering*, *77*, 113-120.

Zendehboudi, A., Li, X., & Wang, B. (2017). Utilization of ANN and ANFIS models to predict variable speed scroll compressor with vapor injection. *International journal of refrigeration*, *74*, 475-487.

Whitley, D. (1994). A genetic algorithm tutorial. *Statistics and computing*, *4*(2), 65-85.

Huang, Y. M., & Tsay, S. N. (2009). Mechanical efficiency optimization of a sliding vane rotary compressor. *Journal of pressure vessel technology*, *131*(6).

Chen, Q. J., & Ooi, K. T. (2021). Geometric Optimisation of a Coupled Vane Compressor. In *IOP Conference Series: Materials Science and Engineering* (Vol. 1180, No. 1, p. 012028). IOP Publishing.

Silva, E., & Dutra, T. (2021). Piston trajectory optimization of a reciprocating compressor. *International Journal of Refrigeration*, *121*, 159-167.

Lu, K., Phung, T. H., & Sultan, I. A. (2021). On the Design of a Class of Rotary Compressors Using Bayesian Optimization. Machines, 9(10), 219.

Sultan, I. A., & Kalim, A. (2011). Improving reciprocating compressor performance using a hybrid two-level optimisation approach. *Engineering Computations*.

Phung, T. H., & Sultan, I. A. (2021). Geometric design of the limaçon-to-circular fluid processing machine. *Journal of Mechanical Design,* 143(10).

Qi, G., Zhu, Z., Erqinhu, K., Chen, Y., Chai, Y., & Sun, J. (2018). Fault-diagnosis for reciprocating compressors using big data and machine learning. *Simulation Modelling Practice and Theory*, 80, 104-127.

Lu, K., Sultan, I. A., & Phung, T. H. (2021). A study on the use of machine learning methods to improve reciprocating compressor reliability via torque tailoring. In *2021 International Conference on Maintenance and Intelligent Asset Management (ICMIAM)* (pp. 1-6). IEEE.

Ma, J., Ding, X., Horton, W. T., & Ziviani, D. (2020). Development of an automated compressor performance mapping using artificial neural network and multiple compressor technologies. *International Journal of Refrigeration*, *120*, 66-80.

AHRI (2020). *2020 Standard for Performance Rating of Positive Displacement Refrigerant compressors*.

Afshari, F., Comakli, O., Adiguzel, N., & Ghasemi Zavaragh, H. (2016). Influence of refrigerant properties and charge amount on performance of reciprocating compressor in air source heat pump. *J. Energy Eng*, *10*.

Karnaz, J., Seeton, C., & Dixon, L. (2017). Identifying lubricant options for compressor bearing designs. In *IOP Conference Series: Materials Science and Engineering* (Vol. 232, No. 1, p. 012092). IOP Pub

Chapter 2. Mathematical modelling and parametric study of the limaçon rotary compressor[‡]

2.1. Abstract

In this chapter, a class of rotary positive displacement compressors which is known as the limaçon compressor is introduced. The main feature of such a compressor is that profiles of its housing and rotor and the motion of its rotor are developed from a mathematical curve called the limaçon of Pascal. A mathematical model of the limaçon compressor, which incorporates the mass flow of the working fluid, the leakage loss, the dynamic response of the discharge valve, as well as the thermodynamic behaviours, is formulated, and the simulation of such a model has been performed to study the operational characteristics of the limaçon compressor. A parametric analysis is also conducted to investigate the effects of various parameters on compressor performance. Based on the results, it is found that the machine performance deteriorates as the operating speed increases despite an initial rise in the volumetric efficiency. Additionally, the isentropic efficiency appears insensitive to the change in the pressure ratio, whereas a negative effect on the volumetric efficiency is noticed when the pressure ratio is increased. The effect of the valve diameter on the over-compression loss has also been studied, and the result indicates that a smaller valve diameter leads to a higher level of fluid over-compression.

Keywords: Rotary compressor; Limaçon of Pascal; Positive displacement compressor; Compressor simulation; Isentropic efficiency; Volumetric efficiency.

[‡] This chapter has been published: Lu, K, Sultan, I. A., and Phung, T. H. (2022) "Mathematical modeling and parametric study of the limaçon rotary compressor," *International Journal of Refrigeration*, *134*, 219-231.https://doi.org/10.1016/j.ijrefrig.2021.11.014

2.2. Introduction

Rotary positive displacement compressors have become increasingly popular in many engineering applications such as in heating, ventilation, and air-conditioning. Compared to the reciprocating compressor, one noticeable advantage of rotary machines is the simple machine structure, making them more compact in size, lighter in weight, and allowing for a lower weight to displacement ratio (Spark and Lu, 2019).

Literature shows that research effort has been dedicated to investigating various types of rotary compressors. Some examples in the field of the rotary compressor are the works of Chen et al. (2002a; 2002b) and Cuevas et al. (2010), which presented detailed investigations on the performance of the scroll compressor with respect to various factors. Stosic et al. (2003) endeavoured to explore the suitable optimization procedure for a given application of the screw compressor. They discovered that the geometric and operating factors exhibit different levels of impact on the machine performance when changing the working condition. Teh and Ooi (2009) proposed a new design of the vane compressor by introducing a mechanism called the revolving vane, which can reduce the frictional loss by 20%. The understanding of the mechanical and thermodynamical characteristics of such a design is further elaborated by the work of Subiantoro and Ooi (2009; 2011; 2012a; 2012b). Zhang et al. (2014) carried out a study on the crankshaft dynamic behaviours of rolling piston compressors. They found that the transverse force exerted on the crankshaft and the wear-out of journal bearings can be reduced when the dynamic balance of the crankshaft maintains at 80%. It is worth noting that the current interest in research is given to such mature technologies as the vane compressor and the scroll compressor. Some of the promising concepts, for example, the limaçon technology, have yet received enough attention from either academia or the industrial communities.

The limaçon compressor utilizes a mathematical curve called the limaçon of Pascal. During the operation, the chord, $p_l p_t$, of length $2L_{cp}$, rotates about its midpoint, c, and sliding at the limaçon pole, o. Both points c and o fall on a stationary circle (i.e., the base circle) of radius r, as shown in Fig. 2-1(a). If introducing a stationary frame $X_o Y_o$ at the pole o, and a moving frame $X_c Y_c$ at c, the sliding distance L_{oc} of the chord, measured from o to c along the X_c-axis, can be expressed as a function of the rotor angular displacement θ, measured from X_o-axis to X_c-axis, as:

$$L_{oc} = 2r \sin\theta \tag{2-1}$$

The radial distance from the pole o to the apex of the chord can be given by adding L_{oc} to half of the chord length, L_{cp},

$$L_{op} = 2r \sin\theta + L_{cp} \tag{2-2}$$

The parametric form of the endpoint p_l can be expressed with respect to the stationary frame $X_o Y_o$ as:

$$\begin{cases} x_{p_l} = r \sin 2\theta + L_{cp} \cos\theta \\ y_{p_l} = r - r \cos 2\theta + L_{cp} \sin\theta \end{cases} \tag{2-3}$$

Subsequently, the machine housing can be generated in accordance with the curve produced by equation (2-3). It should be pointed out that the limaçon curve, in order to be applicable for fluid machinery, has to comply with the restraint of the limaçon aspect ratio, β,

$$0 < \beta = \frac{r}{L_{cp}} \leq 0.25 \tag{2-4}$$

This relationship ensures that points p_l and p_t will not fall inside the base circle, so it is possible to acquire a single-looped and dimple-free profile of the limaçon housing.

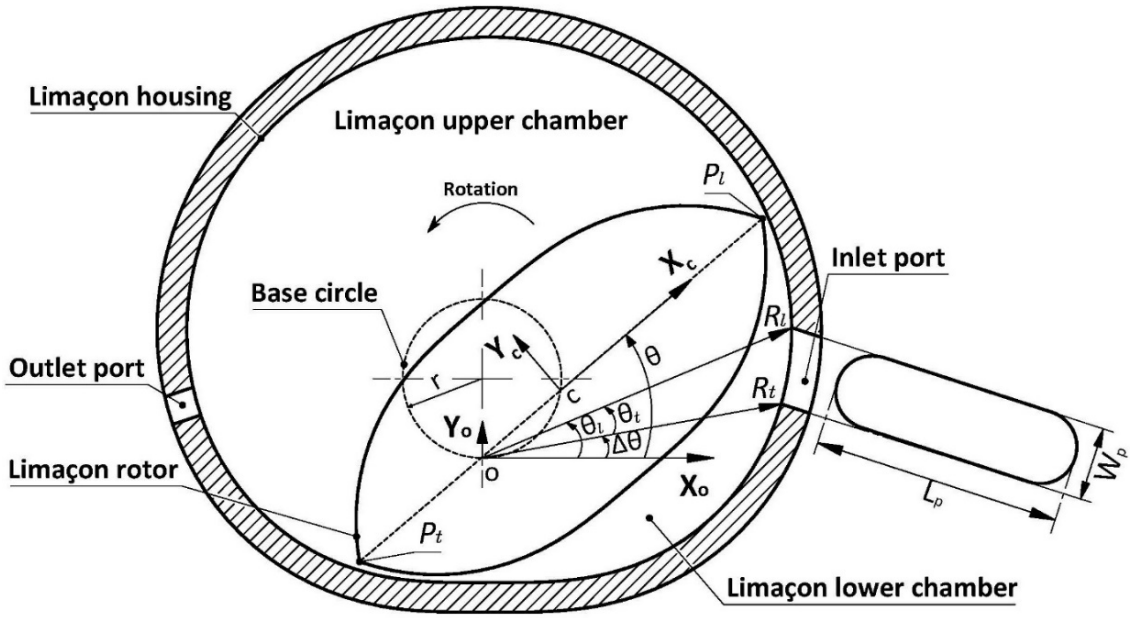

(a)

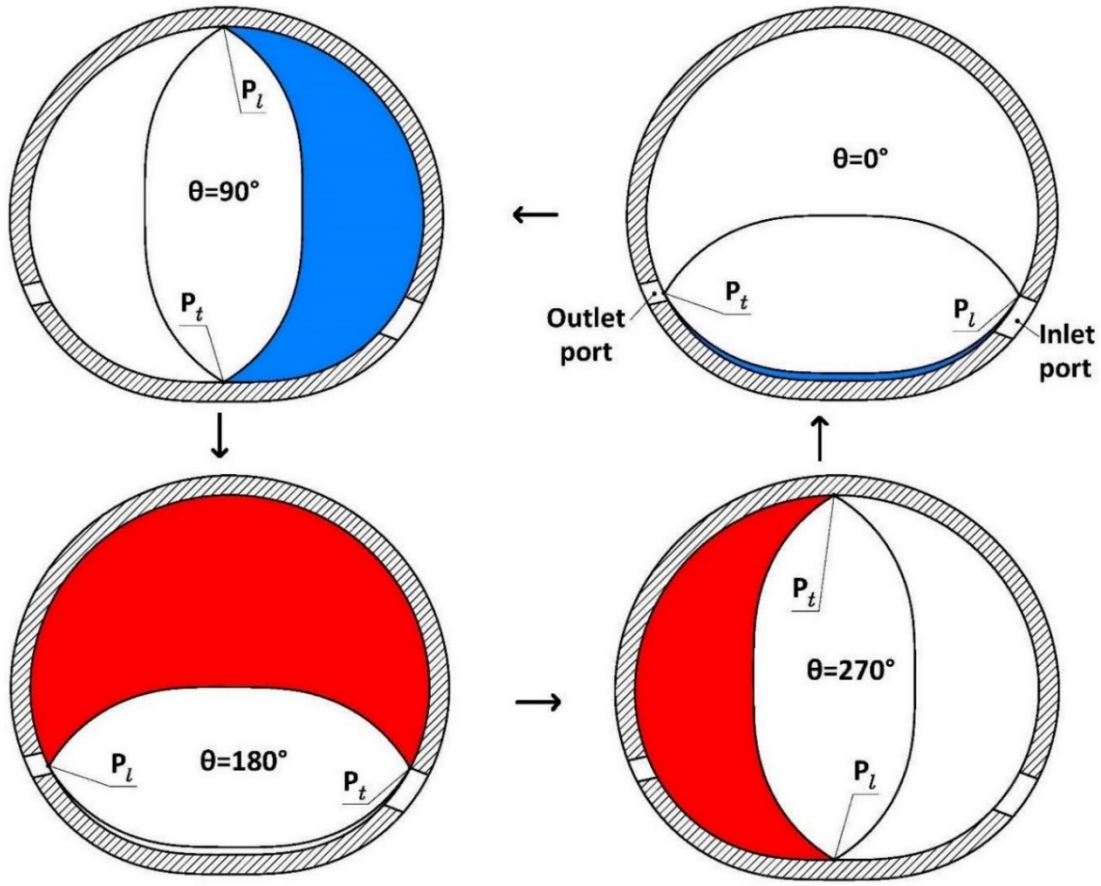

(b)

Fig. 2-1. (a) The limaçon compressor; (b) Illustration of the working process (suction is blue and discharge is red).

It is worth noting here that the housing and rotor share the same chord, resulting in the radial distance of half portion of the rotor, L_r, has an identical form as equation (2-2). However, interference between the housing and rotor occurs due to the same radial distance. This generally leads to a reduction in performance since severe frictional loss may take place during the operation. As such, an apex clearance, l_a, is introduced to equation (2-2) to produce the rotor radial distance with the form:

$$L_r = 2r_r \sin\theta + (L_{cp} - l_a) \tag{2-5}$$

where r_r is the radius of the rotor base circle.

The parametric form of the rotor with respect to the moving frame, X_cY_c, can then be expressed as:

$$\begin{cases} x_r = r_r \sin 2\theta + (L_{cp} - l_a)\cos\theta \\ y_r = r_r - r_r \cos 2\theta + (L_{cp} - l_a)\sin\theta \end{cases} \tag{2-6}$$

The limaçon concept has appeared in fluid machinery since Wheildon (1896) filed the patented design of a rotary engine. Unfortunately, none of those early designs was possible to be machined owing to the lack of adequate mathematical understanding of such technology as well as the limitation of manufacturing methods. In the past two decades, the work of Sultan (2005; 2006; 2007; 2008a; 2008b) has brought the limaçon technology back to the public attention and provided an understanding of the mathematical characteristic of the limaçon machine. The limaçon compressor possesses advantages such as being compact in size and light in weight. Additionally, the two-lobe design of the rotor implies the double-acting nature of the machine, and more importantly, the gap between the housing and rotor apices is constant, which enables a better sealing performance as shown by the work of Phung et al. (2018).

Literature shows that some attempts have been made to explore the gas expander based on the limaçon curve (Sultan and Schaller, 2011; Sultan, 2012; Phung et al., 2016; Phung and Sultan, 2018; Phung and Sultan, 2021). However, it also has been noticed that the application of the limaçon motion in positive displacement compressors has yet been investigated in the available papers, which is also the motivation of this study. In this chapter, a mathematical model is presented to describe the working of the limaçon positive displacement compressor. The computational software, MATLAB, and the database of fluid thermodynamic properties, REFPROP, are utilized to simulate the thermodynamic behaviour of the working fluid. The effects of operating factors on compressor performance are parametrically analysed based on the proposed thermodynamic model.

2.3. Mathematical models of the limaçon compressor

2.3.1. The kinematic model

Analogous to other positive displacement compressors, the volume of the working chamber of the limaçon compressor periodically changes with the angle rotated by the crankshaft. As can be seen in Fig. 2-1, the working chamber is geometrically separated into two portions by the rotor, namely the upper and lower chambers. When the rotor starts to rotate from the dead centre (i.e., $\theta = 0$), the upper chamber begins to contract to perform the compression process, and the lower chamber simultaneously expands to draw fluid from the intake port. The volume of the fluid that the machine processes, V_c, at any crank angle, θ, can be expressed in terms of the machine geometrical parameters as:

$$V_c = HL_{cp}^2\left[\pi\left(\beta^2 - \frac{r_r^2}{L_{cp}^2} + \frac{l_a}{L_{cp}}\left(1 - \frac{l_a}{2L_{cp}}\right)\right) - 4\beta\cos\theta + 4\frac{r_r}{L_{cp}}\left(1 - \frac{l_a}{L_{cp}}\right)\right] \tag{2-7}$$

where H is the axial length of the rotor measured perpendicular to the page. The rate of change of V_c with respect to the angular displacement is given by:

$$\frac{dV_c}{d\theta} = 4\beta L_{cp}^2 H \sin\theta \tag{2-8}$$

From equations (2-7) and (2-8), it is noticed that the size of the working chamber depends on the limaçon aspect ratio, β, when the machine size (as determined by H and L_{cp}) is determined. This is a distinguishing feature of the limaçon compressor as it allows the machine to achieve a larger capacity within a small machine size.

2.3.2. Mass flow rate through the port

2.3.2.1. Instantaneous area of the port

The mass flow rate through the port can be expressed as:

$$\dot{m}_p = \rho_p A_p u_p \tag{2-9}$$

where ρ_p, u_p, and A_p are the density and velocity of the fluid, and the instantaneous area of the port at the downstream side, respectively.

In equation (2-9), the port area can be determined based on the insightful work of Sultan and Schaller (2011). During the machine operation, the rotor leading apex, p_l, successively contacts the two edges of the port, which are called the leading edge and the trailing edge, respectively. The angular positions of the two edges are defined by two angles, θ_l and θ_t, that have a relationship shown in equation (2-10):

$$\theta_t = \theta_l + \Delta\theta \tag{2-10}$$

where $\Delta\theta$ is the angular width of the port. The radial position of these edges is described by using two position vectors, R_l and R_t:

$$\begin{cases} R_l = L_{cp}(2\beta \sin\theta_l + 1)\hat{R}_l \\ R_t = L_{cp}(2\beta \sin\theta_t + 1)\hat{R}_t \end{cases} \tag{2-11}$$

where $\hat{R}_l = \begin{bmatrix} \cos\theta_l \\ \sin\theta_l \\ 0 \end{bmatrix}$ and $\hat{R}_t = \begin{bmatrix} \cos\theta_t \\ \sin\theta_t \\ 0 \end{bmatrix}$ are the unit vectors. The port width, W_p, can then be calculated from the edge vectors of the port as follows:

$$W_p = |R_t - R_l| \tag{2-12}$$

To calculate the full port area, A_f, both the inlet and outlet ports are assumed to be a semi-circular shape as illustrated in Fig. 2-1, thus obtaining the expression as follows:

$$A_f = L_p W_p - W_p^2 \left(1 - \frac{\pi}{4}\right) \tag{2-13}$$

where L_p is the length of the port, and it satisfies the constraint, in which $L_p < H$.

It should be pointed out that the port areas, that are exposed to the working chambers, vary during the suction and discharge processes due to the relative position between the rotor and the port edges. To calculate the instantaneous area opening for the control volume, the position of the rotor leading and trailing apices with respect to the port edges are defined by employing the vector U_l and U_t, respectively:

$$\begin{cases} U_l = L_{cp}(2\beta \sin\theta + 1)\hat{X}_c \\ U_t = L_{cp}(2\beta \sin\theta - 1)\hat{X}_c \end{cases} \tag{2-14}$$

where $\hat{X}_c = \begin{bmatrix} \cos\theta \\ \sin\theta \\ 0 \end{bmatrix}$ is the unit vector of the X_c-axis. The relative positions of the rotor leading apices with respect to the port edges are given by two scalar quantities, S_l and S_t, shown in equation (2-15) as follows:

$$\begin{cases} S_l = (\hat{R}_l \times \hat{X}_c) \cdot (\hat{X}_c \times \hat{Y}_c) \\ S_t = (\hat{R}_t \times \hat{X}_c) \cdot (\hat{X}_c \times \hat{Y}_c) \end{cases} \tag{2-15}$$

where $\hat{Y}_c = \begin{bmatrix} -\sin\theta \\ \cos\theta \\ 0 \end{bmatrix}$ is the unit vector of the Y_c-axis. Subsequently, A_p can be determined in accordance with one of the four following cases of S_l and S_t:

a) $S_l \geq 0$ and $S_t \geq 0$, which indicates that the port is fully open to allow fluid to flow into the working chamber. In this case, A_p can be conveniently set equal to A_f.

b) $S_l \geq 0$ and $S_t < 0$, which indicates that the leading apex of the rotor is passing the port. In this case, the area of the port is obtained by the following equation:

$$A_p = \frac{W_{ins}}{W_p} A_f \tag{2-16}$$

where W_{ins} is the instantaneous port width and it is given by:

$$W_{ins} = |U_l - R_t| \tag{2-17}$$

c) $S_l < 0$ and $S_t \geq 0$, which indicates that the trailing apex of the rotor is passing the port. In this case, the area of the port is obtained by the following equation:

$$A_p = \frac{W_{ins}}{W_p} A_f \tag{2-18}$$

where W_{ins} in this case is given by:

$$W_{ins} = |U_t - R_t| \tag{2-19}$$

d) $S_l < 0$ and $S_t < 0$, which indicates that the port is fully shut off from the working chamber. Hence, A_p is set equal to 0.

2.3.2.2. Velocity of the fluid flowing through the port

For the limaçon compressor, fluid flow through the ports possesses similar characteristics to the flow through a globe valve, in which the change of flow direction occurs. Therefore, Sultan (2012) suggests considering the ports of a limaçon machine as globe valves instead of orifice plates. In this regard, the limaçon compressor investigated in this paper will adopt the same concept to simulate the fluid flow through the ports.

Generally, the flow velocity will be increased as a result of energy conversion when the fluid passes through the port. For compressible flow, the theoretical flow velocity at the downstream side of the port is obtained as follows:

$$u = \sqrt{2\Delta h} \tag{2-20}$$

where Δh is the isentropic enthalpy drop from the upstream to the downstream of the port. In actual workings, the effect of frictional loss and port area variations cannot be ignored during such an energy conversion. Hence, a loss coefficient, $K = \lambda f$, proposed by Massoud (2005) is introduced into equation (2-21):

$$u = \sqrt{\frac{2\Delta h}{\lambda f}} \tag{2-21}$$

where λ is a specific number assigned to each type of flow and f is the friction factor for turbulent flow. Massoud (2005) suggests that the friction factor can be expressed as a function of Reynolds number, $Re = \frac{\rho D u}{\mu}$, by using the McAdams formula:

$$f = \frac{0.184}{Re^{0.2}} = \frac{0.184}{\left(\frac{\rho D u}{\mu}\right)^{0.2}} \tag{2-22}$$

Combining equations (2-21) and (2-22), the flow velocity, u_p, at the downstream side of the port can then be expressed as follows:

$$u_p = \begin{cases} \left(\left(\frac{\rho_p D_p}{\mu_p}\right)^{\frac{1}{10}} \sqrt{\frac{2\Delta h}{0.184\lambda}}\right)^{\frac{10}{9}}, & if\ \sqrt{2\Delta h} < u_{ss} \\ \left(\frac{\rho_p D_p}{\mu_p}\right)^{\frac{1}{10}} \frac{u_{ss}^{1.1}}{\sqrt{0.184\lambda}}, & if\ \sqrt{2\Delta h} \geq u_{ss} \end{cases} \tag{2-23}$$

where D_p and μ_p are the downstream hydraulic diameter and viscosity, respectively, and u_{ss} is the speed of sound at the downstream side of the port.

Equation (2-23) can handle the fluid flow for both single-phase and two-phase situations. For the two-phase case, the viscosity term, μ_p, is gained by using the McAdams formula:

$$\frac{1}{\mu_p} = \frac{x}{\mu_g} + \frac{1-x}{\mu_{liq}} \tag{2-24}$$

where μ_g and μ_{liq} are the viscosities of the fluid in vapour and liquid phases, respectively, and x is the dryness fraction.

2.3.3. Mass flow rate through the discharge valve

For a compressor without a valve, the discharged fluid with high pressure may flow back to the chamber if the pressure at the discharge manifold is greater, thereby raising chamber pressure and more shaft work is required. To manipulate the fluid discharging out of the chamber, the limaçon compressor investigated in the present study equips a spring-loaded discharge valve whose structure is shown in Fig. 2-2. It is worth mentioning that a valve chamber with a volume of V_v lies between the discharge valve and the working chamber. The fluid, after being discharged from the outlet port, will need to fill this valve chamber before reaching the discharge valve. The thermodynamic behaviour of the fluid in the valve chamber shares the same principle as that of the working chamber, which is presented in the thermodynamic model section of this paper. The mass flow rate of the fluid being discharged through the valve, $\dot{m}_v$, is calculated by:

$$\dot{m}_v = \rho_v A_v u_v \tag{2-25}$$

where ρ_v is the density at the downstream side of the valve, u_v is the velocity of the fluid through the valve, which can be obtained by using the equation (2-20) to (2-24), and A_v is the effective area which available for fluid flowing through the valve and it is calculated from the expression suggested by Tuymer and Machu (2001):

$$A_v = \frac{1}{\sqrt{\left(\frac{1}{0.85\pi D_{vp}(z - z_{min})}\right)^2 + \left(\frac{1}{A_{vp}}\right)^2}} \tag{2-26}$$

where D_{vp} and A_{vp} are the effective diameter and effective area of the valve plate, respectively, and z and z_{min} are respectively the instantaneous and the initial displacements of the spring connected to the valve plate, which is obtained from the dynamic

model of the discharge valve. An illustration of the discharge vale section view is shown in Fig. 2-2 below.

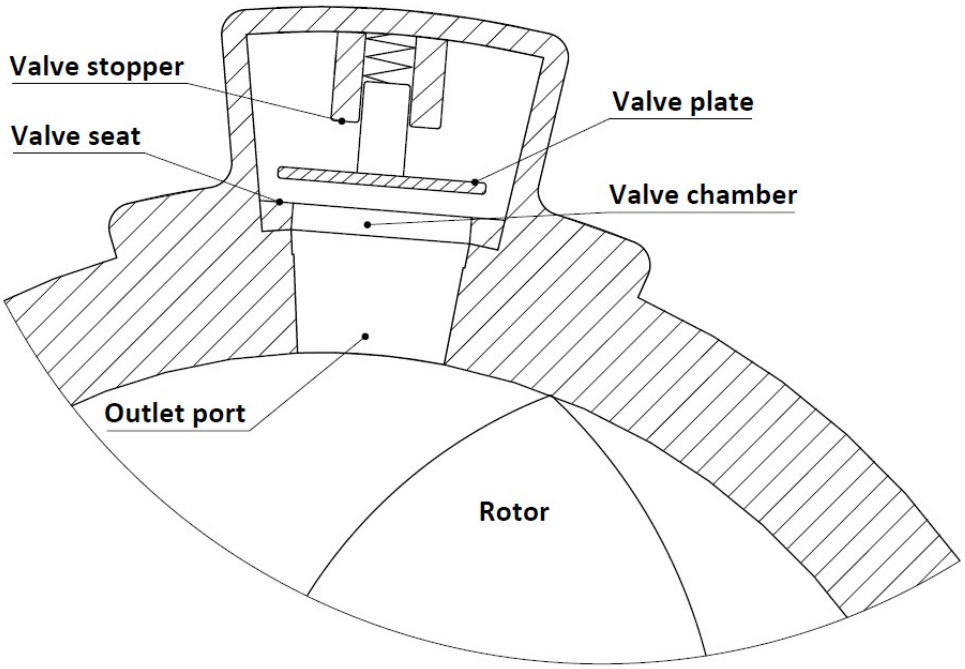

Fig. 2-2. Sectional view of the discharge valve.

2.3.3.1. Dynamic model of the discharge valve

The discharge valve is modelled as a simple spring-mass-damper system, as shown in Fig. 2-3. The equation of motion of the valve plate can be derived based on Newton's second law:

$$m_v \frac{d^2 z}{dt^2} = F - F_v \tag{2-27}$$

where m_v is the mass of the valve plate, t is time. Knowing that $t = \frac{\theta}{\omega}$, where ω is the angular speed of the rotor, so equation (2-27) can be rewritten as:

$$m_v \frac{d^2 z}{d\theta^2} = \frac{F - F_v}{\omega^2} \tag{2-28}$$

In the above equation, F is the force due to the pressure difference between the two sides of the valve, which is expressed as:

$$F = C_d A_{vp}(P_o - P_d) \tag{2-29}$$

where C_d is the drag coefficient, P_o and P_d are the pressures in the outlet port and discharge manifold, respectively.

The resistance force, F_v, provided by the spring-damper system (including springs and dampers of the valve, the valve seat, and the stopper) is calculated in accordance with the valve instantaneous displacement as follows:

$$F_v = \begin{cases} \omega(C_v + C_{se})\dfrac{dz}{d\theta} + (k_v + k_{se})z - k_{se}z_{min}, & z < z_{min} \\ \omega C_v \dfrac{dz}{d\theta} + k_v z, & z_{min} < z < z_{max} \\ \omega(C_v + C_{st})\dfrac{dz}{d\theta} + (k_v + k_{st})z - k_{st}z_{max}, & z < z_{max} \end{cases} \tag{2-30}$$

where C and k denote the damping coefficient and spring stiffness, respectively; the subscripts v, se and st represent the valve plate, the seat, and the stopper, respectively; and z_{max} is the maximum allowable displacement.

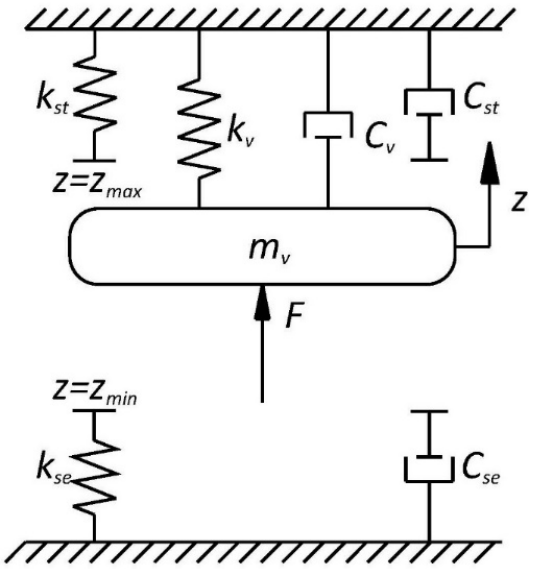

Fig. 2-3. Schematic view of the motion of the discharge valve.

2.3.4. The leakage model

For smooth operation of the compressor, it is necessary to introduce a reasonable clearance between the rotor and housing. However, leakage of the working fluid usually occurs because of the existence of this rotor-housing clearance and the side clearance. For the limaçon compressor, the majority of leakage occurs at the side and apex clearance due to the pressure difference. Hence, the total leakage mass flow rate, $\dot{m}_{le}$, considered in the current study is the sum of the side leakage, $\dot{m}_s$, and the apex leakage, $\dot{m}_a$:

$$\dot{m}_{le} = \dot{m}_s + \dot{m}_a \tag{2-31}$$

2.3.4.1. Leakage at the side clearance

The side clearance is referred to as the gap between the rotor side face and the side housing, as shown in Fig. 2-4(a). During the operation, the high pressure inside the working chambers pushes the fluid through the side clearance to the assembly cavity between the crankshaft and the rotor. In this study, the leakage flowing through the side clearance is treated as the flow through a port. Therefore, the velocity of leakage flow, u_s, can be obtained by using the equations (2-20) to (2-24), and the leakage mass flow rate, $\dot{m}_s$, is calculated as follows:

$$\dot{m}_s = \rho_s A_s u_s \tag{2-32}$$

where ρ_s is the downstream density, A_s is the side leakage flow area that is calculated from the half-length of the chord, L_{cp}, and the side clearance, l_s, as:

$$A_s = 4 l_s L_{cp} \tag{2-33}$$

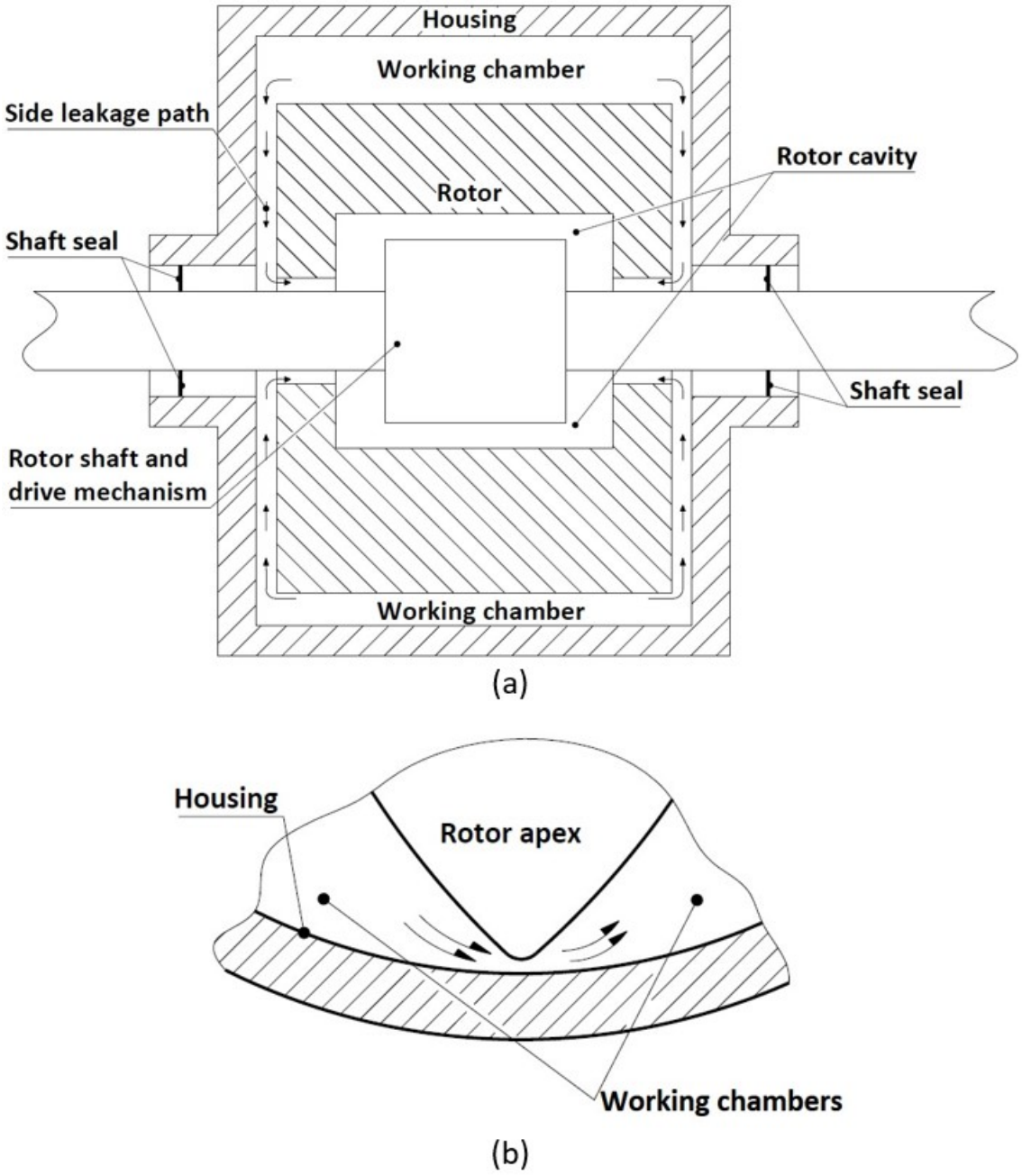

Fig. 2-4. Path of the leakage: (a) Side leakage. (b) Apex leakage.

2.3.4.2. Leakage at the apex clearance

At the apex clearance, the working fluid can flow from the high-pressure chamber to the low-pressure chamber through the gap between the rotor apex and the housing, as demonstrated in Fig. 2-4(b).

Geometrically, the gap is extremely small, which can be considered as a throat section that lies in the middle of the path; the leakage path at the apex clearance can be conveniently considered as a convergent-divergent nozzle. By assuming the fluid is an isentropic single-phase flow at this place, the leakage mass flow rate through the throat, $\dot{m}_a$, can then be calculated from the upstream pressure, P_{au}, and the downstream pressure, P_{ad}, as:

$$\dot{m}_a = \begin{cases} C_f A_a P_{au} \sqrt{\dfrac{2\gamma\rho_{au}}{(\gamma-1)P_{au}}\left[\left(\dfrac{P_{ad}}{P_{au}}\right)^{\frac{2}{\gamma}} - \left(\dfrac{P_{ad}}{P_{au}}\right)^{\frac{\gamma+1}{\gamma}}\right]}, & \dfrac{P_{ad}}{P_{au}} > \left(\dfrac{2}{\gamma+1}\right)^{\frac{\gamma}{\gamma-1}} \\ C_f A_a P_{au} \sqrt{\dfrac{\rho_{au}}{P_{au}}\left(\dfrac{2}{\gamma+1}\right)^{\frac{\gamma+1}{\gamma-1}}}, & \dfrac{P_{ad}}{P_{au}} < \left(\dfrac{2}{\gamma+1}\right)^{\frac{\gamma}{\gamma-1}} \end{cases} \tag{2-34}$$

where C_f is the flow coefficient, ρ_{au} is the upstream density at the throat, γ is the specific heat ratio, A_a is the leakage flow area at the apex clearance, which is calculated as:

$$A_a = 2l_a H \tag{2-35}$$

2.3.5. The thermodynamic model

2.3.5.1. The continuity equation

The mass processed by the limaçon compressor, m_c, complies with the conservation law can be expressed in the derivative form as follows:

$$\frac{dm_c}{d\theta} = \frac{1}{\omega}(\dot{m}_i - \dot{m}_o - \dot{m}_{le}) \tag{2-36}$$

where $\dot{m}_i$ and $\dot{m}_o$ are the mass flow rate through the compressor inlet and outlet ports obtained by referring to the procedure mentioned in the previous section.

Knowing that the continuity equation for the mass processed at the upper chamber, m_c^A, can be expressed as:

$$dm_c^A = d(\rho_c^A V_c^A) = \rho_c^A dV_c^A + V_c^A d\rho_c^A \tag{2-37}$$

where the superscript A denotes the limaçon upper chamber. After manipulating equations (2-36) and (2-37), the following expression may be obtained:

$$\frac{d\rho_c^A}{d\theta} = \frac{1}{V_c^A \omega}\left(\dot{m}_i^A - \dot{m}_o^A - \dot{m}_{le}^A - \rho_c^A \omega \frac{dV_c^A}{d\theta}\right) \tag{2-38}$$

Substituting equation (2-8) to equation (2-38) gives:

$$\frac{d\rho_c^A}{d\theta} = \frac{1}{V_c^A \omega}\left(\dot{m}_i^A - \dot{m}_o^A - \dot{m}_{le}^A - 4\rho_c^A \omega \beta L_{cp}^2 H \sin\theta\right) \tag{2-39}$$

Similarly, the continuity equation for the lower chamber can be expressed as follows:

$$\frac{d\rho_c^B}{d\theta} = \frac{1}{V_c^B \omega}\left(\dot{m}_i^B - \dot{m}_o^B - \dot{m}_{le}^B - 4\rho_c^B \omega \beta L_{cp}^2 H \sin\theta\right) \tag{2-40}$$

where the superscript B denotes the limaçon lower chamber.

2.3.5.2. The first law of thermodynamics

In this paper, the energy transfer from and to the working chamber is considered as an adiabatic process. Thus, the following equation can be yielded by applying the first law of thermodynamics:

$$h_i \frac{dm_i}{d\theta} + \frac{dw}{d\theta} = \frac{d(me)}{d\theta} + h_o \frac{dm_o}{d\theta} + h_{le} \frac{dm_{le}}{d\theta} \tag{2-41}$$

where h_i and h_o represent the enthalpy moving in and out of the working chamber respectively, h_{le} is the enthalpy at the upstream of the leakage flow, and e is the specific internal energy available in the working chamber. From the relationship of the enthalpy, the specific internal energy can be expressed as:

$$e = h_c - pv \tag{2-42}$$

where h_c is enthalpy inside the working chamber and

$$dh_c = Tds + vdp \tag{2-43}$$

Taking the work term, w, as the mechanical work which has the form:

$$dw = P_c dV_c \tag{2-44}$$

where P_c is pressure inside the working chamber.

Consequently, the change of entropy in the upper and lower working chambers can be respectively obtained by combining equations (2-41) to (2-44) as follows:

$$\frac{ds_c^A}{d\theta} = \frac{1}{\rho_c^A V_c^A T_c^A \omega}\left(\dot{m}_i^A(h_i - h_c^A) - \dot{m}_o^A(h_o - h_c^A) - \dot{m}_{le}^A(h_{le} - h_c^A) - 4\rho_c^A \omega \beta L_{cp}^2 H \sin\theta\right) \tag{2-45}$$

and

$$\frac{ds_c^B}{d\theta} = \frac{1}{\rho_c^B V_c^B T_c^B \omega}\left(\dot{m}_i^B(h_i - h_c^B) - \dot{m}_o^B(h_o - h_c^B) - \dot{m}_{le}^B(h_{le} - h_c^B) - 4\rho_c^B \omega \beta L_{cp}^2 H \sin\theta\right) \tag{2-46}$$

where T_c is the chamber temperature. The torque, τ, required by the compressor at any rotor angular displacement is calculated as follows:

$$\tau = (P_c^A - P_c^B)\frac{dV_c}{d\theta} = 4\beta L_{cp}^2 H(P_c^A - P_c^B)\sin\theta \tag{2-47}$$

2.3.5.3. Performance indices

The performance of positive displacement compressors is usually described by a series of indices. One of the most used indices is the isentropic efficiency which is defined in this paper as the ratio of the ideal work to the actual work; the isentropic efficiency can be written in terms of enthalpies, as shown in equation (2-48):

$$\eta_{isen} = \frac{(h_o - h_i)}{(h_{o,actual} - h_i)} \tag{2-48}$$

where $h_{o,actual}$ is the actual enthalpy at the discharge manifold.

For each compression process, the total torque may be obtained by adding up the instantaneous torque at each angle θ ranging from θ_{li} to $\theta_{li}+\pi$, where θ_{li} is the angular position of the inlet port leading edge. In that regard, the thermodynamic model needs to be calculated iteratively in order to compare the value of pressure and density at the start and end of each iteration, and this can be expressed by an error function as follows:

$$\sigma = \sqrt{\sigma_1 + \sigma_2 + \sigma_3 + \sigma_4} \tag{2-49}$$

where σ_1, σ_2, σ_3 and σ_4 are obtained as follows:

$$\sigma_1 = \left(\frac{2\left(P_c^A(\theta_{li}+\pi) - P_c^B(\theta)\right)}{P_c^A(\theta_{li}+\pi) + P_c^B(\theta)} \right)^2 \tag{2-50}$$

$$\sigma_2 = \left(\frac{2\left(P_c^B(\theta_{li}+\pi) - P_c^A(\theta)\right)}{P_c^B(\theta_{li}+\pi) + P_c^A(\theta)} \right)^2 \tag{2-51}$$

$$\sigma_3 = \left(\frac{2\left(\rho_c^A(\theta_{li}+\pi) - \rho_c^B(\theta)\right)}{\rho_c^A(\theta_{li}+\pi) + \rho_c^B(\theta)} \right)^2 \tag{2-52}$$

$$\sigma_4 = \left(\frac{2\left(\rho_c^B(\theta_{li}+\pi) - \rho_c^A(\theta)\right)}{\rho_c^B(\theta_{li}+\pi) + \rho_c^A(\theta)} \right)^2 \tag{2-53}$$

This error function, σ, will continue processing until its value falls within the acceptable range, which reflects the cyclical nature of the thermodynamic process. When such an objective is satisfied, the actual mass of fluid delivered per revolution, m_o, can be expressed as:

$$m_o = \frac{2\delta\theta}{\omega}\left(\sum_{n=1}^{N} (\dot{m}_o^A + \dot{m}_o^B)_n - \frac{(\dot{m}_o^A)_n - (\dot{m}_o^A)_1}{2} - \frac{(\dot{m}_o^B)_n - (\dot{m}_o^B)_1}{2} \right) \tag{2-54}$$

where $\delta\theta$ is the size of the angular interval, n is the successive point on the torque curve, and N is the total number of intervals.

The ideal mass drawn into the working chamber, m_{ideal}, is calculated as follows:

$$m_{ideal} = 2\rho_i V_{swept} \tag{2-55}$$

where ρ_i is the density of the fluid at the inlet port, and V_{swept} is the swept volume obtained by:

$$V_{swept} = V_c(\pi) - V_c(0) \tag{2-56}$$

It is worth noting that the multiplication of a factor of 2 appears in equations (2-54) and (2-55) due to the double-acting nature of the limaçon compressor. Consequently, the volumetric efficiency, η_{vol}, can be expressed as the ratio between m_o and m_{ideal} as shown in equation (2-57):

$$\eta_{vol} = \frac{m_o}{m_{ideal}} \tag{2-57}$$

2.4. Numerical illustration

In this section, a numerical simulation is carried out to illustrate the workings of the limaçon compressor. This simulation is based on the programming language of MATLAB and some of the machine dimensions are set as shown in Table 2-1. Air is selected as the working fluid and the needed state variables, such as entropies, are obtained by using the NIST REFPROP 10 database (Lemmon et al., 2010). The ambient temperature is assumed at $20°C$ and the inlet and discharge pressure are set as $P_i = 100\ kPa$ and $P_d = 300\ kPa$, respectively. The operating speed is assumed to be constant at $1000\ rpm$, and the volume of the valve chamber is set as $\frac{1}{3}$ of the maximum volume of the working chamber.

Table 2-1. Dimensions of the limaçon compressor

Geometric parameters	**Values**
Half-length of the rotor-chord, L_{cp}	$50\ mm$
Axial length of the rotor, H	$65\ mm$
Apex clearance, l_a	$0.1\ mm$
Side clearance, l_s	$0.01\ mm$
Aspect ratio, β	0.1

Table 2 1. Dimensions of the limaçon compressor (Continued)

Geometric parameters	Values
Leading edge of inlet port, θ_{li}	$0°$
Leading edge of outlet port, θ_{lo}	$180°$
Inlet angular width, $\Delta\theta_i$	$11°$
Outlet angular width, $\Delta\theta_o$	$10°$
Inlet port length, L_{pi}	$35\ mm$
Outlet port length, L_{po}	$25\ mm$
Effective diameter of the valve plate, D_{vp}	$20\ mm$
Effective mass of the valve plate, m_v	$0.04\ kg$
Volume of the valve chamber, V_v	$43.63\ cm^3$
Maximum volume per compression stroke, $V_{c,max}$	$130.89\ cm^3$

The friction between machine components is not discussed in the current study as rotor-housing clearance is applied in the simulation. The minimum chamber volume occurs at $\theta = 0°$, which is the rotor dead centre. According to Fig. 2-5, the maximum chamber volume is achieved when $\theta = 180°$, at which the working chamber pressure also starts to increase as shown in Fig. 2-6, signifying the beginning of the compression stroke. The working chamber is exposed to the outlet port when the rotor passes $\theta = 180°$, but it is noticed that the working chamber pressure is not higher than that of the valve chamber until the rotor reaches $\theta \approx 200°$. This leads to the compressed fluid left in the valve chamber from the previous stroke flowing back to the working chamber, and as a result, a sudden increase in fluid mass in the working chamber and a corresponding reduction in the valve chamber are observed in Fig. 2-8. As the rotor rotates to $\theta \approx 300°$, the discharge valve starts to open as illustrated in Fig. 2-7, indicating that the discharge stroke is initiated. When the rotor reaches $\theta = 360°$, a new suction stroke is started. However, the working chamber is exposed to both the inlet and outlet ports at this point, and this results in a

minor backflow of compressed fluid to the inlet port through the rotor-housing clearance. Fig. 2-9 and Fig. 2-10 show the required torque and the P-V diagram during one working cycle, respectively.

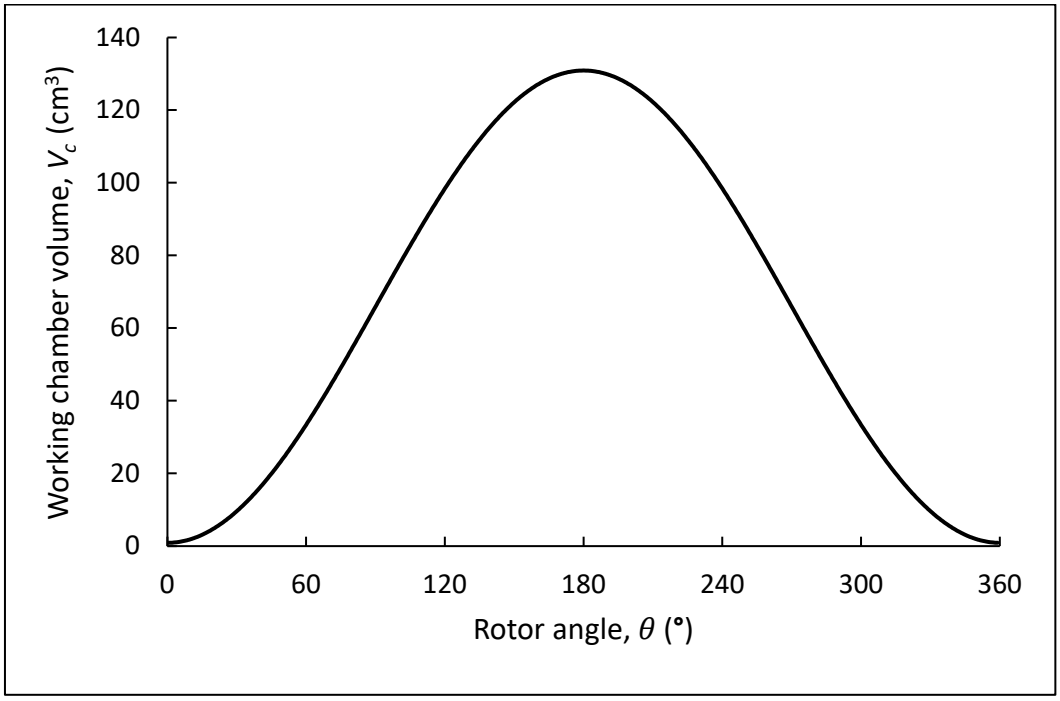

Fig. 2-5. Variation of the working chamber volume.

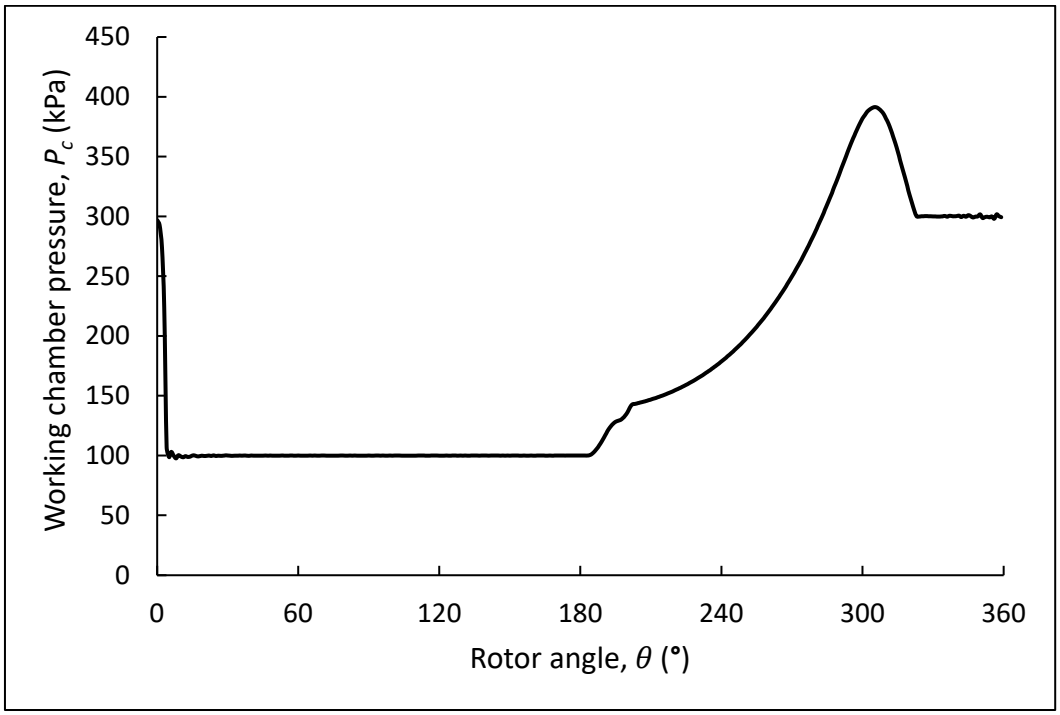

Fig. 2-6. Variation of chamber pressure.

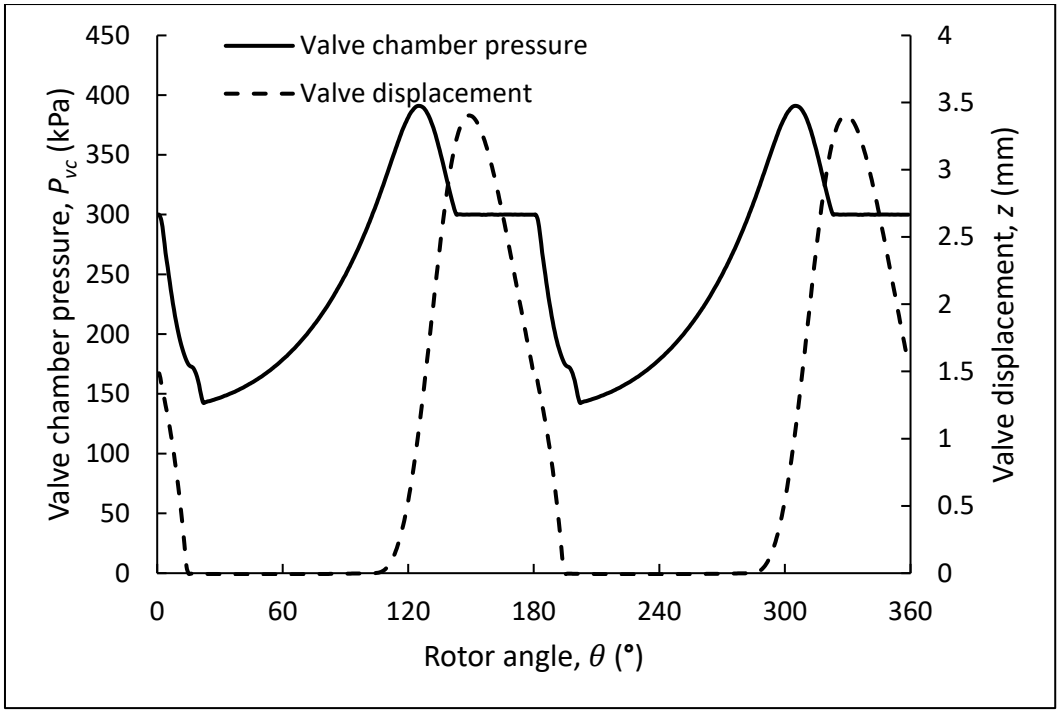

Fig. 2-7. Variation of valve chamber pressure and valve displacement.

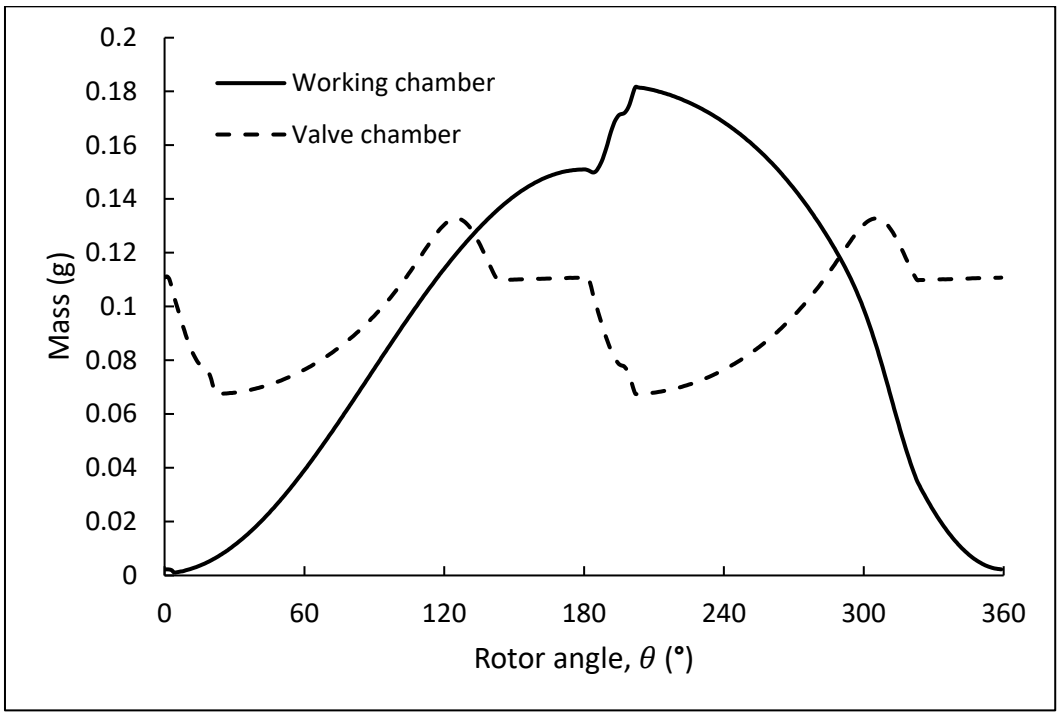

Fig. 2-8. Variation of the fluid mass in the working chamber, m_c, and valve chamber, m_{vc}.

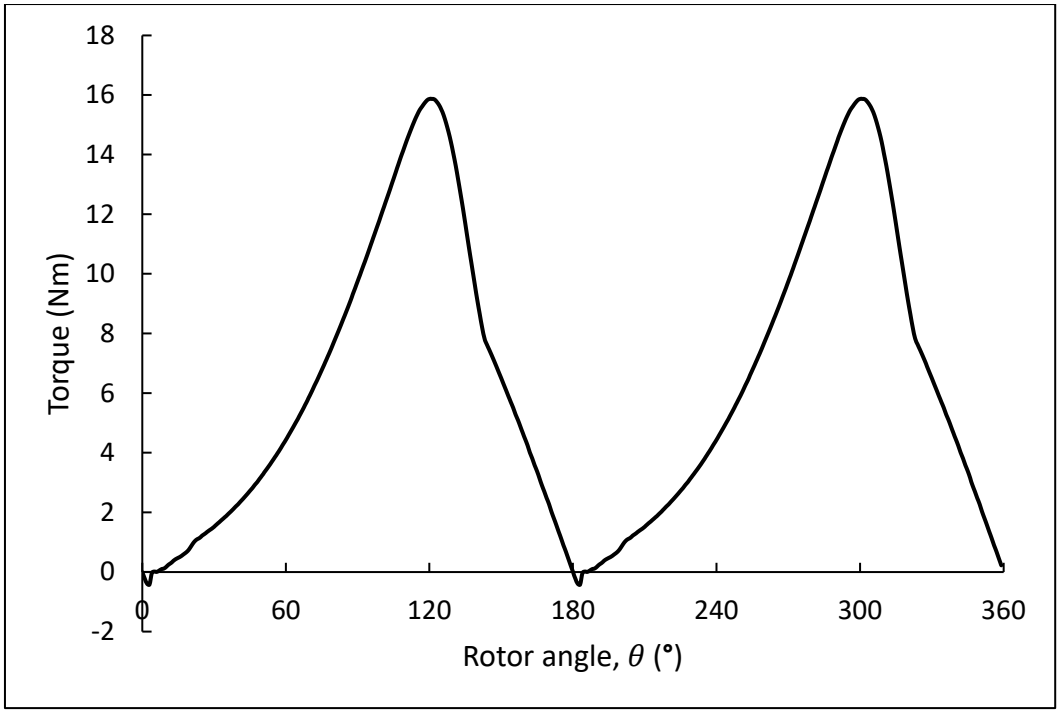

Fig. 2-9. Variation of the torque, τ.

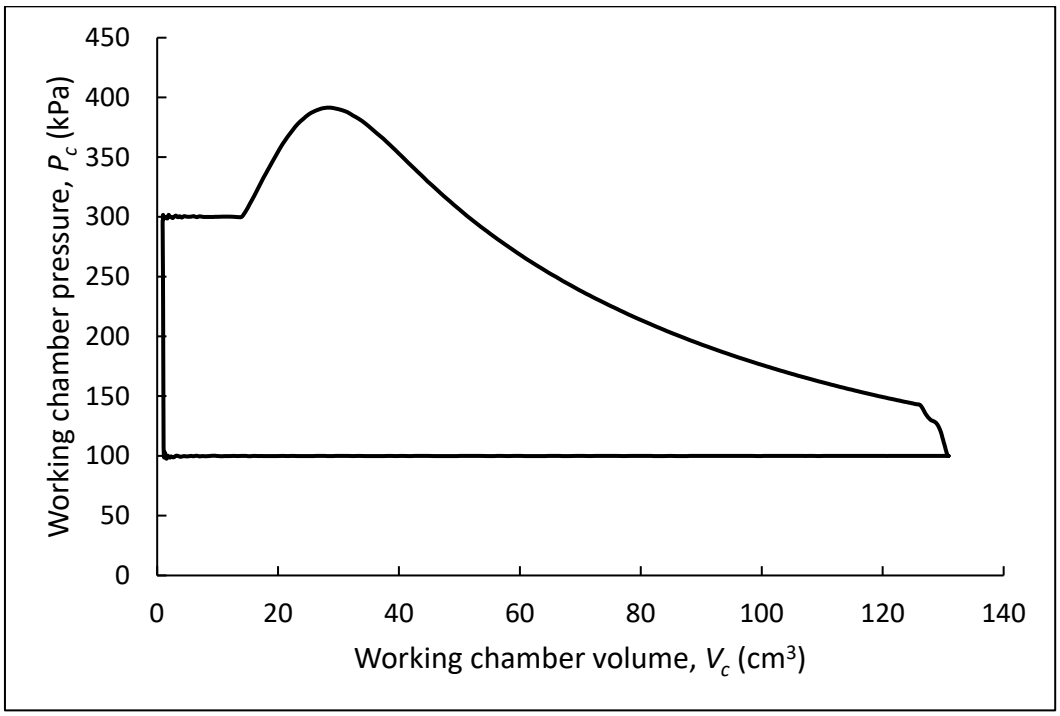

Fig. 2-10. The P-V diagram.

2.5. The effect of various parameters on the performance

In the simulation presented above, the limaçon compressor presents an isentropic efficiency of 88.9% and a volumetric efficiency of 61.5% under the given conditions. The

compressor performance may vary significantly with the change in operating conditions (i.e., change in pressures at inlet and outlet, and the operating speed). Hence, the behaviour of the limaçon compressor under different conditions is to be investigated. For this purpose, the effect of different parameters, including the operating speed, the pressure ratio (i.e., the ratio of the discharge pressure to the inlet pressure), and the size of the discharge valve, will be discussed in this section. All results presented in the following sections are obtained by using the same dimensions as listed in Table 2-1, and the ambient temperature is assumed constant at $20°C$.

2.5.1. Effects of operating speed

Fig. 2-11 shows the variation of isentropic and volumetric efficiencies against different operating speeds. This simulation is carried out with air as the working fluid under a constant pressure ratio of 3. As shown in Fig. 2-11, the volumetric efficiency increases at the speed range from $600\ rpm$ to $1800\ rpm$. This might be attributed to the considerable reduction of the leakage mass, and the opening of the discharge valve, as indicated by Fig. 2-12, increases with the operating speed, allowing more fluid to be discharged through the valve. However, as the speed keeps increasing, there will be less time available for the fresh charge to fill the working chamber. Additionally, the closing of the discharge valve is delayed, as shown in Fig. 2-12, which raises the possibility of the high-pressure fluid backflow into the other chamber. Moreover, the backflow can make its way through the inlet port out of the working chamber, causing the amount of fluid admitted into the chamber to be reduced. Therefore, the machine performance may deteriorate if the operating speed increases beyond the design limit.

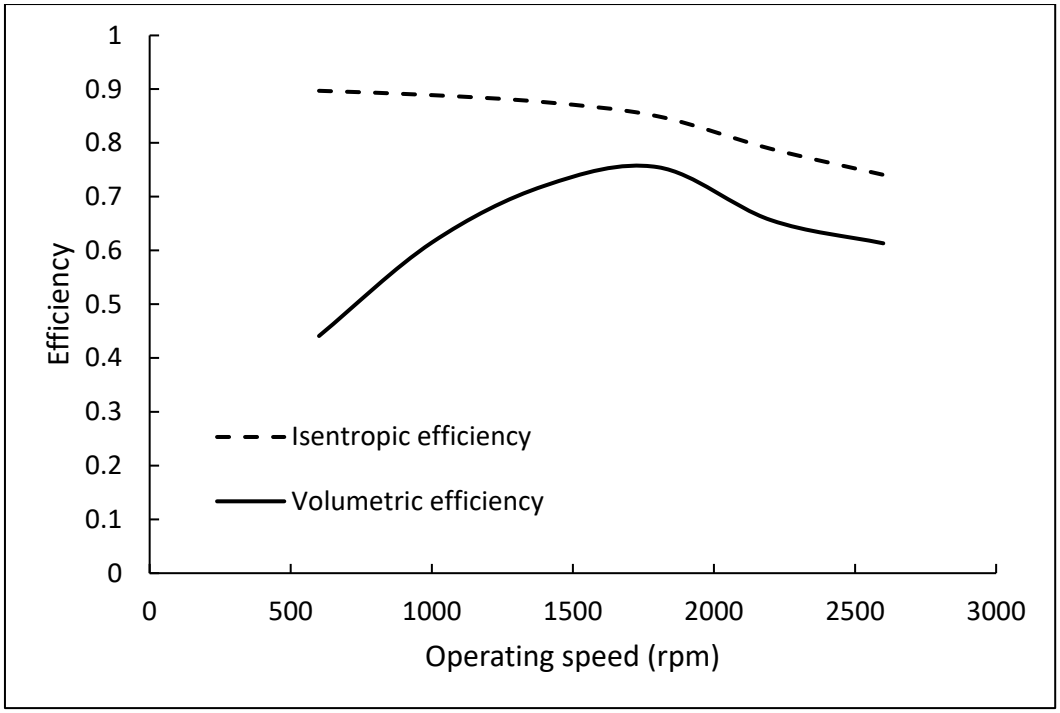

Fig. 2-11. Performance at different operating speeds.

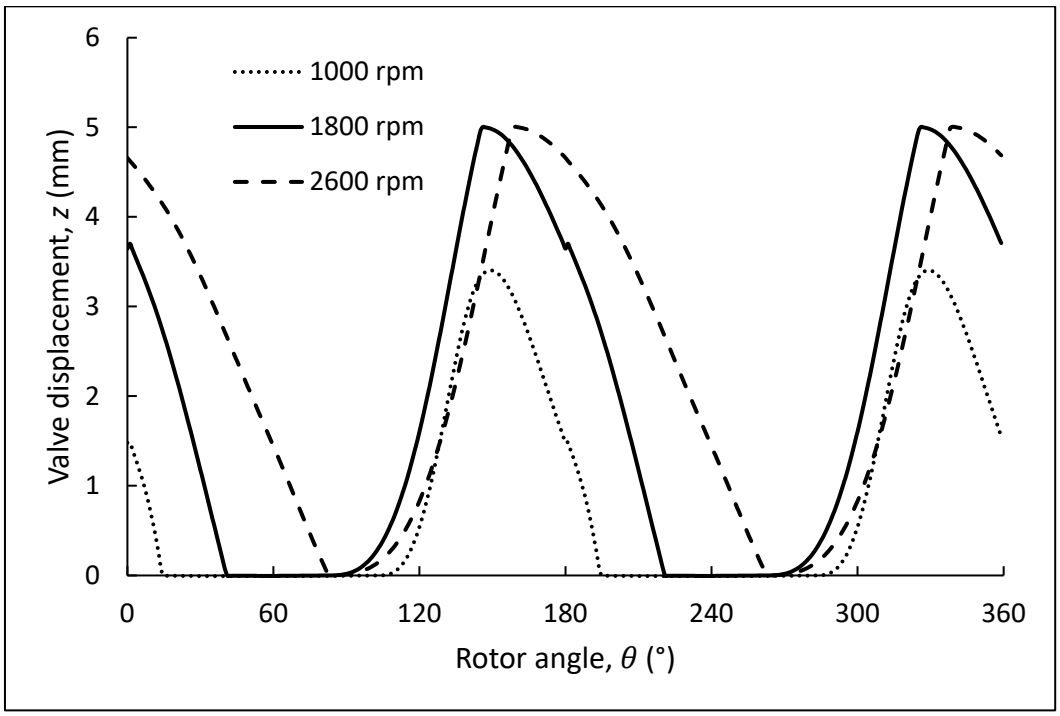

Fig. 2-12. Valve displacement at three specific operating speeds.

2.5.2. Effects of pressure ratio

The effects of changes in pressure ratio on isentropic and volumetric efficiencies are shown in Fig. 2-13. The simulation employs air as a working fluid and runs at a constant

inlet pressure and operating speed, which are respectively $100\ kPa$ and $1000\ rpm$. According to Fig. 2-13, the volumetric efficiency exhibits a downward trend with the pressure ratio rising from 3 to 13. This is due to the fact that the opening of the discharge valve is affected by the increased discharge pressure. As the discharge pressure increases, the opening of the valve will decrease, thereby reducing the time available for the discharge stroke. As a result of this, the discharged mass will be reduced, and more importantly, the amount of fluid drawn into the working chamber will also be reduced since the backflow formed by the undischarged fluid flows out of the working chamber through the inlet port. Compared to the volumetric efficiency, the isentropic efficiency is found to be relatively insensitive to the change in the pressure ratio, especially since the isentropic efficiency curve tends to be flat as the pressure ratio keeps increasing, showing an overall difference of less than 7% (Fig. 2-13).

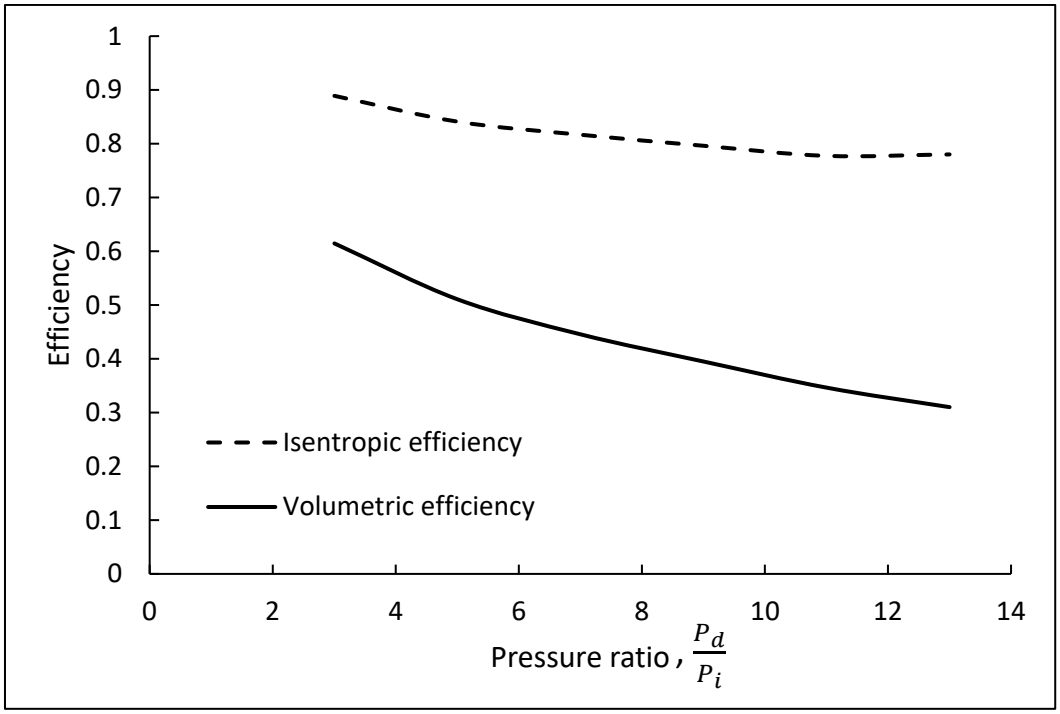

Fig. 2-13. Performance at different pressure ratios.

2.5.3. Effects of the diameter of the valve

During the compression stroke, the working fluid usually needs to be compressed to a higher level than it is desired. This is to overcome the stiffness of the spring attached to the valve, which realizes the opening of the discharge valve and initiates the discharge stroke. However, the fluid over-compression causes that extra input power in the form of shaft torque to be required, thus increasing the power consumption. Fig. 2-14 shows the variation of the chamber pressure with respect to the different sizes of the valve. Based on the figure, it is found that the level of fluid over-compression increases with the reduction of the diameter of the valve. The direct influence of the valve diameter is in the area of the valve, which affects the force acting on the valve plate. As the valve diameter decreases, the pressure has to be increased in order to reach the force that can open the valve.

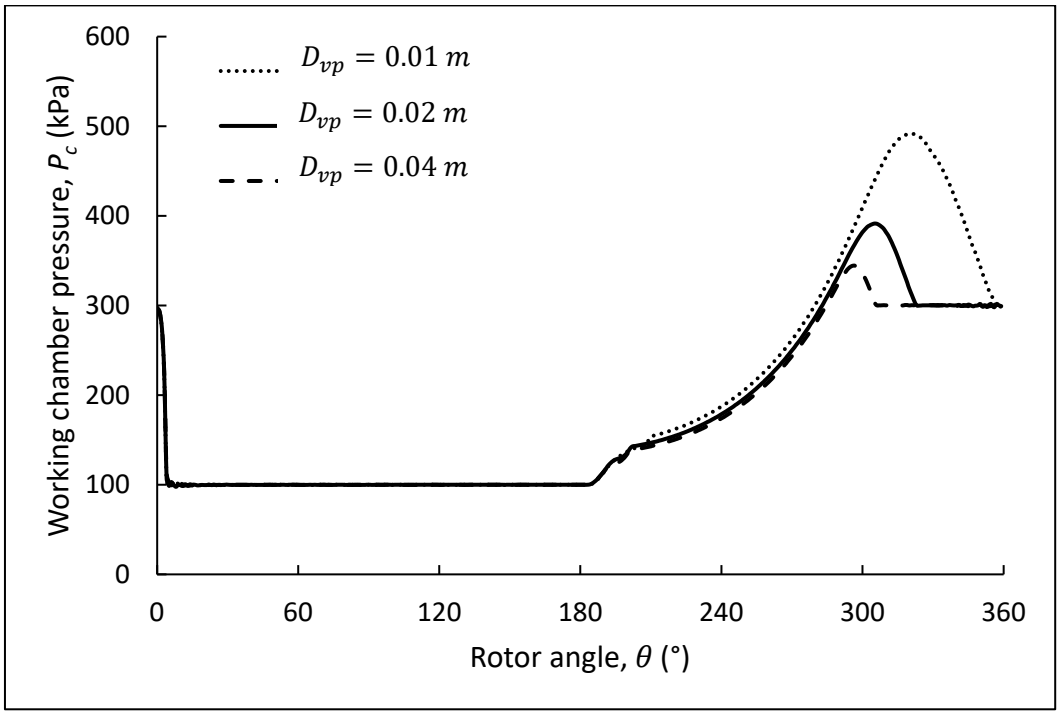

Fig. 2-14. Effect of the diameter of the valve on the variation of chamber pressure.

2.6. Conclusion

In this paper, a mathematical model, which incorporates the mass flow of the working fluid, the leakage loss, the dynamic response of the discharge valve, as well as the thermodynamic behaviours, is established to theoretically study the workings of the proposed limaçon compressor. Furthermore, a parametric analysis is carried out, which reveals the effect of different parameters on the performance. Based on the results, the following has been revealed:

(1). At the speed range of 600 to 1800 rpm, the volumetric efficiency increases with speed as a result of the reduction of the leakage. As the speed keeps increasing, however, the amount of working fluid flowing through the port is reduced due to the shorter time that is available for the inlet port to expose to the working chamber, thus the volumetric efficiency starts decreasing.

(2). Furthermore, the discharge valve stays open for a longer period at a higher speed, which increases the chance of backflow of the discharged high-pressure fluid. As a result, the chamber pressure will be increased in the subsequent cycle, which degrades the machine performance.

(3). Isentropic efficiency is relatively insensitive to the changes in pressure ratio, while the volumetric efficiency decreases as the pressure ratio increases. This is due to the effect of the discharge pressure on the opening of the discharge valve, which affects the amount of fluid flowing out and drawn into the working chamber.

(4). The change occurring in the valve diameter affects the discharge loss due to the fluid over-compression. It is found that a smaller valve diameter leads to a higher level of over-compression.

This paper demonstrates the potential of the limaçon technology to be used as a positive displacement compressor, and the information provided through the mathematical modelling will benefit future work on the limaçon compressor, especially the optimization procedure for the prototype.

2.7. References

Spark, I. J., Lu, K. (2019). The orbital displacer: Implications and applications. In I. A. Sultan & T. H. Phung (Eds.), Positive Displacement Machines (pp. 3-34): Academic Press.

Chen, Y., Halm, N. P., Groll, E. A., Braun, J. E. (2002a). Mathematical modeling of scroll compressors—part I: compression process modeling. International Journal of Refrigeration, 25(6), 731-750. doi: https://doi.org/10.1016/S0140-7007(01)00071-8

Chen, Y., Halm, N. P., Braun, J. E., Groll, E. A. (2002b). Mathematical modeling of scroll compressors — part II: overall scroll compressor modeling. International Journal of Refrigeration, 25(6), 751-764. doi:https://doi.org/10.1016/S0140-7007(01)00072-X

Cuevas, C., Lebrun, J., Lemort, V., & Winandy, E. (2010). Characterization of a scroll compressor under extended operating conditions. Applied thermal engineering, 30(6-7), 605-615.

Stosic, N., Smith, I., Kovacevic, A. (2003). Opportunities for innovation with screw compressors. Proceedings of the Institution of Mechanical Engineers, Part E: Journal of Process Mechanical Engineering, 217, 157-170. doi: 10.1177/095440890321700301

Teh, Y. L., & Ooi, K. T. (2009). Theoretical study of a novel refrigeration compressor–Part I: Design of the revolving vane (RV) compressor and its frictional losses. international journal of refrigeration, 32(5), 1092-1102.

Subiantoro, A., Ooi, K. T. (2009). Introduction of the Revolving Vane Expander. HVAC&R Research, 15(4), 801-816. doi:10.1080/10789669.2009.10390865

Subiantoro, A., Ooi, K. T. (2011). Analytical study of the endface friction of the revolving vane mechanism. International Journal of Refrigeration, 34(5), 1276-1285. doi:https://doi.org/10.1016/j.ijrefrig.2011.01.019

Subiantoro, A., Ooi, K. T. (2012a). Analysis of the revolving vane (RV-0) expander, Part 1: Experimental investigations. International Journal of Refrigeration, 35(6), 1734-1743. doi:https://doi.org/10.1016/j.ijrefrig.2012.04.015

Subiantoro, A., Ooi, K. T. (2012b). Analysis of the Revolving Vane (RV-0) expander, part 2: Verifications of theoretical models. International Journal of Refrigeration, 35(6), 1744-1756. doi:https://doi.org/10.1016/j.ijrefrig.2012.04.014

Zhang, H., Wu, J., Xie, F., Chen, A., & Li, Y. (2014). Dynamic behaviors of the crankshafts in single-cylinder and twin-cylinder rotary compressors. International journal of refrigeration, 47, 36-45.

Wheildon, W. M. (1896). U.S. Patent No. 553,086. Washington, DC: U.S. Patent and Trademark Office.

Sultan, I. A. (2005). The Limaçon of Pascal: Mechanical Generation and Utilization for Fluid Processing. Proceedings of the Institution of Mechanical Engineers, Part C: Journal of Mechanical Engineering Science, 219(8), 813-822. doi: 10.1243/095440605x31698

Sultan, I. A. (2006). Profiling Rotors for Limaçon-to-Limaçon Compression-Expansion Machines. Journal of Mechanical Design, 128(4), 787-793. doi: 10.1115/1.2202877 %J Journal of Mechanical Design

Sultan, I. A. (2007). A surrogate model for interference prevention in the limaçon-to-limaçon machines. Engineering Computations, 24, 437-449.

Sultan, I. A. (2008a). Inverse geometric design for a class of rotary positive displacement machines. Inverse Problems in Science and Engineering, 16(2), 127-139. doi: 10.1080/17415970601162164

Sultan, I. A. (2008b). A geometric design model for the circolimaçon positive displacement machine. Journal of Mechanical Design, 130(6).

Phung, T. H., Sultan, I. A. (2018). Characterization of Limaçon Gas Expanders with Consideration to the Dynamics of Apex Seals and Inlet Control Valve. Journal of Engineering for Gas Turbines and Power, 140(12).

Sultan, I. A., Schaller, C. G. (2011). Optimum Positioning of Ports in the Limaçon Gas Expanders. Journal of Engineering for Gas Turbines and Power-Transactions of the ASME, 133(10).

Sultan, I. A. (2012). Optimum design of limaçon gas expanders based on thermodynamic performance. Applied Thermal Engineering, 39, 188-197. doi: https://doi.org/10.1016/j.applthermaleng.2012.01.039

Phung, T., Sultan, I., Boretti, A. (2016). Design of Limaçon Gas Expanders. In R. N. Jazar & L. Dai (Eds.), Nonlinear Approaches in Engineering Applications: Advanced Analysis of Vehicle Related Technologies (pp. 91-119). Cham: Springer International Publishing.

Phung, T. H., Sultan, I. A., & Appuhamillage, G. K. (2018). On the apex seal analysis of limaçon positive displacement machines. Mechanism and Machine Theory, 127, 126-145.

Phung, T. H., & Sultan, I. A. (2021). Geometric Design of the Limaçon-to-Circular Fluid Processing Machine. Journal of Mechanical Design, 143(10). doi:10.1115/1.4050383

Massoud, M. (2005). *Engineering thermofluids* (Vol. 2005). Springer-Verlag Berlin Heidelberg.

Tuymer, W. J., Machu, E. H., & Hanlon, P. C. (2001). Compressor valves. Compressor handbook, 20-1.

Lemmon, E. W., Huber, M. L., McLinden, M. O. (2010). NIST Reference Fluid Thermodynamic and Transport Properties—REFPROP Version 10.0. Gaithersburg, Maryland 20899: U.S. Department of Commerce - Technology Administration - National Institute of Standards and Technology.

Chapter 3. On the design of a class of rotary compressors using Bayesian optimisation [§] [**]

3.1. Abstract

The optimization process of compressors is usually regarded as a 'black-box' problem, in which the mathematical form underlying the relationship between design parameters and the design objective is impractical and costly to be obtained. To solve the 'black-box' problem, Bayesian optimization has been proven as an accurate and efficient method. However, the application of such a method in the design of compressors is rarely discussed, particularly no work has been reported in terms of the positive displacement type compressor. Therefore, this chapter aims to introduce Bayesian optimisation to the design of positive displacement compressors through the optimisation process of the novel limaçon compressor. In this chapter, a two-stage optimisation process is presented, in which the first stage optimizes the geometric parameters as per design requirements and the second stage focuses on revealing an optimum setting of port geometries that improves machine performance. A numerical illustration is offered to prove the validity of the presented approach.

Keywords: positive displacement; limaçon of Pascal; rotary compressor; optimization; Bayesian optimization

[§] This chapter has been published: Lu, K., Phung, T. H., and Sultan, I. A. (2021). On the Design of a Class of Rotary Compressors Using Bayesian Optimization. Machines, 9(10), 219. https://doi.org/10.3390/machines9100219

[**] A detailed version of the geometric design of the limaçon compressor has been presented at 3rd ICEP conference (Nov 18-20, Ching Mai, Thailand): Lu, K., Sultan, I. A. and Phung, T. H. (2021) "Geometric Design of The Limaçon Rotary Compressor Using Bayesian Optimization", The 3rd Int. Conf. on Energy and Power (ICEP2021)., Nov 18-20, Chiang Mai, Thailand.

3.2. Introduction

In compressor design, information solely obtained from the simulation of the mathematical model is usually insufficient to reflect the thorough relationship between the design parameters and design objective in terms of performance. As such, designers often need to rely on optimization strategies to reveal the optimum design scenario before reaching the final decision on the prototype.

The published literature shows that various optimization techniques have been applied to the design optimization of the positive displacement machine and compressor in particular. Ooi (2005) applied the direct-search method to seek a set of six machine dimensions and seven design constraints, which can minimize the mechanical losses of the rolling piston compressor. The author reported that a predicted 50% reduction in mechanical loss, which increases 14% of the coefficient of performance, can be achieved with a proper combination of design dimensions. Liu et al. (2010) employed the gradient search method to determine optimum dimensions of bearing components that can reduce the frictional loss occurring in the scroll compressor. Based on the optimization result, the author found that the frictional loss can be reduced in the range of 14.1% to 18.1%. Sultan and Kalim (2011) adopted the simultaneous perturbation stochastic approximation (SPSA) method to find the best piston trajectory of the reciprocating compressor, and the authors also employed gradient-based optimization to determine the machine dimensions which can realize such a trajectory. Recently, the SPSA approach has also been utilized in the work of Phung and Sultan (2021) to design a new embodiment of the limaçon machine referred to as the limaçon-to-circular machine. Like other limaçon machine embodiments, this new design can be used as expanders, compressors, and potentially pumps. Cavazzini et al. (2020) adopted topology optimization, which combines the particle swarm method

with computational fluid dynamics, to determine the geometric parameters that can maximize the machine efficiency of the scroll compressor. The authors discovered that the compressor performance is more sensitive to the variation of three parameters, which are the size of the discharge port, the number of coils, and the radius of orbiting scroll. Silva and Dutra (2021) used the genetic optimization algorithm to find an optimum piston trajectory that maximizes the performance of the reciprocating compressor. The authors reported that the optimum piston trajectory reduces the losses from heat transfer and leakage, increasing the thermodynamic efficiency from 88.3% to 92.1% and the volumetric efficiency from 70.9% to 72%. In their latest work, Aw and Ooi (2021) presented a comprehensive review of the previous investigation conducted on sliding-vane and rolling piston compressors. The authors discussed various aspects of these two types of compressors and pointed out the importance of the optimization process with respect to the development and design evolution of rotary type compressors.

It is worth mentioning that the process executed by the compressor is rather intricate, and the mathematical expression underlying such a process is impractical to be obtained, leading to the optimization of the compressor becoming a 'black-box' problem. For this kind of optimization problem, iterative methods such as direct-search or gradient-search are generally time-consuming and costly. One preferable alternative is the surrogate-based technique such as Bayesian optimization. In fact, many studies have proven that Bayesian optimization is an efficient and accurate tool for problems in which the evaluation of objective function is computationally expensive (Pelikan et al., 1999; Snoek et al., 2012; Frazier and Wang, 2016). In the past decade, this method has become popular in many areas of science and engineering, including integrated system design (Torun et al., 2018), chemical engineering (Griffiths and Hernández-Lobato, 2017), policy optimization

(Letham et al., 2019), and rail network (Hickish et al., 2020). Despite the successful application in various disciplines, the utilization of Bayesian optimization in the design of compressors is rarely discussed, particularly no work has been reported in terms of the positive displacement type compressor. Therefore, this chapter attempts to introduce the concept of Bayesian optimization to the field of positive displacement compressors by way of presenting the optimization process of the novel limaçon compressor. The proposed optimization process will be implemented through a two-stage process, in which the first stage optimizes the geometric parameters that determine the overall size of the machine as per design requirements. Based on the result of the first stage, the second stage is intended to reveal the parameters of the port geometry, which contains the angular location, angular width, and the length of the port, that can maximize the machine performance, such as the isentropic efficiency and the volumetric efficiency.

3.3. Geometric Characteristics of the Limaçon Compressor

One feature distinguishing the limaçon compressor from other types of rotary compressors is that the profiles of the housing and rotor are developed from a mathematical curve named the limaçon of Pascal. In fact, the use of limaçon technology in fluid machinery can be traced back to the 1800s, but none of those early designs received enough attention from either industrial or academic communities owing to the limitation of manufacturing methods and the lack of mathematical understanding. Over the last two decades, the work of Sultan (2005; 2006; 2007; 2008) offered good insights into the limaçon technology, and some studies on the application of the limaçon technology in the gas expander have been reported recently (Sultan and Schaller, 2011; Sultan, 2012; Phung and Sultan, 2018). However, the investigation of this technology in the compressor is still

rarely reported in the available literature. This section is intended to present the geometric characteristics of the limaçon compressor.

Analogous to other types of rotary compressors, the limaçon compressor has advantages such as being compact in size and light in weight. Additionally, the limaçon compressor possesses better sealing performance as the rotor apices are in constant contact with the housing during the operation, and the two-lobe design of the rotor also implies the double-acting nature of the machine. Most distinctively, a larger capacity can be realized by adjusting the limaçon aspect ratio without changing the machine size, thereby allowing for a higher power-to-weight ratio.

Fig. 3-1 below shows a typical limaçon compressor and its working process. As shown in Fig. 3-1(a), the rotor chord, p_1p_2, performs sliding and rotational motion about the limaçon pole, o, during its operation. As the rotor moves, the midpoint of the chord, m, is kinematically connected to the circumference of the housing base circle whose radius is r; the profile of the limaçon housing can be obtained by tracing the path of the chord apex, p_1 or p_2. To readily describe the parametric coordinates of the chord apices, two Cartesian frames, X_oY_o and X_mY_m, are respectively introduced at o and m. The housing profile in the X_oY_o coordinate can be expressed as:

$$\begin{cases} x_h = r\sin 2\theta + L\cos\theta \\ y_h = r - r\cos 2\theta + L\sin\theta \end{cases} \tag{3-1}$$

where L is half rotor chord length and θ is the angular displacement swept by the chord from the X_o- to the X_m-axis. It is worthy of mentioning here that the shape of the housing profile is dependent on a geometric factor which is referred to as the limaçon aspect ratio, $\beta = \frac{r}{L}$. For a limaçon curve that is applicable to fluid machinery, the limaçon aspect ratio

needs to be less than 0.25 so that the housing profile can be produced as single-looped and dimple-free.

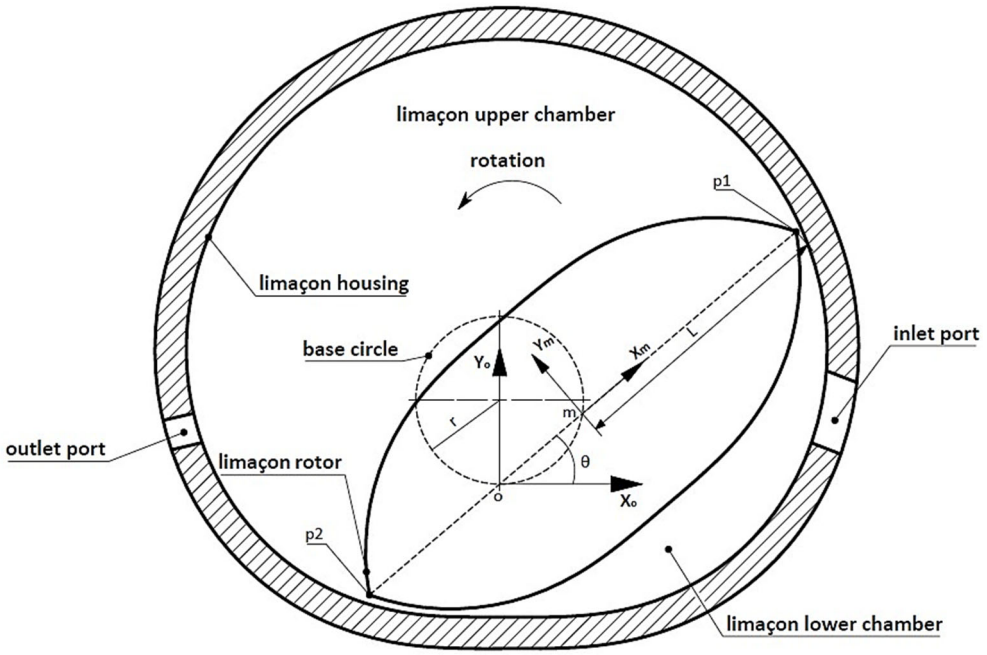

(a)

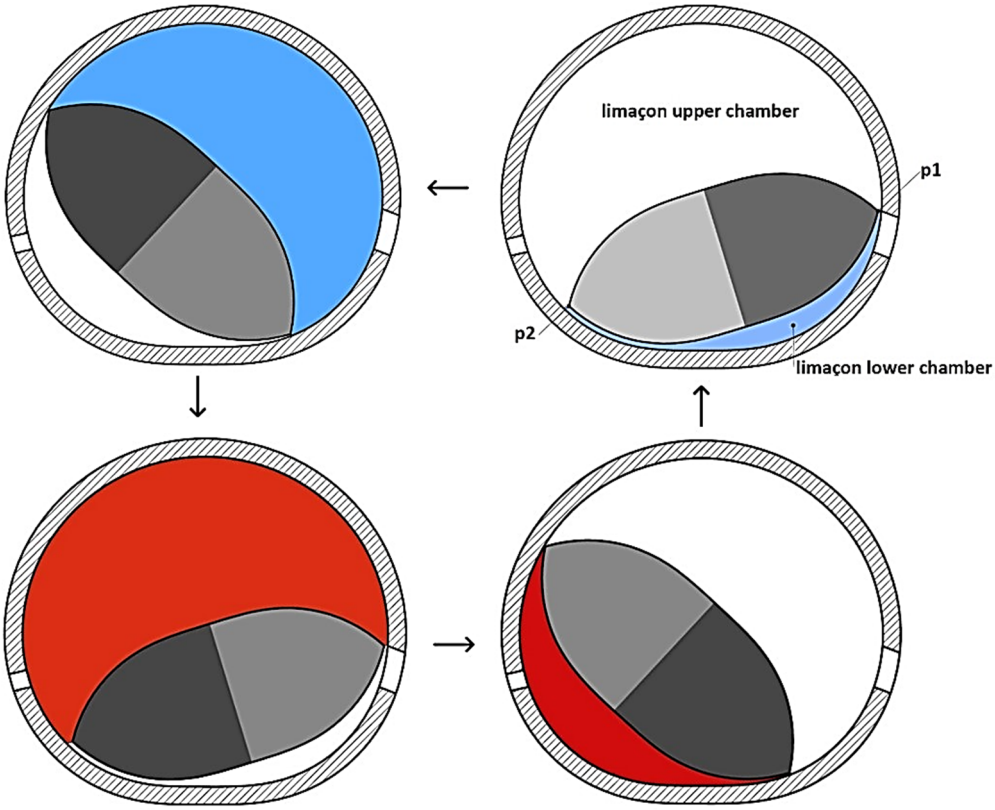

(b)

Fig. 3-1. (a) The limaçon compressor; (b) illustration of the working process (suction is blue and delivery is red).

The lenticular profile of the rotor can be developed by mirroring the lower portion of the limaçon housing (i.e., $\theta \in [\pi, 2\pi]$) about the chord. However, this could lead to undesirable housing-rotor interference at the lower portion of the housing as the limaçon curves that are respectively used for the housing and rotor profiles share the same base circle. To avoid this interference, it is necessary to shorten the half rotor chord length,L, by a distance L_c; the parametric expression of the rotor with respect to the moving frame, $X_m Y_m$, can then be obtained as follows:

$$\begin{cases} x_r = r_r \sin\theta_r + (L - L_c)\cos\theta_r \\ y_r = r_r - r_r \cos 2\theta_r + (L - L_c)\sin\theta_r \end{cases} \tag{3-2}$$

where r_r is the radius of the rotor base circle which is identical to r in this design, and $\theta_r \in [\pi, 2\pi]$ is the angle measured from the X_m-axis to any point on the rotor profile.

Of important note is that the value of L_c needs to be carefully regulated in order to ensure the clearance, Δ, between the housing and the rotor would not fall below a minimum allowable value, Δ_{min}, assigned to the design. The expression of Δ has been proposed by Sultan (2006) as follows:

$$\Delta = \frac{-2\beta L_3 \sin(\theta - \varphi) - \frac{L_3^2}{L}}{\sqrt{\frac{L_3^2}{L^2} + 4\beta \sin\theta \left(\beta \sin\theta + \frac{L_3}{L}\cos\varphi\right)}} + L \tag{3-3}$$

where φ is the angle measured from the X_m-axis to the radial line L_3 connecting m to a point p_3 on the rotor profile as shown in Fig. 3-2. L_3 has the expression as follows:

$$L_3 = 2r_r \sin(\varphi + \pi) + (L - L_c) \tag{3-4}$$

To obtain an appropriate value for L_c which can produce Δ that meets the design requirements, the following conditions must be simultaneously satisfied:

$$\begin{cases} \dfrac{\partial \Delta}{\partial \theta} = 0 \\ \dfrac{\partial \Delta}{\partial \varphi} = 0 \\ \Delta - \Delta_{min} \geq 0 \end{cases} \tag{3-5}$$

The two angles, θ and φ, obtained from Equation (3-5) are to locate the angular position of the minimum clearance, making sure that Equation (3-3) using these angles will always yield the lowest value of L_c in terms of the proposed Δ_{min}.

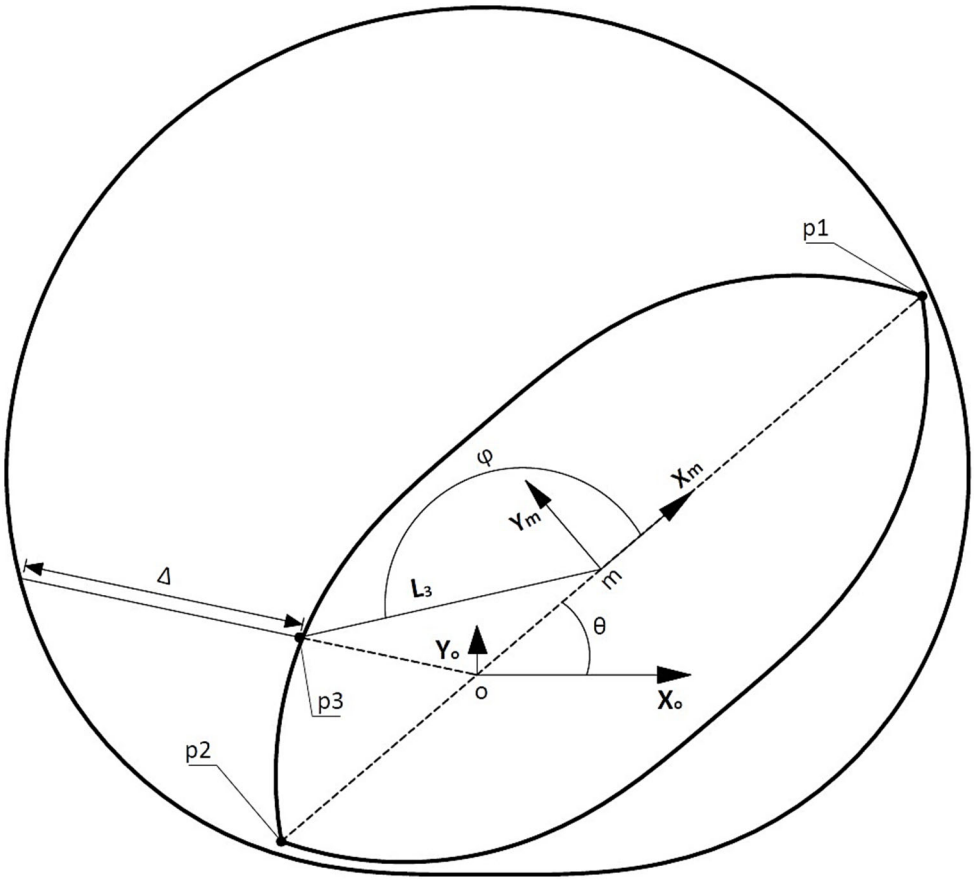

Fig. 3-2. The rotor-housing clearance.

As shown in Fig. 3-1, the working chamber of the limaçon compressor is separated by the rotor into the upper and the lower portions. Such a configuration implies the fact that the limaçon compressor is a double-acting machine by nature, i.e., the suction process correspondingly occurs in the lower chamber when the discharge process is being conducted in the upper chamber. As such, the limaçon compressor is capable of compressing

the working fluid twice per revolution of the crankshaft, and the net volume available for each compression charge can be expressed as a function of θ as follows:

$$V_c = HL^2\left[\pi\left(\beta^2 - \frac{r_r^2}{L^2} + \frac{L_c}{L}\left(1 - \frac{L_c}{2L}\right)\right) - 4\beta\cos\theta + 4\frac{r_r}{L}\left(1 - \frac{L_c}{L}\right)\right] \tag{3-6}$$

where H is the axial length of the rotor measured perpendicular to the page.

Equation (3-6) shows that the variation of chamber volume follows a sinusoidal manner where the maximum and the minimum values are at $\theta = \pi$ and $\theta = 0$, respectively. Generally, the minimum volume, provided that the rotor-housing clearance condition is satisfied, should be kept as small as practical so that the volumetric performance and machine capacity would not significantly deteriorate. To determine whether the limaçon compressor can present a satisfactory performance, a volumetric ratio, R, is employed. This volumetric ratio, R, is defined as the minimum volume to the maximum volume of the working chamber as follows:

$$R = \frac{\pi\left(\beta^2 - \frac{r_r^2}{L^2} + \frac{L_c}{L} - \frac{L_c^2}{2L^2}\right) - 4\left(\frac{r_r L_c}{L^2} + \beta - \frac{r_r}{L}\right)}{\pi\left(\beta^2 - \frac{r_r^2}{L^2} + \frac{L_c}{L} - \frac{L_c^2}{2L^2}\right) - 4\left(\frac{r_r L_c}{L^2} - \beta - \frac{r_r}{L}\right)} \tag{3-7}$$

In addition, the volume of the working fluid, V_i, induced into the chamber by each suction stroke can be used to indicate the machine capacity and which is calculated as:

$$V_i = V_c|_{\theta=\theta_{cut}} - \mu V_c|_{\theta=0} \tag{3-8}$$

where $\theta_{cut} \in (0, \pi]$ indicates the end of the suction process. The clearance volume factor, μ, is assigned by the designer to include the effect of residual fluid in the minimum chamber on the suction process. The expression for this factor is shown below:

$$\mu = \frac{\rho_o}{\rho_i} \tag{3-9}$$

where ρ_i and ρ_o are the densities of the fluid flowing in and out of the compressor, respectively. By combining Equations (3-6) and (3-8), V_i can be expressed in a detailed fashion as follows:

$$V_i = HL^2(1-\mu)\left[\pi\left(\beta^2 - \frac{r_r^2}{L^2} + \frac{L_c}{L}\left(1-\frac{L_c}{2L}\right)\right) + 4\frac{r_r}{L}\left(1-\frac{L_c}{L}\right)\right] - 4\beta HL^2\cos(\theta_{cut}-\mu) \tag{3-10}$$

3.4. Optimization Process

3.4.1. Bayesian Optimization Method

Bayesian optimization is a class of surrogate-based global optimization targeting to find the minima (or maxima) of an output y over an input x in a domain $\mathbb{d}$, and it can be concisely expressed as follows:

$$x = \underset{x \in \mathbb{d}}{\operatorname{argmin}}\, y \tag{3-11}$$

where the mathematical expression underlying the relationship between x and y cannot readily be explicitly defined. In practice, Bayesian optimization starts with building a prior distribution based on observations to express assumptions about the black box objective function. It is necessary to point out that the actual value of the function generally differs from the observed one as errors occurring in aspects, such as recording or measuring, are not avoidable. Therefore, the optimization procedure will be more realistic if the observation used to develop the prior distribution is added up with a noise factor, ε, such that those errors can be considered into the process, and the actual function value y is then calculated as:

$$y = f + \varepsilon \tag{3-12}$$

where f is the observed function value.

Suppose that there are n sets of observations have been made, Bayesian optimization employs statistical methods, particularly Gaussian Process (GP), to sample the observations, which is associated with the input x as follows (Rasmussen and Williams, 2006):

$$f = (K_x + \sigma^2 I)w \tag{3-13}$$

where σ is the standard deviation, I is the identity matrix, w is a vector of weights, and K_x is the covariance matrix that has the form:

$$K_x = \begin{bmatrix} k(x_1, x_1) & k(x_2, x_1) & \dots & \dots & k(x_n, x_1) \\ k(x_1, x_2) & \dots & \dots & \dots & \dots \\ \dots & \dots & \dots & \dots & \dots \\ \dots & \dots & \dots & \dots & \dots \\ k(x_1, x_n) & \dots & \dots & \dots & k(x_n, x_n) \end{bmatrix} \tag{3-14}$$

In Equation (3-14), each element in the matrix is a covariance function that describes the relationship between points x_i and x_j $(i, j = 1,2, \dots, n)$. For the optimization of the limaçon compressor, the $Matérn\ 5/2$ covariance function is used, which has the form:

$$k(x_i, x_j) = c_1 \left(1 + \sqrt{5l^2(x_i, x_j)} + \frac{5}{3} l^2(x_i, x_j)\right) \exp\left(-\sqrt{5l^2(x_i, x_j)}\right) \tag{3-15}$$

where $l^2(x_i, x_j) = \sum_n \frac{(x_i - x_j)^2}{c_2^2}$ is the radial basis function, and c_1 and c_2 are the hyperparameters.

Given that one seeks to predict the function value at a new point x^*, one can set up the relationship between x^* and observed points as follows:

$$K_x^* = [k(x^*, x_1) \quad k(x^*, x_2) \quad \dots \quad k(x^*, x_n)] \tag{3-16}$$

The predicted function value at the point x^* can then be computed as:

$$f^* = [K_x^*]^T (K_x + \sigma^2 I)^{-1} f \tag{3-17}$$

In Bayesian optimization, Equation (3-17) is referred to as the surrogate model of the objective function, and the variance σ^{*2} that describes the uncertainty in the prediction can be calculated as:

$$\sigma^{*2} = k(x^*, x^*) - [K_x^*]^T (K_x + \sigma^2 I)^{-1} K_x^* \tag{3-18}$$

Based on the above equations, the objective function can be evaluated at any input point, and the obtained function value can be verified by using the selected input in the real process. From the optimization point of view, however, it would be time-consuming and wasteful if the evaluation is conducted on any point that is arbitrarily selected in the searching domain. As such, Bayesian optimization employs the acquisition function to guide the search for the next query point. The mechanism of the acquisition function for selecting the next query point is based on the prediction (f^*) and the uncertainty (σ^{*2}) of the candidate point. In fact, the acquisition function can be regarded as the examiner of a scoring process. With low prediction (for minimization problems) and high uncertainty, the candidate point obtains a high score from the acquisition function, and the candidate point with the highest score will be selected as the next query point.

Currently, there are many available acquisition functions, e.g., Probability of Improvement (PI) and Expected Improvement (EI). For the optimization of the limaçon compressor, the scaled expected-improvement acquisition function (ScaledEI) is used (Noè and Husmeier, 2018), which has the following form:

$$ScaledEI(x^*) = \frac{EI(x^*)}{\sqrt{VI(x^*)}} \tag{3-19}$$

In Equation (3-19), EI is the normal expected-improvement acquisition function that takes the form:

$$EI(x^*) = \begin{cases} (f_{min} - f^*)\Phi(Z) + \phi(Z)\sigma^*, & if\ \sigma^* > 0 \\ 0, & if\ \sigma^* = 0 \end{cases} \tag{3-20}$$

where f_{min} is the minimum function value that is observed, Φ and ϕ denote the probability density function and cumulative density function, respectively, and Z is expressed as:

$$Z = \frac{f_{min} - f^*}{\sigma^*} \tag{3-21}$$

The term VI in Equation (3-19) is the variance of the improvement quantifier, which has the form:

$$VI(x^*) = \sigma^{*2}(Z^2 + 1)\Phi(Z) + (Z)\phi(Z) - EI(x^*)^2 \tag{3-22}$$

A comprehensive explanation of ScaledEI can be sought in the work by Noè and Husmeier (2018).

Subsequently, the selected query point and its corresponding function value of the real process will be used to update the GP and the process will be repeated till the terminating criteria are satisfied. This also reveals another feature of the Bayesian optimization technique, that is the knowledge of the surrogate function is kept updating along the optimization process, thereby refining the surrogate model.

3.4.2. Two-Stage Optimization

The optimization of the limaçon compressor in this paper employs the Bayesian optimization presented in the above section. Due to the fact that the thermodynamic model is complex and computationally intensive, the optimization procedure is implemented by a two-stage process to reduce the computational cost of the overall optimization process. The first stage is to optimize the geometric parameters, including the half chord length, L, the limaçon aspect ratio, β, and the rotor clearance, L_c, to meet the specified design requirements. The obtained outcome is evaluated in terms of an evaluation function shown below:

$$E_{o1} = \sqrt{w_1 F_1 + w_2 F_2 + w_3 F_3} \tag{3-23}$$

where w_1, w_2, and w_3 are weighting factors assigned by the designer to highlight the significance of the corresponding term in the evaluation; F_1, F_2, and F_3 are evaluation functions of design requirements associated with Δ, R and V_i, which are respectively expressed as follows:

$$\begin{cases} F_1 = \left(R - R_{req}\right)^2 \\ F_2 = \left(V_i - V_{req}\right)^2 \\ F_3 = \left(\Delta - \Delta_{req}\right)^2 \end{cases} \tag{3-24}$$

where the subscript req denotes the design requirement. One should note that Δ used in F_3 is the lowest value of the rotor-housing clearance in terms of the proposed outcome. Therefore, conditions in Equation (3-5) must be satisfied on top of Equation (3-24), and the input vector of design variables for the first stage, x_{o1}, is then given as:

$$x_{o1} = [L \quad \beta \quad L_c]^T \tag{3-25}$$

In the first stage, 10 sets of x_{o1} will be randomly generated and the corresponding E_{o1} will be calculated by using the geometric model proposed in Section 2. These pre-collected data will be regarded as observations that are employed by GP to build the surrogate model. Subsequently, 1500 sets of new input points, x_{o1}^*, will be sampled from the search domain and feed to the acquisition function to determine the next query point. The determined query point will be then used to calculate the corresponding E_{o1}^*, which will be saved and used to update the GP till the terminating criteria are reached. When the terminating criteria are satisfied, the machine size will be determined based on the x_{o1}^* that achieves the lowest value of the recorded E_{o1}^*, and the second stage optimization will be implemented on top of these geometric parameters to improve the machine performance by modifying the setting of the inlet and outlet ports by utilizing the thermodynamic model presented in Section 3.4. The design variables of this stage, x_{o2}, is given as follows:

$$x_{o2} = [\theta_{li} \quad \theta_{lo} \quad \Delta\theta_i \quad \Delta\theta_o \quad Lp_i \quad Lp_o]^T \tag{3-26}$$

where θ_l, $\Delta\theta$, and Lp are the angular location of the port leading edge measured from the X_o-axis, the port angular width, and the port length, respectively; the subscript i and o represent the inlet port and the outlet port, respectively. The evaluation function of this stage is given by incorporating the performance indices (i.e., isentropic efficiency, η_{is}, and volumetric efficiency, η_{vol}) obtained from the mathematical model:

$$E_{o2} = \sqrt{w_4(1-\eta_{is})^2 + w_5(1-\eta_{vol})^2} \tag{3-27}$$

where w_4 and w_5 are weighting factors assigned by the designer. The steps of the second stage are similar to that of the first stage, except that 20 sets of x_{o2}^* and the corresponding E_{o2}^* will be collected before initiating the optimization process. It should be mentioned here that it is relatively impractical to extract the exact combination of design variables that can produce the global optimum of E_{o1}^* and E_{o2}^* due to the high complexity of the relationship between design variables and design objectives. Instead, a more feasible way is that the optimum outcome is reflected by a set of results obtained from the optimization procedure. Fig. 3-3 illustrates the process of the two-stage optimization employed in the current study.

3.1. Numerical Illustration

In this section, a numerical illustration is presented, and assumptions of the optimization process, such as operating conditions and weighting factors, are listed in Table 3-1. Mathematically, the searching domain of design variables can be simply set according to the corresponding geometric constraints, e.g., $L \in [0, +\infty]$. For a real compressor, however, it is unrealistic for L to be zero or a very large value. Hence, by considering the actual design situation, the searching domain of each design variable is selected, as shown in

Table 3-2. The mathematical model presented in Chapter 2 is used to obtain the performance indices, i.e., the volumetric and isentropic efficiencies.

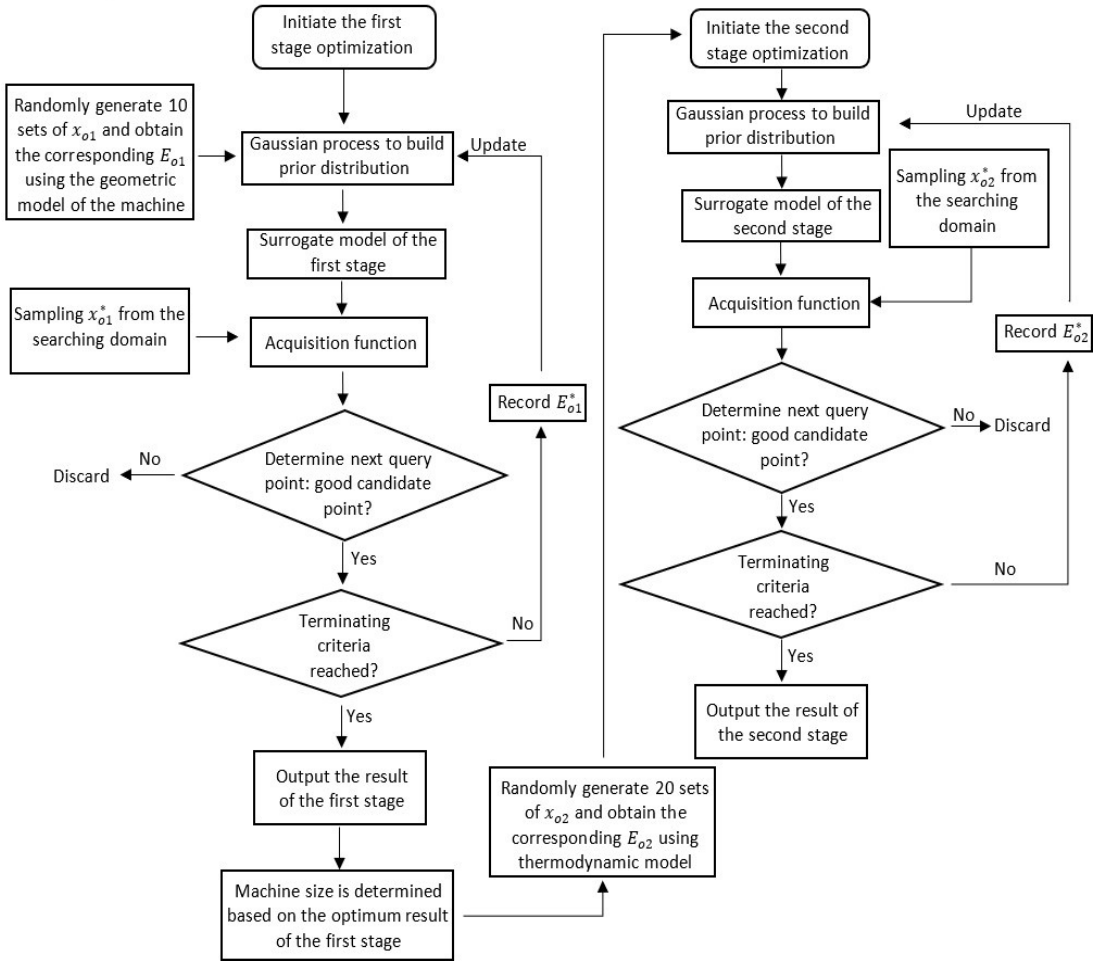

Fig. 3-3. Illustration of the two-stage optimization process.

Table 3-1. Assumptions of optimisation process

Parameters		**Value**
Speed of the crankshaft		$1400\ rpm$
Temperature at inlet port, T_i		$20°C$
Pressure at inlet port, P_i		$100\ kPa$
Pressure at outlet port, P_o		$300\ kPa$
Clearance volume factor, μ		5
Cut-off angle of the suction process, θ_{cut}		π
Weighting factors	w_1	1
	w_2	1000
	w_3	100

Table 3 1. Assumptions of optimisation process (Continued)

Parameters		Value
Weighting factors	w_4	1
	w_5	1

Table 3-2. Searching domain of each design variable

Design variable	Lower limit	Upper limit
Half chord length, L	$0.04\ m$	$0.15\ m$
Aspect ratio, β	0.04	0.22
Rotor clearance, L_c	$0.5\ mm$	$1.5\ mm$
Leading edge of inlet port, θ_{li}	$-7.5\ °$	$3\ °$
Leading edge of outlet port, θ_{lo}	$175\ °$	$200\ °$
Angular width of inlet port, $\Delta\theta_i$	$4\ °$	$16\ °$
Angular width of outlet port, $\Delta\theta_o$	$4\ °$	$16\ °$
Length of inlet port, Lp_i	$0.02\ m$	$0.09\ m$
Length of outlet port, Lp_o	$0.02\ m$	$0.09\ m$

Fig. 3-4(a) depicts a histogram that shows the distribution of E_{o1} based on results obtained from the first stage. It is clear that the majority of the result is concentrated in the low-value region (i.e., the first cluster in the figure), indicating that the proposed optimization tends to produce promising outcomes. Fig. 3-4(b–d) presents the distribution of each design variable that yields the result of the first cluster of Fig. 3-4(a), which provides useful information to guide the setting of design variables in order to obtain an optimum outcome. The combination of design variables that achieve the minimum E_{o1} is used to calculate objective parameters, which are compared with the design requirements as shown in Table 3-3. With the selected design variables, the limaçon compressor is designed with a volumetric displacement of $720\ \mathrm{cm}^3$ per revolution of the crankshaft.

Table 3-3. Comparison of obtained result and required result

Objective parameters	Required value	Obtained value
Volume ratio, R	0.02	0.0193
Induced volume per suction process, V_i	$3 \times 10^{-4}\ m^3$	$3.316 \times 10^{-4}\ m^3$
Rotor-housing clearance, Δ	$5 \times 10^{-4}\ m$	$5.9 \times 10^{-4}\ m$

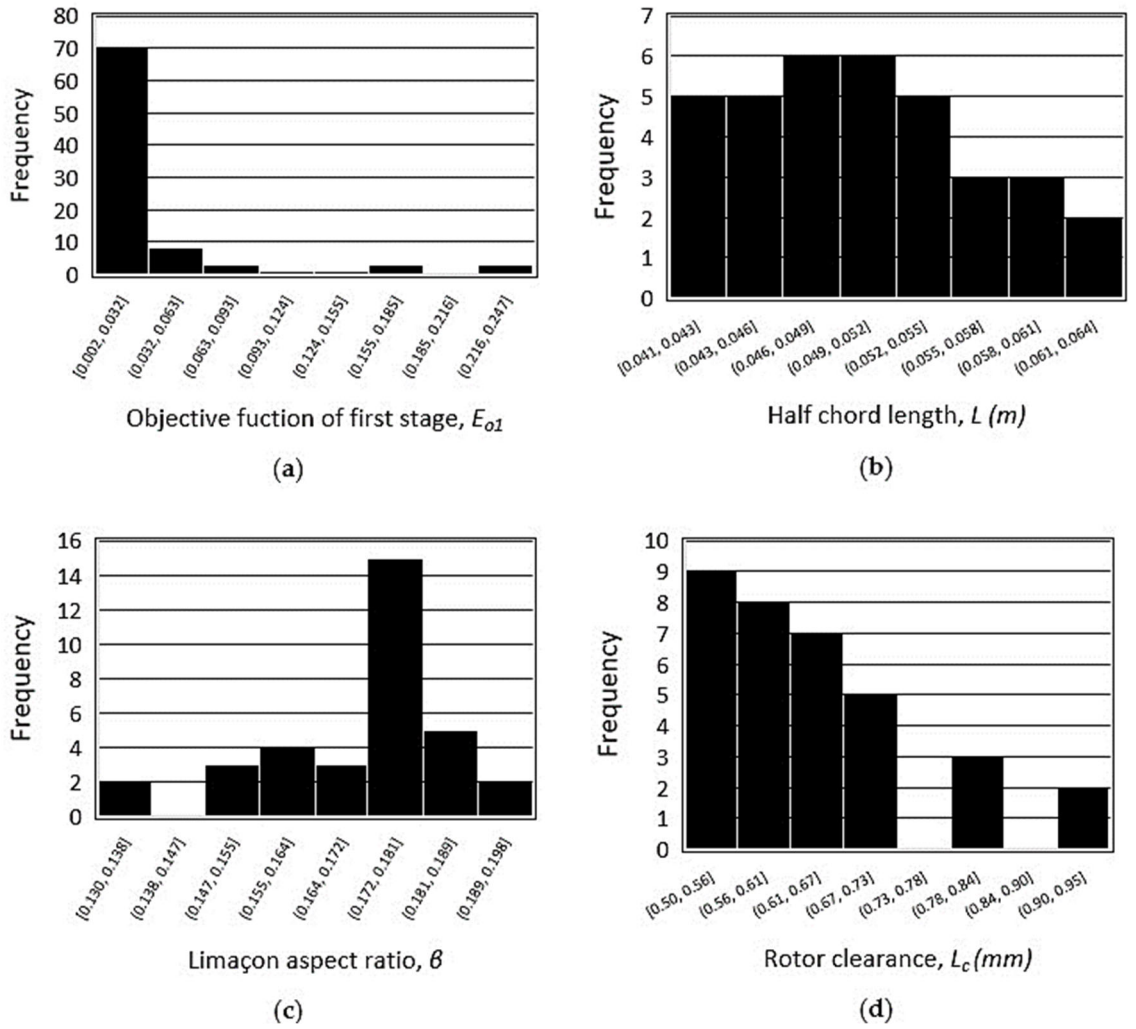

Fig. 3-4. Result of the first stage: (a) distribution of E_{o1}; and distribution of first stage design variables: (b) half chord length; (c) aspect ratio; (d) rotor clearance.

Fig. 3-5 depicts the distribution of E_{o2}, which exhibits a similar pattern to that of E_{o1}. The distribution of design variables of the second stage is presented in Fig. 3-6. Based on the first cluster of Fig. 3-5, the optimization yields an average isentropic efficiency of

93.81%, peaking at 97.05% and an average volumetric efficiency of 83.62% with the highest of 86.99%.

Based on the results, the designer will obtain a range for every design parameter from which an acceptable design can be manufactured. However, it should be pointed out that the optimization is conducted by assuming the compressor is working under a constant operating speed and pressure ratio, making the optimum design only valid for the given working condition. In actual applications, the machine is generally required to handle various tasks while maintaining acceptable performance; therefore, it is necessary to evaluate the design under different working conditions. In the current work, the result whose design variables achieve the minimum E_{o1} and E_{o2} is considered as the optimum design.

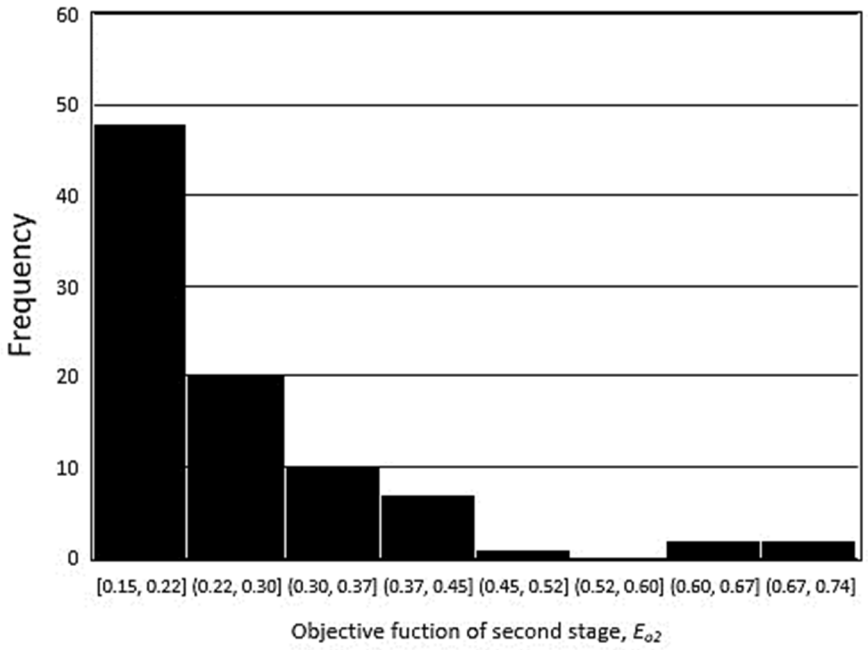

Fig. 3-5. Distribution of E_{o2}.

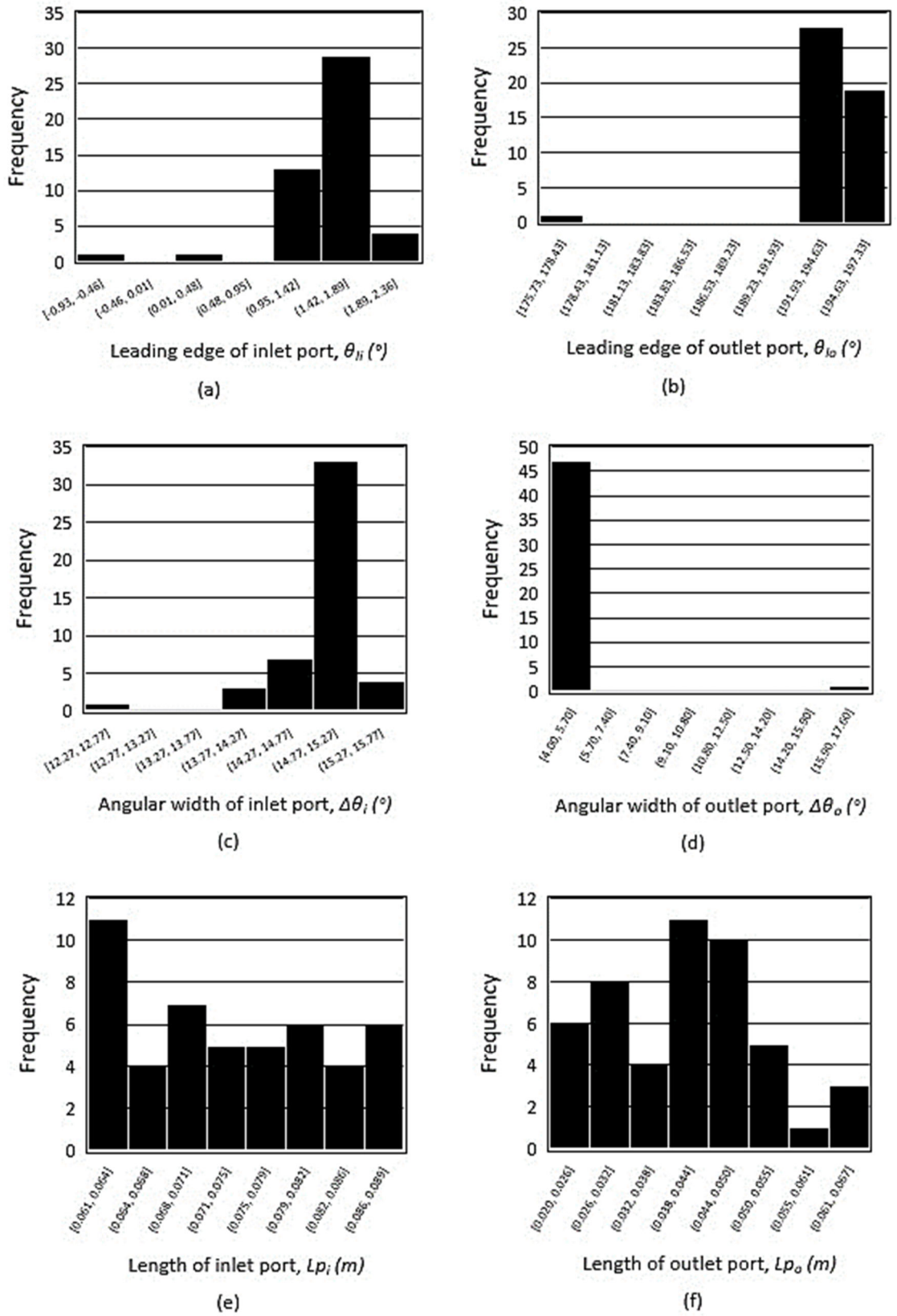

Fig. 3-6. Distribution of second stage design variables: (a) leading edge of inlet port; (b) leading edge of outlet port; (c) inlet port angular width; (d) outlet port angular width; (e) inlet port length; (f) outlet port length.

Fig. 3-7 shows the performance of the proposed optimum design with respect to different speeds of the crankshaft. It is found that the optimum design can exhibit relatively stable performance when the speed varies within a small percentage around that used in the optimization. Fig. 3-8 depicts the machine performance under different outlet pressure. It is obvious that the isentropic efficiency is not sensitive to the changes occurring in the outlet pressure, as reflected by the nearly flat curve in Fig. 3-8. For the volumetric efficiency, it decreases as the outlet pressure increases, but the reduction is not significant when the outlet pressure fluctuates around the value used in the optimization, thus suggesting a reasonable level of robustness. Based on Fig. 3-7 and Fig. 3-8, the best performance is found to be 99.09% for isentropic efficiency and 86.25% for volumetric efficiency, and they are compared with the reported performance of other types of rotary compressors to highlight the significant potential of the limaçon compressor, as shown in Table 3-4.

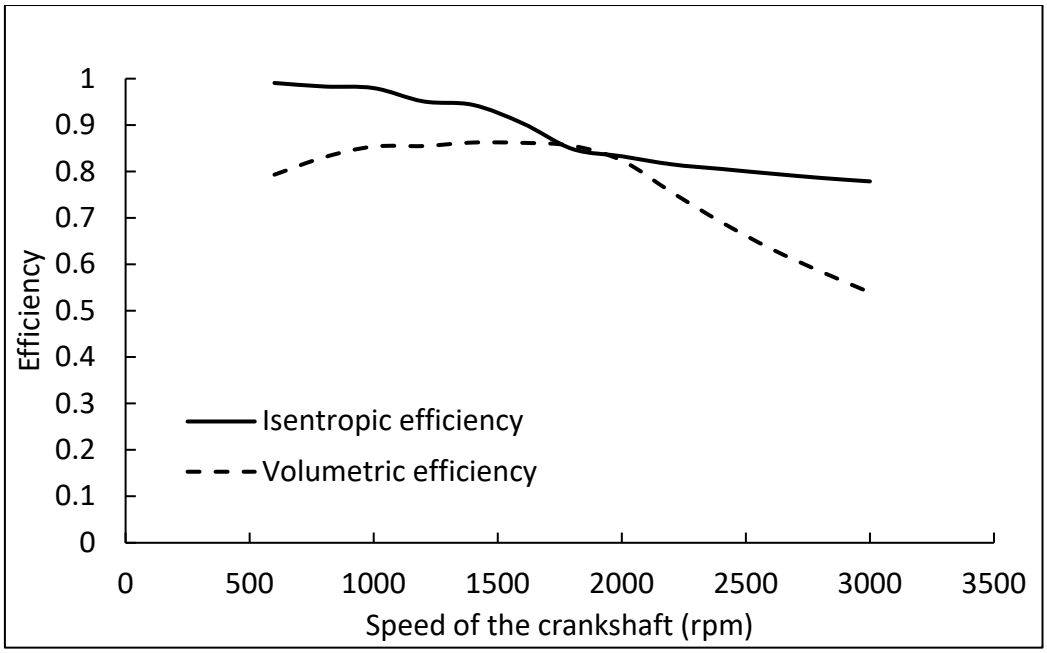

Fig. 3-7. Performance of the optimized compressor under different speeds (at P_o = 300 kPa).

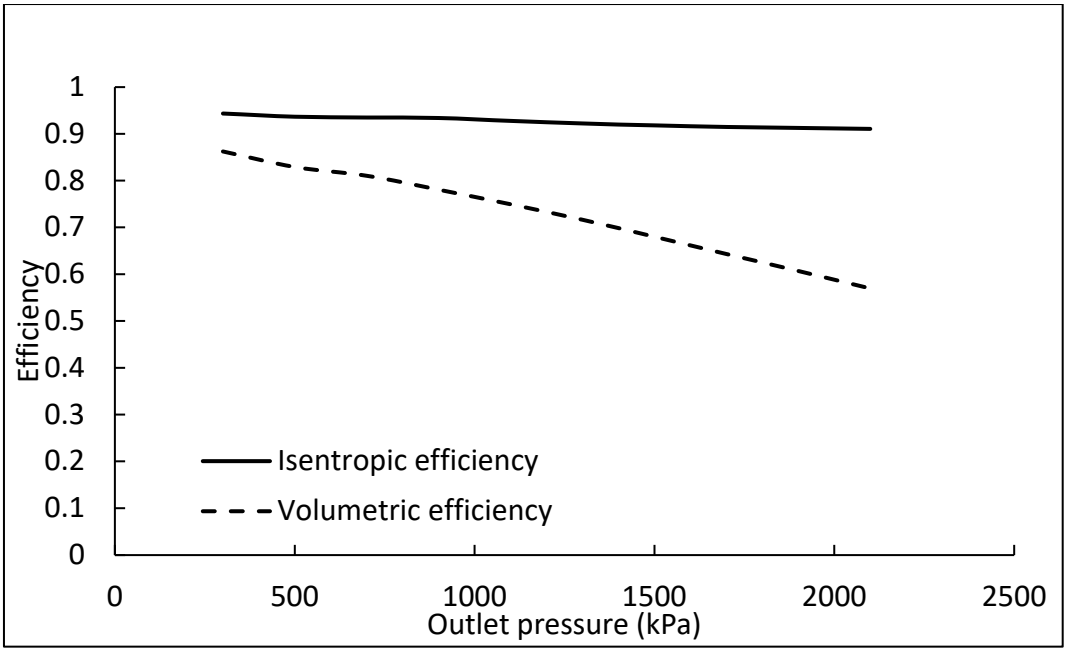

Fig. 3-8. Performance of the optimized compressor under different outlet pressure (at 1400 rpm).

Table 3-4. Performance comparison of other types of rotary compressors

Type	**Volumetric Dis-placement per Revolution**	**Working Fluid**	**Reported Maximum Performance**
Limaçon	$720\ \mathrm{cm}^3$	Air	$86.25\%\ (Volumetric)$, $99.09\%\ (Isentropic)$
Hermetic scroll (Cuevas et al., 2010)	-	R134A	$72\%\ (Isentropic)$
Swing-vane (Pan et al., 2019)	$10.49\ \mathrm{cm}^3$	R410A	$91\%\ (Volumetric)$, $79\%\ (Isentropic)$
Coupled-vane (Shakya and Ooi, 2020)	$44\ \mathrm{cm}^3$	Air	$79\%\ (Volumetric)$
Asymmetrical sliding vane (Wang et al., 2021)	$1.79\ \mathrm{cm}^3$	Air	$73.27\%\ (Volumetric)$

3.2. Conclusions

In this chapter, the Bayesian optimisation technique is applied in a two-stage optimisation process of the limaçon compressor, where the first stage determines the size of the compressor as per design requirements and the second stage aims to optimise the setting of the port to improve machine performance. The results of the numerical illustration prove the validity of the proposed method for the given design tasks with obtaining satisfactory machine performance. Additionally, a discussion is presented on the effects of operating parameters (pressure ratio and speed) on the performance of the optimized design. It is found that the optimized design exhibits relatively stable isentropic efficiency over the tested range of the speed and the outlet pressure, whereas volumetric efficiency can be maintained within an acceptable range when the operating condition is around that used in the optimization. This provides the designer useful information on the suitable operating conditions for the optimized design in real applications, and more importantly, it highlights the importance of the optimization process before the prototype is produced for a specific application.

3.3. References

Ooi, K. (2005). Design optimization of a rolling piston compressor for refrigerators. Applied Thermal Engineering, 25(5-6), 813-829. doi: 10.1016/j.applthermaleng.2004.07.017

Liu, Y., Hung, C., & Chang, Y. (2010). Design optimization of scroll compressor applied for frictional losses evaluation. *International Journal of Refrigeration*, *33*(3), 615-624. doi: 10.1016/j.ijrefrig.2009.12.015

Sultan, I., & Kalim, A. (2011). Improving reciprocating compressor performance using a hybrid two-level optimisation approach. *Engineering Computations*, *28*(5), 616-636. doi: 10.1108/02644401111141046

Phung, T. H., & Sultan, I. A. (2021). Geometric Design of the Limaçon-to-Circular Fluid Processing Machine. *Journal of Mechanical Design, 143*(10). doi:10.1115/1.4050383

Cavazzini, G., Giacomel, F., Ardizzon, G., Casari, N., Fadiga, E., Suman, A. & Pinelli, M. (2020). CFD-based optimization of scroll compressor design and uncertainty quantification of the performance under geometrical variations. *Energy*, *209*, 118382. doi: 10.1016/j.energy.2020.118382

Silva, E., & Dutra, T. (2021). Piston trajectory optimization of a reciprocating compressor. *International Journal of Refrigeration*, *121*, 159-167. doi: 10.1016/j.ijrefrig.2020.09.021

Aw, K. T., & Ooi, K. T. (2021). A Review on Sliding Vane and Rolling Piston Compressors. Machines, 9(6), 125. doi:10.3390/machines9060125.

Pelikan, M., Goldberg, D. E., & Cantú-Paz, E. (1999). BOA: The Bayesian optimization algorithm. In Proceedings of the Genetic and Evolutionary Computation Conference GECCO-99 (Vol. 1, pp. 525-532).

Snoek, J., Larochelle, H., & Adams, R. P. (2012). Practical Bayesian optimization of machine learning algorithms. In Proceedings of the Advances in neural information processing systems, 2951-2959.

Frazier, P. I. and Wang, J. (2016). Bayesian optimization for materials design. In Lookman, T., Alexander, F. J., and Rajan, K. (eds.), *Information Science for Materials Discovery and Design*, pages 45–75. Springer.

Torun, H., Swaminathan, M., Kavungal Davis, A., & Bellaredj, M. (2018). A Global Bayesian Optimization Algorithm and Its Application to Integrated System Design. *IEEE Transactions on Very Large Scale Integration (VLSI) Systems*, *26*(4), 792-802. doi: 10.1109/tvlsi.2017.2784783

Griffiths, R. R., & Hernández-Lobato, J. M. (2017). Constrained Bayesian optimization for automatic chemical design. arXiv preprint arXiv:1709.05501.

Letham, B., Karrer, B., Ottoni, G., & Bakshy, E. (2019). Constrained Bayesian Optimization with Noisy Experiments. *Bayesian Analysis*, *14*(2). doi: 10.1214/18-ba1110

Hickish, B., Fletcher, D., & Harrison, R. (2019). Investigating Bayesian Optimization for rail network optimization. *International Journal of Rail Transportation*, *8*(4), 307-323. doi: 10.1080/23248378.2019.1669500

Sultan, I. A. (2005). The Limaçon of Pascal: Mechanical Generation and Utilization for Fluid Processing. *Proceedings of the Institution of Mechanical Engineers, Part C: Journal of Mechanical Engineering Science, 219*(8), 813-822. doi: 10.1243/095440605x31698

Sultan, I. A. (2006). Profiling Rotors for Limaçon-to-Limaçon Compression-Expansion Machines. *Journal of Mechanical Design*, *128*(4), 787-793. doi: 10.1115/1.2202877

Sultan, I. A. (2007). A Surrogate Model for Interference Prevention in the Limaçon-to-Limaçon Machines. Engineering Computations, 24(5), 437-449.

Sultan, I. A. (2008). Inverse geometric design for a class of rotary positive displacement machines. *Inverse Problems in Science and Engineering, 16*(2), 127-139. doi: 10.1080/17415970601162164

Sultan, I. A, & Schaller, C. (2011). Optimum Positioning of Ports in the Limaçon Gas Expanders. *Journal of Engineering for Gas Turbines and Power*, *133*(10). doi: 10.1115/1.4003195

Sultan, I. A. (2012). Optimum design of limaçon gas expanders based on thermodynamic performance. *Applied Thermal Engineering*, *39*, 188-197. doi: 10.1016/j.applthermaleng.2012.01.039

Phung, T., Sultan, I., & Appuhamillage, G. (2018). On the apex seal analysis of limaçon positive displacement machines. *Mechanism and Machine Theory*, *127*, 126-145. doi: 10.1016/j.mechmachtheory.2018.05.003

Tuymer, W.J. and Machu, E.H. (2001), “Compressor valves”, in Hanlon, P.C. (ed.), *Compressor Handbook*, McGraw-Hill, New York, NY.

Rasmussen, C. E. and Williams, C. K. I. (2006) Gaussian Processes for Machine Learning. MIT Press, Cambridge, Massachusetts.

Noè, U., & Husmeier, D. (2018). On a new improvement-based acquisition function for bayesian optimization. arXiv preprint arXiv:1808.06918.

Cuevas, C., Lebrun, J., Lemort, V., & Winandy, E. (2010). Characterization of a scroll compressor under extended operating conditions. *Applied thermal engineering*, *30*(6-7), 605-615.

Pan, X., Tian, C., Wu, S., Xing, Z., & Pan, S. (2019). Experimental study of the swing compressor with no valves. *Applied Thermal Engineering*, *163*, 114274. doi: 10.1016/j.applthermaleng.2019.114274

Shakya, P., & Ooi, K. (2020). Introduction to Coupled Vane compressor: Mathematical modelling with validation. *International Journal of Refrigeration*, *117*, 23-32. doi: 10.1016/j.ijrefrig.2020.01.027

Wang, J., Liu, Y., Chen, Z., & Tan, Q. (2021). Geometric model and pressurization analysis on a novel sliding vane compressor with an asymmetrical cylinder profile. *International Journal of Refrigeration*, *129*, 175-183. doi: 10.1016/j.ijre

Chapter 4. A comparative study of two embodiments of the limaçon rotary compressor based on theoretical modelling of apex seal dynamics and leakage[††]

4.1. Abstract

As an emerging technology, the limaçon rotary compressor possesses great potential for fluid-processing applications. However, the technology and associated cost required to fabricate the limaçon machine could sometimes be beyond the capability of some manufacturers. To reduce the production cost, circolimaçon embodiment whose rotor and housing are constructed of circular arcs has been proposed. This paper is intended to investigate the viability of the circolimaçon embodiment of limaçon technology based on sealing performance. A nonlinear three-degree of freedom model is presented to describe the dynamic behaviour of the apex seal during the machine operation. Additionally, the leakage through the seal-housing gap is formulated by considering the inertia and viscous effects on the flow. A numerical illustration is offered to compare the performance of the circolimaçon embodiment with that of the limaçon-to-limaçon (L2L) type machine at different pressure ratios and operating speeds. The effect of the limaçon aspect ratio on the apex seal dynamics is also investigated. Based on the results, it is found that the circolimaçon embodiment exhibits comparable performance to the L2L-type machine, despite having more significant seal vibrations. The differences in the volumetric and isentropic

[††] This chapter has been published: Lu, K, Sultan, I. A., and Phung, T. H., (2022) " A comparative study of two embodiments of the limaçon rotary compressor based on theoretical modelling of apex seal dynamics and leakage". *International Journal of Refrigeration*. https://doi.org/10.1016/j.ijrefrig.2022.10.004

efficiencies between the two machines are found within 8% and 3%, respectively. Additionally, it is also discovered that the circolimaçon compressor with a small capacity undergoes a lower level of seal dynamics, suggesting better machine reliability.

Keywords: Positive displacement compressor; Compressor performance; Circolimaçon; Apex seal; Seal dynamics; Leakage.

4.2. Introduction

By virtue of their compact size and less susceptibility to vibration, rotary compressors have received particular popularity in many fluid-processing applications, ranging from domestic refrigeration to industrial gas transmission. In a recent market analysis, rotary compressors accounted for the largest share of the global compressor market and are anticipated to remain the leader through 2028 (Grand View Research, 2021). In this context, substantial research efforts have been devoted to improving the performance of rotary compressors. The work by Ooi (2005) presents an example of such effort as the author optimised the geometric parameters that can reduce the mechanical loss of the rolling piston compressor up to 50%, thereby increasing the coefficient of performance by 14%. Blunier et al. (2009) proposed a reference frame to describe the scroll symmetry of scroll compressors, which could describe the chamber volume without considering any special cases for initial involute angles. Liu et al. (2010) optimised the bearing components of the scroll compressor based on the gradient-search method. Based on the result, the author reported that the frictional losses at bearing components could be reduced by at least 14.1% after optimisation. Stosic (2015) utilised the quasi-one-dimensional model and the three-dimensional (3D) computational fluid dynamics (CFD) to analyse the heat transfer that occurred in screw compressors. Through the analysis, the author suggested

that implementing a proper cooling method could bring down the maximum rotor temperature from 700K to 350K, thus enhancing the reliability of machine components. Noh et al. (2016) investigated the effect of the cylinder slenderness ratio on the performance of the rolling piston compressor. The authors found that a smaller cylinder slenderness ratio could increase the volumetric efficiency by 6.3%, resulting in a 3.7% rise in the overall efficiency. In a recent study, Cavazzini et al. (2020) analysed the effect of geometric parameters on the performance of the scroll compressor. The authors discovered that the machine performance was mainly affected by three geometric parameters: the size of the discharge port, the number of coils, and the radius of orbiting scroll.

Although the industrial and research effort still concentrates on such well-established technologies as the vane- and screw-type devices, the ever-changing needs for applications have pushed for the emergence of many novel designs of rotary compressors. For example, Shin et al. (2019) proposed the dual cylinder design that utilises the inner space of the rotor as an additional working chamber. Compared to the conventional rolling piston compressor, the proposed design is able to reduce mechanical losses and increase compressor efficiency by up to 16.64%. Gu et al. (2021) introduced the rotating cylinder mechanism by which the friction losses at the vane tips between the rotor and cylinder can be reduced to 0.25% and 10.23%, respectively. In addition, the maximum volumetric and isentropic efficiencies of the proposed design could reach 97.14% and 90.33%, respectively. In their recent works, Lu et al. (2021; 2022) mathematically modelled a class of rotary compressors that features the profiles of the rotor and housing generated based on the limaçon of Pascal. The authors parametrically analysed the effects of various fac-

tors, such as operating speed and pressure ratio, on machine performance, and they developed a two-stage optimisation procedure based on the Bayesian method to optimise the geometry of the inlet and outlet ports.

In fact, the potential of the limaçon technology applied in fluid machinery was previously discussed by Sultan (2005). Compared to other types of rotary machines, the limaçon machine has clear geometric parameters that control the machine performance, and this benefits the optimisation procedure. The work of Sultan and Schaller (2011) is such an example in which geometric parameters of the ports were used as design variables to optimise the performance of limaçon gas expanders. In the past, when manufacturing technology was not so advanced, manufacturing a limaçon machine could have been quite a task. Nowadays, however, manufacturing technology has progressed to the point where producing these machines does not present any technical challenges. The limaçon machine whose rotor and housing are developed from the limaçon curve is referred to as the limaçon-to-limaçon (L2L) machine, and one noticeable advantage of the L2L machine is that the gap between the rotor apex and the housing remains constant, enabling excellent sealing performance as shown by the work of Phung et al. (2018). Despite being achievable, the cost and technology required to machine the accurate limaçon profile may still be beyond the capability of some manufacturers. Therefore, Sultan (2008) suggested substituting the limaçon curves of the housing and the rotor with circular profiles, which can simplify manufacturing and reduce production costs. This idea has been elaborated by the work of Phung and Sultan (2018; 2021) as they proposed a design variant known as the limaçon-to-circular machine, in which the rotor profile is based on the circular curve.

Another alternative is the circolimaçon embodiment, in which its housing and rotor are constructed of circular curves. Sultan (2008) discussed the geometric and volumetric

aspects of this type of machine. However, the feasibility of the circolimaçon embodiment in fluid-processing applications has yet been discussed. Hence, the work presented in this paper is intended to investigate the potential of the circolimaçon machine for use as a compressor based on the sealing performance. A dynamic model is presented to describe the vibration of the apex seal, and the leakage past through the seal gap is modelled with considering the viscous and inertia effects on the flow. The sealing performance of the circolimaçon embodiment is compared with that of the L2L-type machine at different pressure ratios and operating speeds, and the effect of the limaçon aspect ratio on the machine reliability is also investigated.

The next section features geometric characteristics of circolimaçon embodiment of the limaçon technology.

4.3. Background on the limaçon technology

4.3.1. Geometric characteristics

The limaçon technology is characterised by its profile and operation based on a mathematical curve known as the limaçon of Pascal. Fig. 4-1 shows an illustration of the limaçon machine (L2L-type). During the operation, the chord, $p_l p_t$, is made to slide and rotate about the limaçon pole, o, and the path of the midpoint, m, of the chord is referred to as the housing base circle whose radius is r. To readily describe the kinematics of the limaçon motion, a stationary frame, $X_o Y_o$, and a moving frame, $X_m Y_m$, are introduced at points o and m, respectively. The sliding distance, s, measured from o to m along the X_m-axis is then expressed as a function of the angular displacement of the chord, $\theta \in [0, 2\pi]$, measured from X_o- to the X_m- axis,

$$s = 2r \sin\theta \tag{4-1}$$

The radial distance of the limaçon housing, R, measured from o to the chord apices can be obtained as follows,

$$R = 2r\sin\theta + L \tag{4-2}$$

where L is the half-length of the chord.

The limaçon profile of the machine housing is the trajectory of the chord leading apex, p_l (or trailing apex, p_t,), which can be described with respect to X_oY_o frame as,

$$\begin{cases} x_{p_l} = R\cos\theta = r\sin 2\theta + L\cos\theta \\ y_{p_l} = R\sin\theta = r - r\cos 2\theta + L\sin\theta \end{cases} \tag{4-3}$$

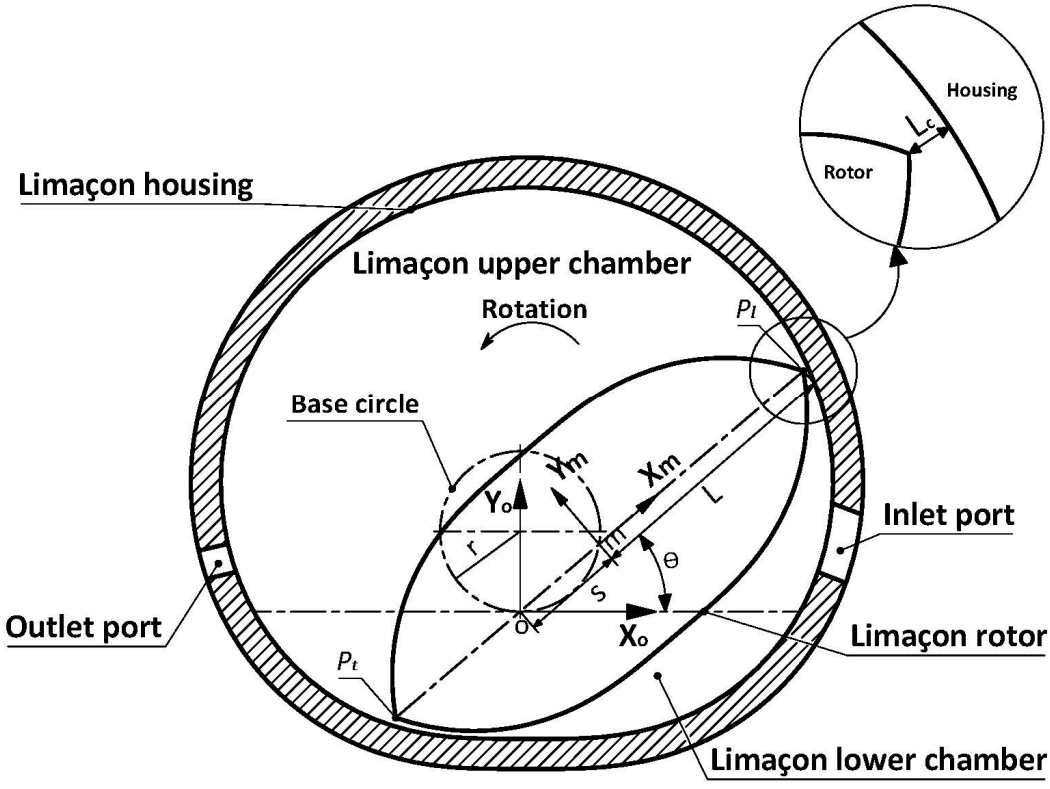

Fig. 4-1. A limaçon-to-limaçon machine.

It is worth mentioning that the shape of the limaçon profile is determined by the limaçon aspect ratio, β, which is defined as the ratio of the radius of the base circle to the chord half-length,

$$\beta = \frac{r}{L} \tag{4-4}$$

With the increase in the limaçon aspect ratio, the limaçon curve will exhibit a flatter bottom portion as illustrated in Fig. 4-2. However, the limaçon aspect ratio must be kept below 0.25 in order to produce a limaçon curve that is free of dimples and kinks, which is suitable for fluid-processing applications.

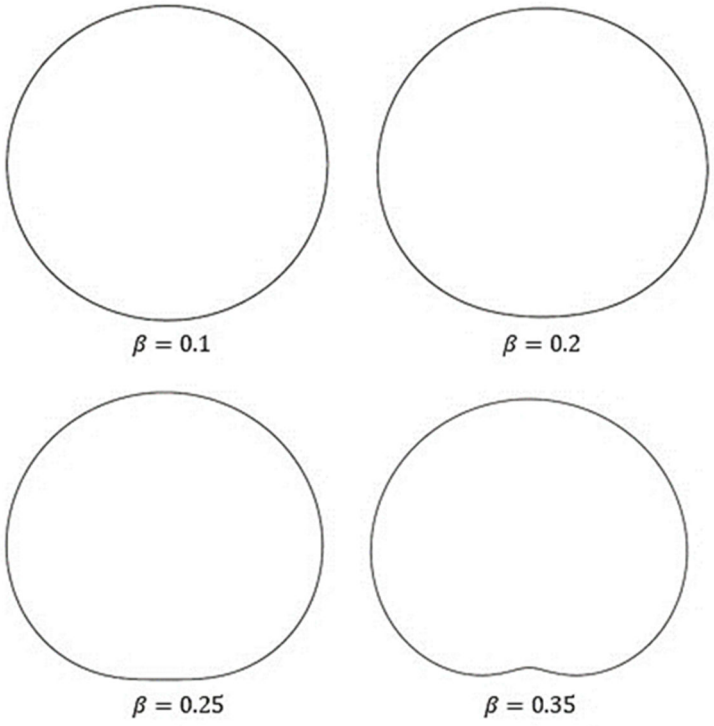

Fig. 4-2. Limaçon curves based on different limaçon aspect ratios.

The rotor profile is developed from the lower portion of the housing profile (i.e., $\theta \in [\pi, 2\pi]$) and mirrored about the chord. However, this results in rotor-housing interference, which severely affects the machine performance. Therefore, it is necessary to introduce the apex clearance, L_c, to prevent such an interference issue, the parametric form of the rotor can then be obtained as follows,

$$\begin{cases} x_r = r_r \sin 2\theta_r + (L - L_c)\cos\theta_r \\ y_r = r_r - r_r \cos 2\theta_r + (L - L_c)\sin\theta_r \end{cases} \tag{4-5}$$

where r_r is the radius of the rotor base circle, $\theta_r \in [\pi, 2\pi]$ is the angle measured from X_m-axis to any points on the rotor profile. Sultan (2006) suggests that the value of r_r can be determined by using the equation below,

$$\frac{r_r}{L} = \begin{cases} \dfrac{a\beta(1-C_L)}{\sqrt{1-4\beta^2}}, & a \geq 1 \\ \beta, & a < 1 \end{cases} \tag{4-6}$$

where $C_L = \frac{L_c}{L}$ is the clearance ratio, and the term a in equation (4-6) is referred to as the rotor design factor, which assists to select a proper apex clearance to prevent rotor-housing interference. When the value of a is set equal to or greater than 1, a small apex clearance will be enough to prevent the interference issue. However, based on equations (4-4) and (4-6), the base circle of the rotor shares the same radius as that of the housing when a is set less than 1. In this case, a relatively larger apex clearance needs to be applied. It is worth noting here that the lenticular profile of the rotor geometrically divides the working chamber into two parts, namely the upper and lower chamber, as shown in Fig. 4-1. This indicates the double-acting nature of the limaçon technology, which can execute two discharge strokes in one revolution of the crankshaft.

4.3.2. The circolimaçon machine

The circolimaçon design shares the same operating characteristics as the L2L-type machine, but the profiles of its housing and rotor are developed from circular arcs rather than the limaçon curve. As shown in Fig. 4-3, the centre of circular profiles for the housing and the rotor locates at C_h and C_r, respectively. It should be mentioned that C_h falls above the limaçon pole and it is fixed at the point where the Y_o-axis intersects with the base circle, while the actual position of C_r varies with the rotation of the rotor. The radius of housing, R_h, and rotor, R_r, can be calculated as shown in equation (4-7),

$$\begin{cases} R_h = L\sqrt{1+4\beta^2} \\ R_r = L(1-C_L)\sqrt{1+4\beta^2 a^2} \end{cases} \tag{4-7}$$

where a is the rotor design factor assigned as 1 in this investigation.

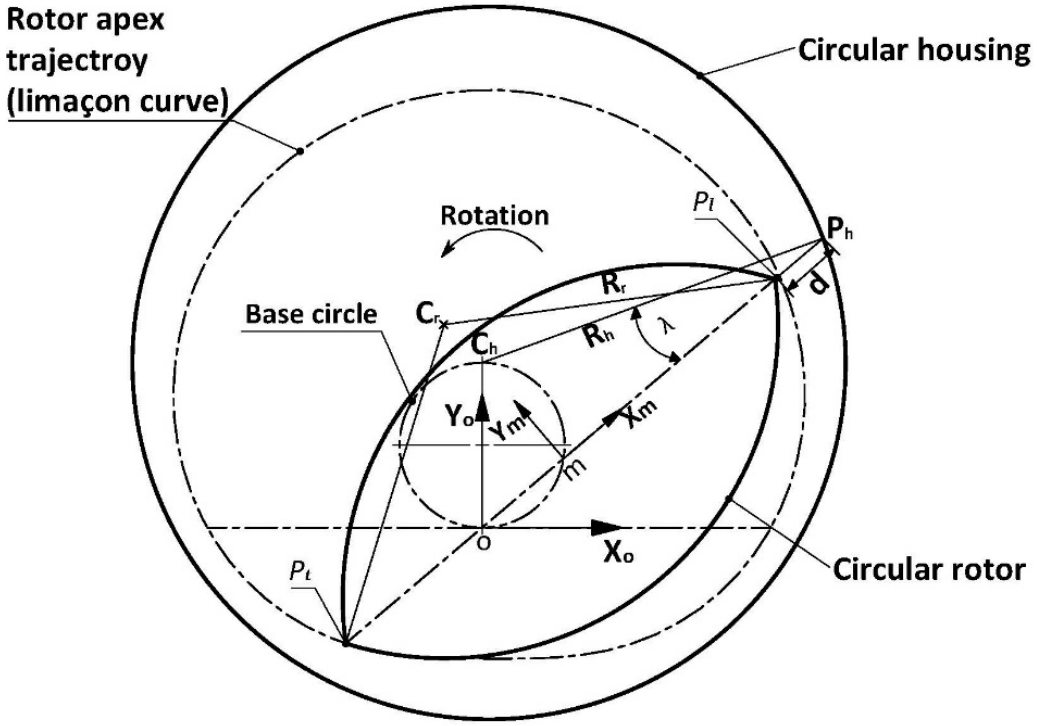

Fig. 4-3. An illustration of the circolimaçon machine.

For fluid-processing applications, the volume of the working fluid, V_c, that the circolimaçon machine processes in one compression stroke can be expressed in the following form,

$$V_c = H(A_b - A_r) \tag{4-8}$$

where H is the axial length of the housing, and A_b and A_r are respectively the area of the housing and rotor section falls below the X_m-axis, which are obtained as shown in the equation below,

$$\begin{cases} A_b = R_h^2\left(\dfrac{\pi}{2} - \lambda\right) - 2r(L - L_c + d)\cos\theta \\ A_r = R_r^2\left(\dfrac{\pi}{2} - \tan^{-1} 2\beta a\right) - 2a\beta L^2(1 - C_L) \end{cases} \tag{4-9}$$

where d denotes the distance between the rotor apex and the point P_h, at which the rotor chord intersects with the housing, and the expression of d is givens as,

$$d = L\left(C_L - 1 + \sqrt{1 + 4\beta^2 \sin^2\theta}\right) \tag{4-10}$$

The term, λ, in equation (4-9) is the angle between $p_l p_t$ and $P_h C_h$, which can be expressed as follows,

$$\lambda = \tan^{-1}\left(\frac{2\beta\cos\theta}{\sqrt{1+4\beta^2\sin^2\theta}}\right) \tag{4-11}$$

Combining equations (4-9) to (4-11), expressions of A_b and A_r can be rewritten as,

$$\begin{cases} A_b = L^2\left[(1+4\beta^2)\left(\frac{\pi}{2}-\lambda\right) - 2\beta\cos\theta\sqrt{1+4\beta^2\sin^2\theta}\right] \\ A_r = L^2(1-C_L)^2\left[(1+4\beta^2 a^2)\left(\frac{\pi}{2}-\tan^{-1}2\beta a\right) - 2\beta a\right] \end{cases} \tag{4-12}$$

The swept volume of the circolimaçon machine, V_s, can then be calculated by subtracting the minimum volume, $V_{c|\theta=0}$, from the maximum volume, $V_{c|\theta=\pi}$, as follows,

$$V_s = V_{c|\theta=\pi} - V_{c|\theta=0} = 2HL^2[(1+4\beta^2)\tan^{-1}2\beta + 2\beta] \tag{4-13}$$

Equation (4-13) shows that the ideal capacity of the machine will depend on the limaçon aspect ratio, β, when the machine size (as determined by H and L) is fixed. This highlights a distinguishing feature of the limaçon technology, which is the ability to achieve larger capacity within a small machine size. In addition, clear geometric parameters, as reflected in equation (4-13), control the volumetric performance of the limaçon technology, which lends the optimisation procedure to be easily developed.

4.4. Dynamic model of apex seal

It is noted that the apex gap, d, varies with the angular displacement of the chord as indicated by equation (4-10), and this differs from the situation in the L2L-type device in which the apex gap maintains constant. Therefore, it can be expected that the seal dynamic behaviour of the circolimaçon embodiment will be different from that of the L2L machine.

Fig. 4-4 depicts the kinematics of the apex seal applied to the circolimaçon machine. The apex seal is modelled as the spring-mass-damper system in which the spring is attached to the inner end of the groove and the seal. As shown in Fig. 4-4, w_g and w_s are widths of the groove and the seal, respectively. L_s signifies the length of the seal and the term, z, is the truncation distance, which is expressed as,

$$z = L(1 - C_L) - \sqrt{R_r^2 - \left(2a\beta L(1 - C_L) + \frac{w_g}{2}\right)^2} \tag{4-14}$$

To readily describe the kinematics of the seal, two frames, XY and X_sY_s, are introduced at the geometric centre, O_g, of the groove and the centre of gravity, C, of the seal, respectively. It should be pointed out that O_g is also the initial position of C, and the position of C can then be described by a position vector, $\overrightarrow{r_c}$, with respect to the XY-frame,

$$\overrightarrow{r_c} = \begin{bmatrix} x \\ y \end{bmatrix} \tag{4-15}$$

The XY and X_sY_s frames can be related by using the frame transformation equation as follows,

$$\begin{bmatrix} \hat{X}_s \\ \hat{Y}_s \end{bmatrix} = \begin{bmatrix} \cos\phi & -\sin\phi \\ \sin\phi & \cos\phi \end{bmatrix} \begin{bmatrix} \hat{X} \\ \hat{Y} \end{bmatrix} \tag{4-16}$$

where $\begin{bmatrix} \hat{X}_s \\ \hat{Y}_s \end{bmatrix}$ and $\begin{bmatrix} \hat{X} \\ \hat{Y} \end{bmatrix}$ are unit vectors along the seal and the groove frames, respectively, and ϕ signifies the angular displacement measured from X- to X_s-axis in a right-handed sense.

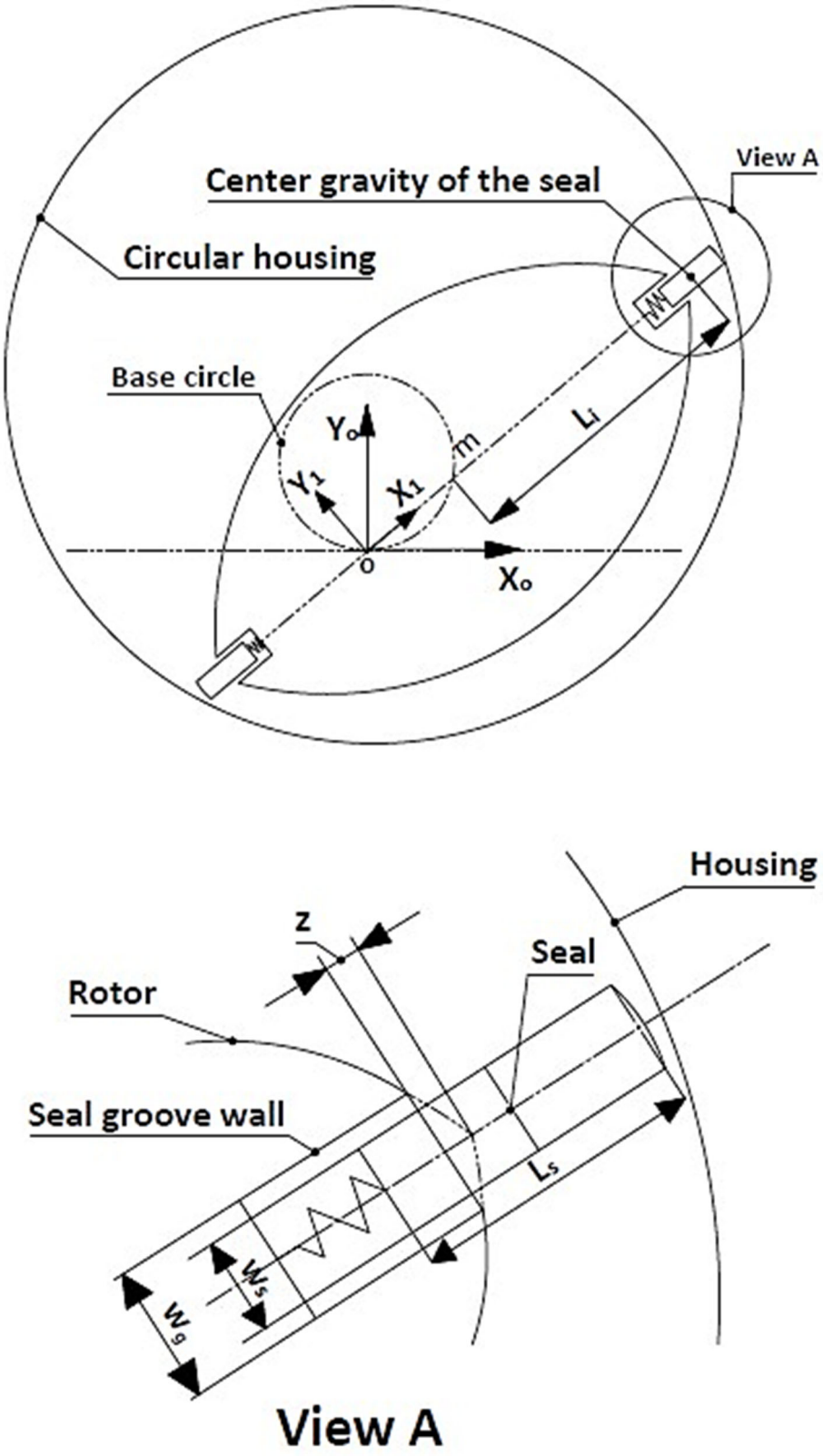

Fig. 4-4. Kinematics of the apex seal.

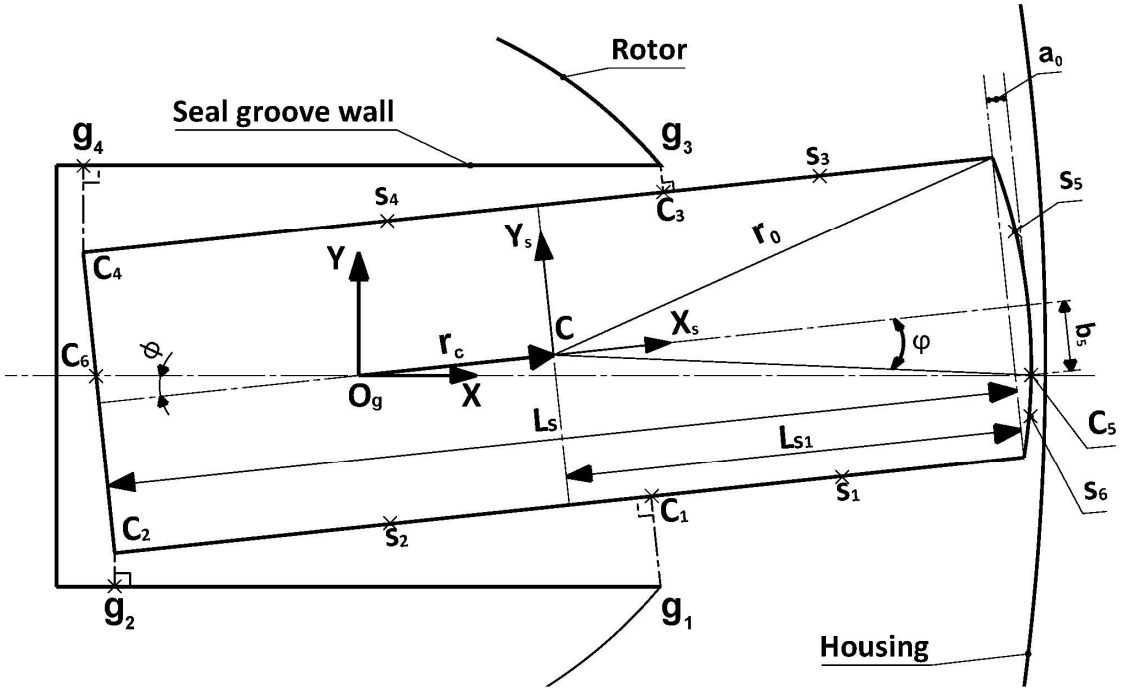

Fig. 4-5. Dynamics of the apex seal.

As shown in Fig. 4-5, the contact points on the groove are denoted as g_i $(i = 1, 2, 3, 4)$, and the corresponding points on the seal are denoted as c_i. Points c_5 and c_6 represent points where the seal touches the machine housing and the spring, respectively. The points that subject forces due the pressure are labelled from s_1 to s_6. In the circolimaçon machine, the kinematics of these points will exhibit similar patterns to that of the L2L machine, which was investigated by Phung et al. (2018). However, the interaction between the seal tip and the housing at the point c_5 is expected to be different as the apex gap that exists in the circolimaçon machine varies with the rotation of the rotor. The position of c_5 in XY frame can be expressed as,

$$\overrightarrow{r_{c_5}} = \vec{r_c} + (L_{s1} - a_0)\hat{X}_s + b_5\hat{Y}_s \tag{4-17}$$

which can be rewritten as,

$$\overrightarrow{r_{c_5}} = (x + (L_{s1} - a_0)\cos\phi - b_5\sin\phi)\hat{X} + (y + (L_{s1} - a_0)\sin\phi + b_5\cos\phi)\hat{Y} \tag{4-18}$$

where L_{s1} is the half-length of L_s measured from C to the outer edge of the seal; a_0 and b_5 are shown in Fig. 4-4 and can, respectively, be obtained from the equation below,

$$\begin{cases} a_0 = r_0(1 - \cos\varphi) \\ b_5 = r_0 \sin\varphi \end{cases} \tag{4-19}$$

In equation (4-19), r_0 is the radius of the curved face of the seal outer edge, and φ is the angle measured from the seal centre line to the radial line connecting r_o and c_5. Noting that point c_5 always sits on the X-axis, making the Y-axis component to be zero. Therefore, the Y-axis component in equation (4-18) can be written as,

$$y + (L_{s1} - a_0)\sin\phi + b_5\cos\phi = 0 \tag{4-20}$$

Combining equations (4-19) and (4-20), φ can be expressed as,

$$\varphi = \sin^{-}\left[\left(1 - \frac{L_{s1}}{r_0}\right)\sin\phi - \frac{y}{r_0}\right] - \phi \tag{4-21}$$

Thus, the position of c_5 can then be simplified as

$$\overrightarrow{r_{c_5}} = (x + (L_{s1} - a_0)\cos\phi - b_5\sin\phi)\hat{X} \tag{4-22}$$

To determine whether the seal and the machine housing come into contact, the position of c_5 needs to be compared to its initial position, and the difference, Δx_{c_5}, is calculated as,

$$\Delta x_{c_5} = x + (L_{s1} - a_0)\cos\phi - b_5\sin\phi - L_{s1} - \Delta d + \delta_w \tag{4-23}$$

where δ_w is the initial deflection of the machine housing and Δd is the change in the apex gap, d, compared to its value, d_o, obtained at the angle where the suction stroke is initiated, which can be expressed as,

$$\Delta d = d - d_o \tag{4-24}$$

If a positive value ($\Delta x_{c_5} > 0$) is obtained from the equation (4-23), it indicates that the seal has contacted the machine housing, thereby resulting in contact force, F_w, from the machine housing. Of note that is the contact force F_w acting on c_5 consists of an elastic

force, F_s, and a damping force, F_d. The elastic force F_s can be obtained from the equation below,

$$F_s = k_w \Delta x_{c_5} \tag{4-25}$$

where k_w is the stiffness of the machine housing.

The damping force F_d depends on the velocity at the point c_5, which takes the form as,

$$\overrightarrow{v_{c_5}} = \overrightarrow{v_c^1} + \vec{\omega} \times \overrightarrow{\Delta \dot{d}} + \left(\vec{\omega} + \vec{\dot{\phi}}\right) \times \left[(L_{s1} - a_0)\hat{X}_s + b_5 \hat{Y}_s\right] \tag{4-26}$$

where $\overrightarrow{v_c^1}$ is the velocity of point C with respect to the base frame, $X_1 Y_1$, whose origin is the same as the $X_o Y_o$ frame but rotates with the rotor at a constant angular velocity, ω, as shown in Fig. 4-4. The expression of $\overrightarrow{v_c^1}$ is given as,

$$\overrightarrow{v_c^1} = (2r\omega \cos\theta + \dot{x} - \omega y)\hat{X}_1 + \left(2r\omega \sin\theta + \dot{y} + \omega(x + L_i)\right)\hat{Y}_1 \tag{4-27}$$

where $\hat{X}_1$ and $\hat{Y}_1$ are unit vectors along X_1 and Y_1 direction, respectively, and the symbol $(\dot{})$ denotes differentiation with respect to time. L_i is the distance between the midpoint, m, of the rotor chord to the point C at the initial position, which can be calculated as,

$$L_i = L + d_o - L_{s1} + \delta_w \tag{4-28}$$

Equation (4-26) can be rewritten with respect to the XY frame as,

$$\overrightarrow{v_{c_5}} = v_{c_{5_x}} \hat{X} + v_{c_{5_y}} \hat{Y} \tag{4-29}$$

where the velocity components, $v_{c_{5_x}}$ and $v_{c_{5_y}}$, are given as follows,

$$\begin{cases} v_{c_{5_x}} = \dot{x} + \omega(2r\cos\theta - y - \dot{\Delta d}) - \left(\omega + \dot{\phi}\right)\left((L_{s1} - a_0)\sin\phi + b_5\cos\phi\right) \\ v_{c_{5_y}} = \dot{y} + \omega(2r\sin\theta + L_i + x) + \left(\omega + \dot{\phi}\right)\left((L_{s1} - a_0)\cos\phi - b_5\sin\phi\right) \end{cases} \tag{4-30}$$

It should be pointed out that the sign convention and magnitude of the damping force, F_d, is determined by $v_{c_{5_x}}$ shown in equation (4-30). Such a condition can be expressed as follows,

$$F_d = \begin{cases} C_w v_{c_{5_x}}, & v_{c_{5_x}} > 0 \\ 0, & v_{c_{5_x}} \leq 0 \end{cases} \tag{4-31}$$

where C_w is the damping coefficient of the machine housing.

Consequently, if $\Delta x_{c_5} > 0$, the contact force, F_w, from the machine housing can then be expressed by combining equations (4-25) and (4-31) as follows,

$$F_w = \begin{cases} k_w \Delta x_{c_5} + C_w v_{c_{5_x}}, & v_{c_{5_x}} > 0 \\ k_w \Delta x_{c_5}, & v_{c_{5_x}} \leq 0 \end{cases} \tag{4-32}$$

The force, $\overrightarrow{F_{c_5}}$, acting on the seal at c_5 and the moment, $\overrightarrow{M_{c_5}}$, about the centre of gravity can then be found as,

$$\begin{cases} \overrightarrow{F_{c_5}} = \overrightarrow{F_{c_{5x}}} + \overrightarrow{F_{c_{5y}}} \\ \overrightarrow{M_{c_5}} = \overrightarrow{r_{c_5}} + \overrightarrow{F_{c_5}} \end{cases} \tag{4-33}$$

where the force components, $\overrightarrow{F_{c_{5x}}}$ and $\overrightarrow{F_{c_{5y}}}$, are calculated from the equation below,

$$\begin{cases} \overrightarrow{F_{c_{5x}}} = -F_w \hat{X} \\ \overrightarrow{F_{c_{5y}}} = -F_w \dfrac{(\tan\lambda) - \mu}{1 + \mu(\tan\lambda)} \hat{Y} \end{cases} \tag{4-34}$$

where μ signifies the coefficient of friction between the seal and the machine housing.

The forces acting on points, other than c_5, of the seal and the corresponding moments about the seal centre gravity can be calculated by using the seal model proposed by Phung et al. (2018). To obtain the seal displacement (x, y, and ϕ) at each rotor angular displacement, θ, a general equation of motion is expressed as shown in equation (4-35),

$$\begin{bmatrix} m_s & 0 & 0 \\ 0 & m_s & 0 \\ 0 & 0 & I_c \end{bmatrix} \begin{bmatrix} \ddot{X}_1 \\ \ddot{Y}_1 \\ \ddot{\phi} \end{bmatrix} = \begin{bmatrix} \sum F_x \\ \sum F_y \\ \sum M_c \end{bmatrix} \tag{4-35}$$

where m_s is the mass of the seal, I_c is the mass moment of inertial about the centre of gravity, $\sum F_x$ and $\sum F_y$ denote the sum of forces acting on the seal in the x- and y-direction, respectively, and $\sum M_c$ is the sum of moments about the seal centre of gravity, $\ddot{\phi}$ is the

angular acceleration of the seal, $\ddot{X}_1$ and $\ddot{Y}_1$ are the acceleration of the seal with respect to the X_1Y_1 frame, which can be, respectively, found as follows,

$$\begin{cases} \ddot{X}_1 = \ddot{x} - 2\omega\dot{y} - \omega^2(4r\sin\theta + L_i + x) \\ \ddot{Y}_1 = \ddot{y} + 2\omega\dot{x} + \omega^2(4r\cos\theta - y) \end{cases} \quad (4\text{-}36)$$

4.5. Leakage through the seal-housing gap

With the application of the apex seal, the leakage through the apex clearance can be reduced considerably. However, if the seal moves momentarily away from the machine housing (i.e., $\Delta x_{c5} < 0$ obtained from equation (4-23)), a gap will exist between the seal tip and the machine housing, resulting in leakage due to the pressure difference between the two chambers, as shown in Fig. 4-6.

The leakage path can be approximated as the flow channel shown in Fig. 4-6, in which a frame, X_LY_L, attached to the housing is introduced. As shown in Fig. 4-6, w_L signifies the projection of the seal width along X_L direction, and h_L denotes the height of the leakage path at any x_L. This section is intended to present the procedure introduced in this paper to calculate the leakage past the apex seal. To model the leakage flow in the current study, some assumptions have been employed, which are:

- Leakage flow is adiabatic and two-dimensional
- Steady state
- State properties are uniform in the y-direction and only vary in the x-direction.

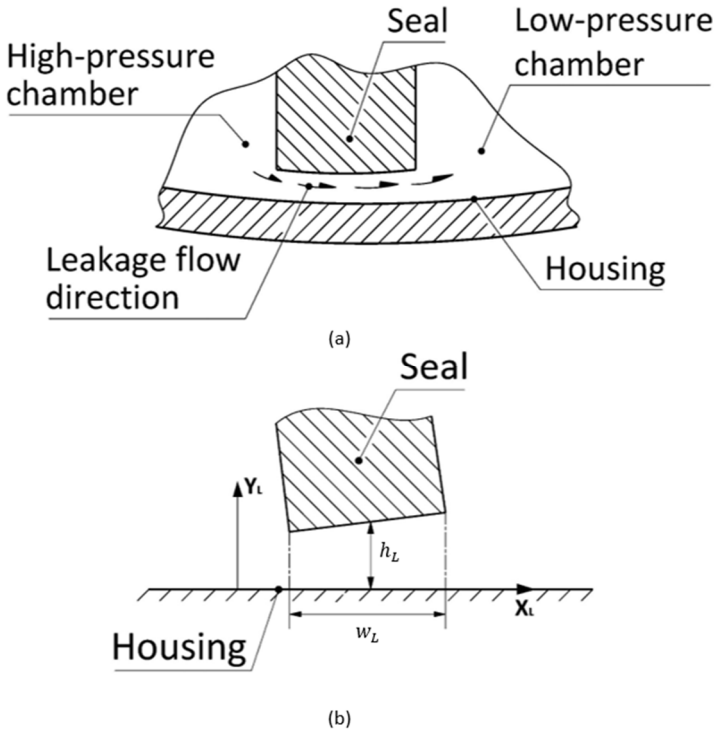

Fig. 4-6. Schematic diagram of leakage path: (a) actual flow path, (b) approximated flow path.

4.5.1. Conservation of momentum

The x-direction momentum of the leakage flow can be obtained from the Navier-Stokes equation, which takes the form as,

$$\rho u \frac{\partial u}{\partial x_L} + \rho v \frac{\partial u}{\partial y_L} = -\frac{\partial P}{\partial x_L} + \mu \frac{\partial^2 u}{\partial y_L^2} \tag{4-37}$$

where P and μ are the pressure and viscosity of the leakage flow, respectively.

In equation (4-37), terms on the left-hand side represent the inertia effects on the flow, while the right-hand side terms are the normal and viscous shear stresses. As proposed by Yuan et al. (1992), the inertia terms in equation (4-37) can be averaged along the Y_L direction as shown in the equation below,

$$F_{x_L} = \frac{1}{h_L} \int_0^{h_L} \left(\rho u \frac{\partial u}{\partial x_L} + \rho v \frac{\partial u}{\partial y_L} \right) dy_L \tag{4-38}$$

where F_{x_L} denotes the averaged inertia effects. Utilising this approximation, equation (4-37) can be rewritten as,

$$\frac{\partial^2 u}{\partial y_L^2} = \frac{1}{\mu}\left(F_{x_L} + \frac{\partial P}{\partial x_L}\right) \tag{4-39}$$

Substituting an x_L-function, B, for $\frac{1}{2\mu}\left(F_{xL} + \frac{\partial P}{\partial x_L}\right)$, equation (4-39) can then be simplified as,

$$\frac{\partial^2 u}{\partial y_L^2} = 2B \tag{4-40}$$

Knowing the boundary conditions are,

$$\begin{cases} u = 0 & at\ \ y_L = 0 \\ u = V_{x_L} & at\ \ y_L = h_L \end{cases}$$

where V_{x_L} is the velocity of the seal along the X_L direction (i.e., $\dot{y}$ obtained from the dynamic model of the seal).

Taking the boundary conditions into equation (4-40) and integrating twice to obtain expressions for $\frac{\partial u}{\partial y_L}$ and u, consecutively,

$$\frac{\partial u}{\partial y_L} = B(2y_L - h_L) + \frac{V_{x_L}}{h_L} \tag{4-41}$$

and

$$u = B(y_L^2 - y_L h_L) + y_L \frac{V_{x_L}}{h_L} \tag{4-42}$$

The mean flow velocity, $\overline{U}$, along Y_L direction is calculated as,

$$\overline{U} = \frac{1}{h_L}\int_0^{h_L} u\, dy_L = -\frac{B}{6}h_L^2 + \frac{V_{x_L}}{2} \tag{4-43}$$

4.5.2. Continuity equation

The steady state continuity equation for the leakage flow can be expressed in the following integral form

$$v = -\int \left(\frac{\partial u}{\partial x_L} + \frac{u}{\rho}\frac{\partial \rho}{\partial x_L}\right) dy_L + C_v \tag{4-44}$$

where the constant, C_v, can be found from the boundary condition that $v(h_L) = V_{y_L}$. It is worthy of noting here that V_{y_L} is the velocity of the seal along the y_L direction (i.e., $\dot{x}$ obtained from the dynamic model of the seal).

4.5.3. Conservation of energy

As the leakage flow is assumed adiabatic, the conservation of energy can be expressed as,

$$\rho u \frac{\partial h}{\partial x_L} = u \frac{\partial P}{\partial x} + \mu \frac{\partial^2 u}{\partial y_L^2} \tag{4-45}$$

where h is the enthalpy of the leakage flow.

Utilising Maxwell thermodynamics relations, the following expression can be written,

$$\frac{dh}{dx_L} = T \frac{dS}{dx_L} + \frac{1}{\rho} \frac{dP}{dx_L} \tag{4-46}$$

where S and T are the entropy and temperature of the leakage flow, respectively.

Combining equations (4-41), (4-45), and (4-46), the change in entropy can be obtained as follows,

$$\frac{\partial S}{\partial x_L} = \frac{\mu}{\rho T \overline{U}} \left(B(2y_L - h_L) + \frac{V_{x_L}}{h_L} \right)^2 \tag{4-47}$$

Averaging equation (4-47) along Y_L direction,

$$\frac{\partial S}{\partial x_L} = \frac{\mu \left(B^2 h_L^4 + 3V_{x_L}^2 \right)}{3\rho T \left(-\frac{B}{6} h_L^2 + \frac{V_{x_L}}{2} \right)} \tag{4-48}$$

The solution procedure starts by setting $v(0) = 0$ to obtain the following functional relationship,

$$\frac{dB}{dx_L} = f\left(B, \frac{dh_L}{dx_L}, \frac{d\rho}{dx_L}, \rho, h_L \right) \tag{4-49}$$

Utilising the reference fluid properties program, REFPROP 10, to provide equation of state information, and the fact that h_L and its derivative are known at any value of x_L, the differential equation in (4-49) is solved numerically with the help of equation (4-48) to find the values of the variable B and the state properties at n sequential points along the x_L-axis. The pressure distribution is calculated during the procedure via the following equation,

$$\frac{dP}{dx_L} = 2\mu B - F_{xL} \tag{4-50}$$

At any position, x_L, the values of the entropy, S, obtained from (4-48) and the pressure, P, obtained from (4-50), can be employed to obtain the density, ρ, and the viscosity, μ, by using the appropriate functions available on REFPROP 10 (Lemmon et al., 2010). The leakage mass flowrate, $\dot{m}_L$, can then be calculated from the following averaging expression,

$$\dot{m}_L = \frac{1}{n}\sum_{i=1}^{n} \rho_i h_{Li} \overline{U}_i H \tag{4-51}$$

where the subscript i signifies point number i on the x_L-axis. As expected, the values of mass flowrate obtained at various x_L points are close to each other in value. However, the averaging formula helps reduce the impact of computational errors on the calculated outcome. By way of demonstrating air leakage through a $4.2\ \mu m$ gap between the seal and the housing with the seal tilted 0.22 °, Fig. 4-7 shows sample results obtained from the leakage model presented above for an inlet state of $110\ kPa$ and $4.23\ kg \cdot m^{-3}$ and outlet pressure of $100\ kPa$. The figure suggests that the leakage mass flowrate remains almost constant, which confirms the continuity equation.

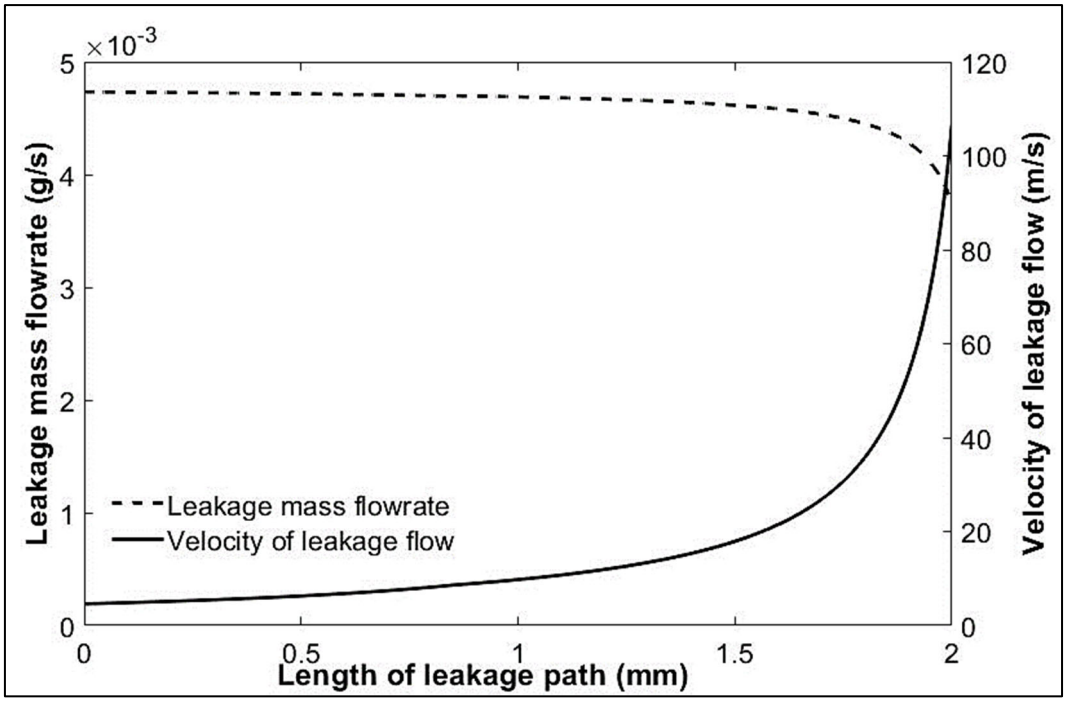

Fig. 4-7. Sample results of the leakage model.

4.6. Comparative analysis

In this section, a numerical simulation is carried out to illustrate the seal dynamics of the circolimaçon compressor, which is also compared to that of the L2L compressor under the same conditions. The simulation is assumed to operate at 600 rpm and uses air as the working fluid, and the inlet pressure is set as $P_i = 100kPa$ and the pressure ratio, $P_r = \frac{P_o}{P_i} = 3$ (where P_o is the outlet pressure). As the circolimaçon and L2L compressors are only different from each other with respect to geometry, key geometric parameters listed in Table 4-1 and the thermodynamic model are adopted from the work of Lu et al. (2022). A flowchart to illustrate the simulation process is shown in Fig. 4-8.

Table 4-1. Dimensions of the circolimaçon compressor

Machine dimensions	**Values**
Half-length of the rotor chord, L	$0.05\ m$

Table 4 1. Dimensions of the circolimaçon compressor (Continued)

Machine dimensions	**Values**
Axial length of the housing, H	$0.065\ m$
Limaçon aspect ratio, β	0.18
Apex clearance, L_c	$0.001\ m$
Rotor design factor, a	0.9
Width of the seal, w_s	$0.002\ m$
Width of the seal groove, w_g	$0.0022\ m$
Length of the seal, L_s	$0.01\ m$
Mass of the seal, m_s	$0.01\ kg$

4.6.1. Comparison of seal dynamics

As mentioned in section 4.3, the lenticular design of the rotor geometrically separates the working chamber into the upper and lower chambers. During the operation, the pressure profiles of the two chambers are similar to each other but π different in phase, as shown in Fig. 4-9. and such pressure differences directly cause the two sides of the seal subject to different forces, which is the main reason for the vibration of the seal. It is noticed that the working fluid is compressed to a higher pressure than it is expected. The reason for the over-compression is to overcome the stiffness of the spring attached to the discharge valve, as pointed out by Lu et al. (2022). The valve design can be optimised to minimise over-compression.

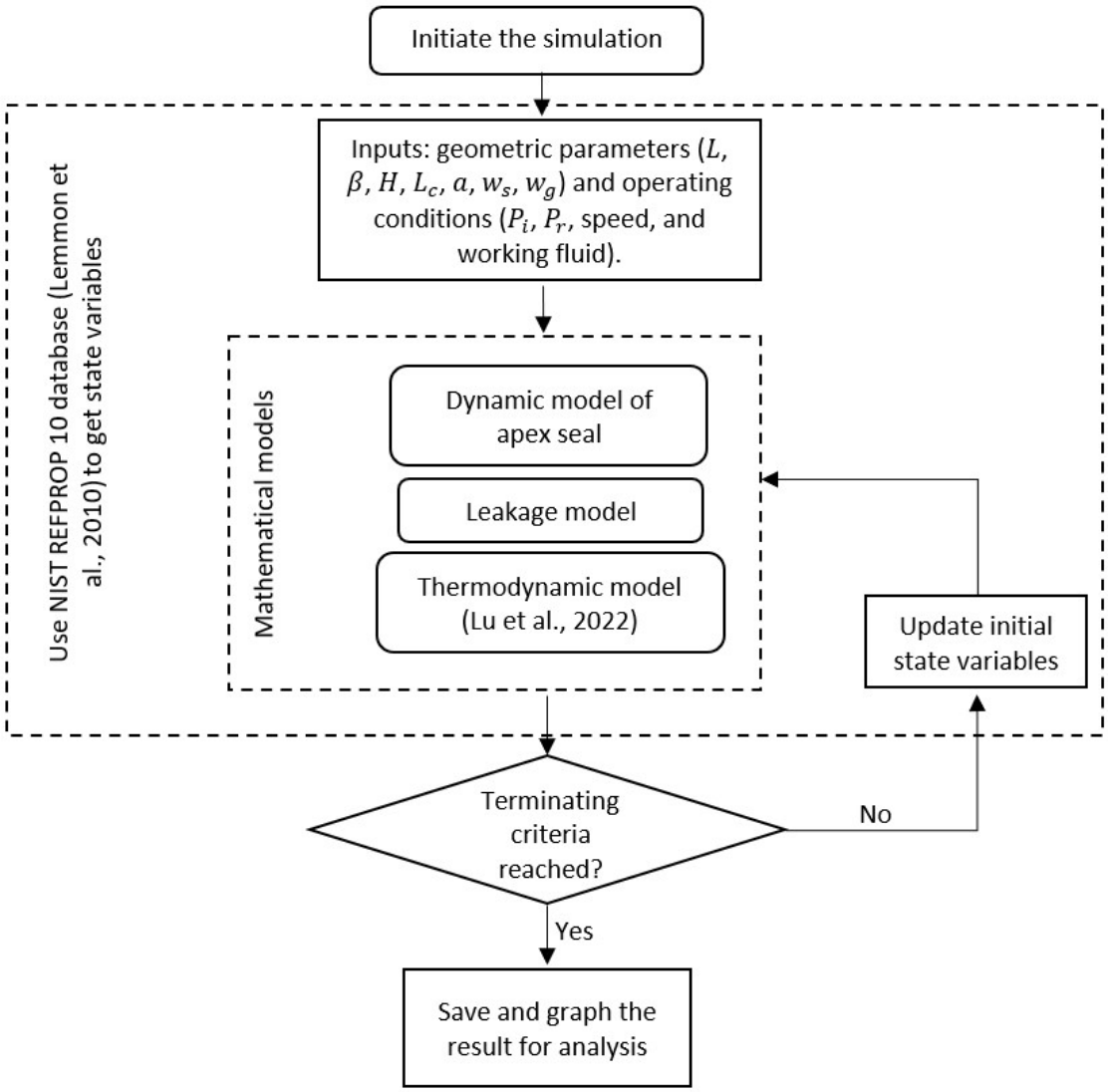

Fig. 4-8. Flowchart of the simulation process.

Fig. 4-10 depicts the seal displacements in X and Y directions and the seal angular displacement, ϕ, respectively. It is apparent that the seal vibration of the circolimaçon compressor is more significant than that of the L2L machine, especially along the X-axis. This is mainly attributed to the fact that the apex gap, as illustrated in Fig. 4-11, in the circolimaçon machine varies with the rotor angle. Fig. 4-11 also depicts the seal position along the X-axis. It can be observed that the two curves closely overlap each other, which indicates that the seal exhibits satisfactory sealing performance. In the current case study, the maximum apex gap is $4.2\ mm$, which is observed at around $90°$ and $270°$. It is noticed that small fluctuations occurred at which the rotor angle swept from $60°$ to $80°$ and from

$240°$ to $260°$. This is because the change in the apex gap takes place rapidly as reflected by the slope of the curve, and consequently, the vibration of the seal is relatively intensified.

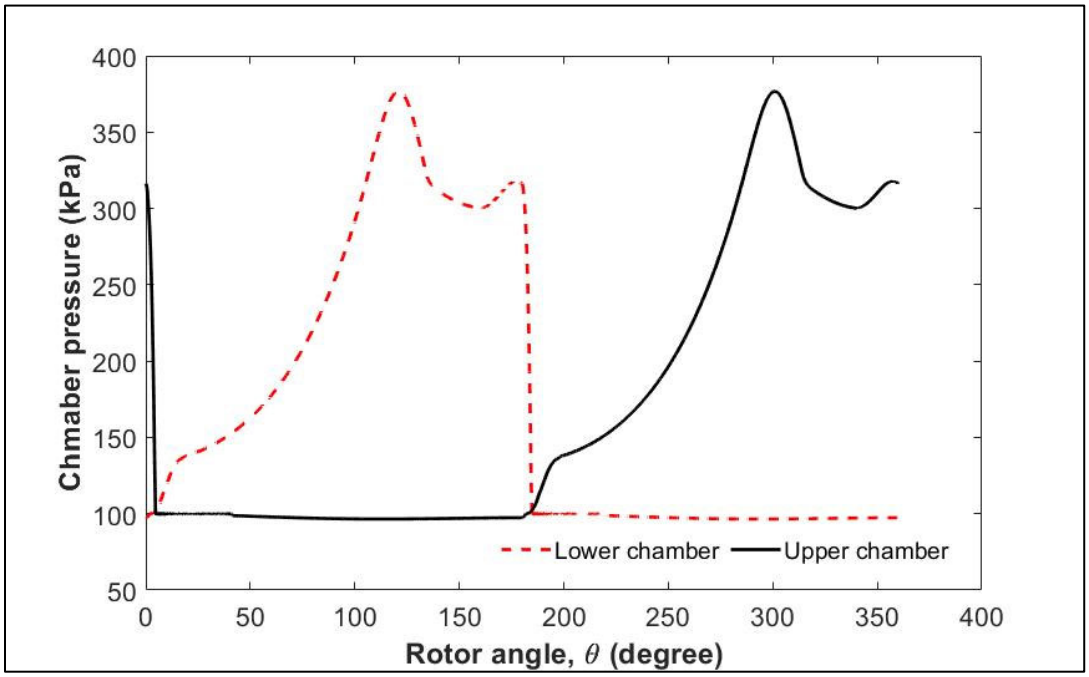

Fig. 4-9. Pressure of the upper and lower chambers of the circolimaçon compressor.

As shown in Fig. 4-10, the circolimaçon compressor experiences more noticeable seal vibrations compared with the L2L-type machine. This would result in negative effects on machine reliability and increase the risk of seal component failure. In Fig. 4-12, the contact forces between the seal and seal groove acting on points c_1, c_2, c_3, c_4, and the spring force acting on c_6 are obtained by using the seal dynamic model proposed by Phung et al. (2018), while the profile of the contact force between the seal and housing acting on point c_5 is calculated from the modified model presented in Section 4.4. Based on Fig. 4-12, the locations on the seal, seal groove, and housing that undergo severe contact forces can be revealed. This information benefits designers to introduce reinforcements to the contact surface at these locations, thereby preventing component failures and improving the reliability of the machine.

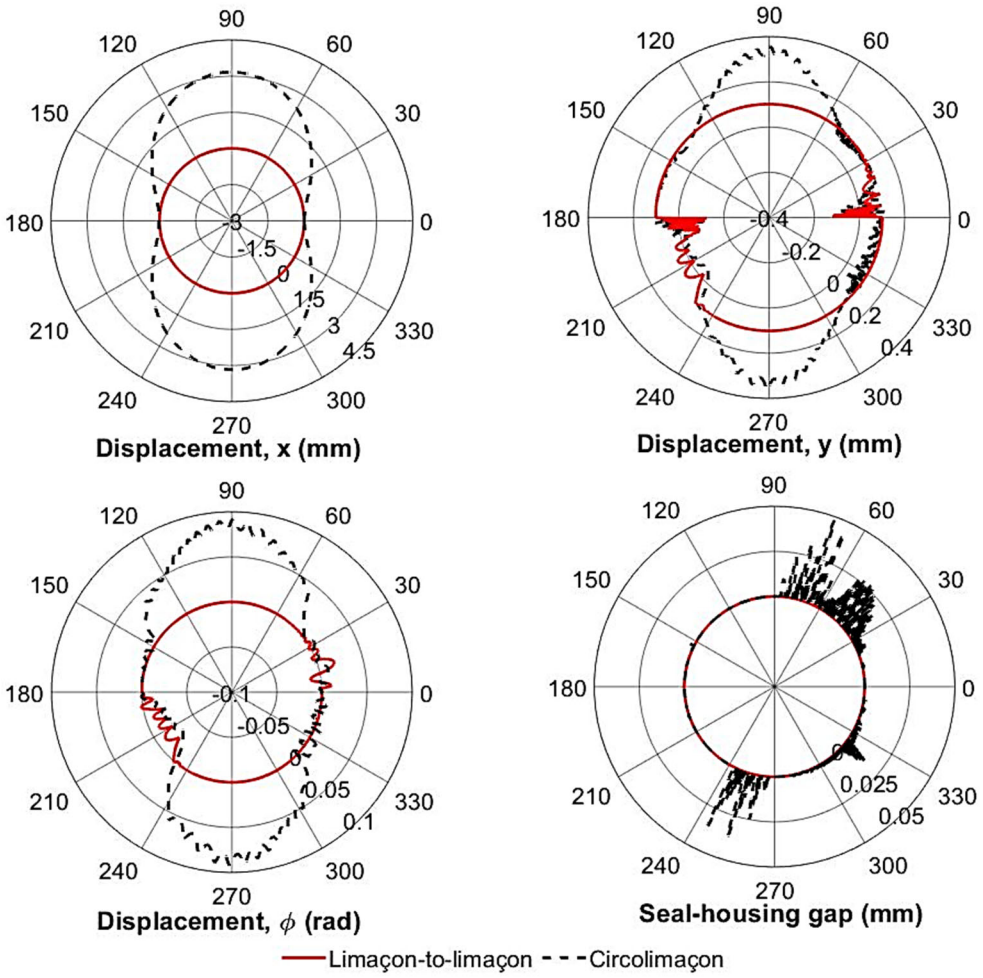

Fig. 4-10. Comparison of seal dynamics between the circolimaçon and L2L compressors.

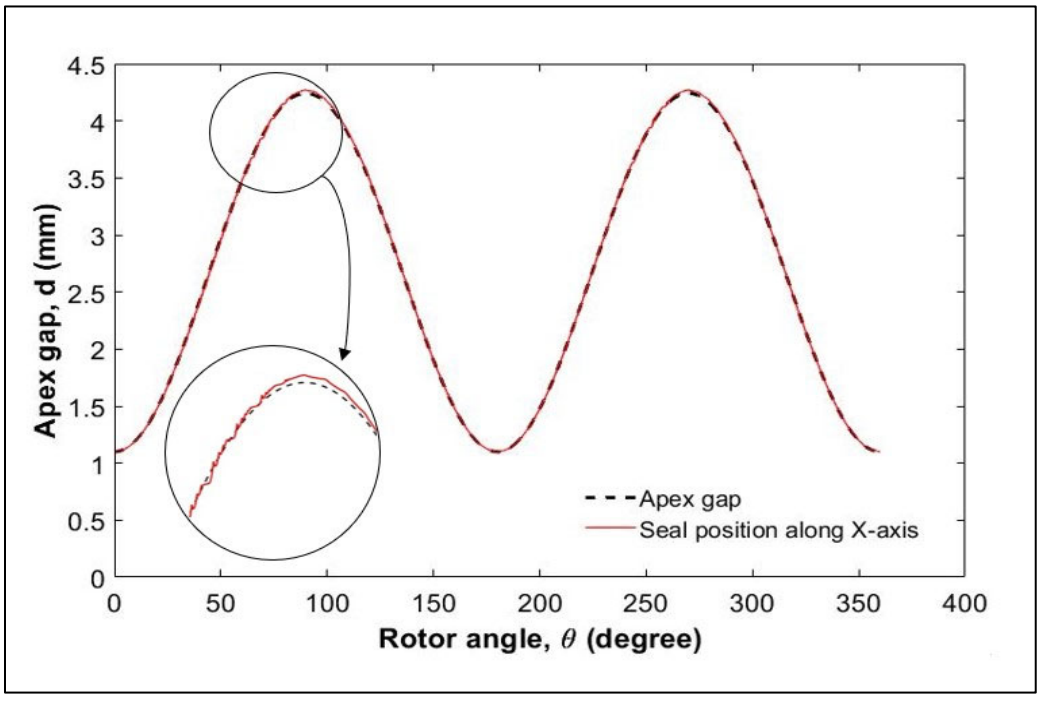

Fig. 4-11. Seal movement to cover the apex-housing gap in the circolimaçon machine.

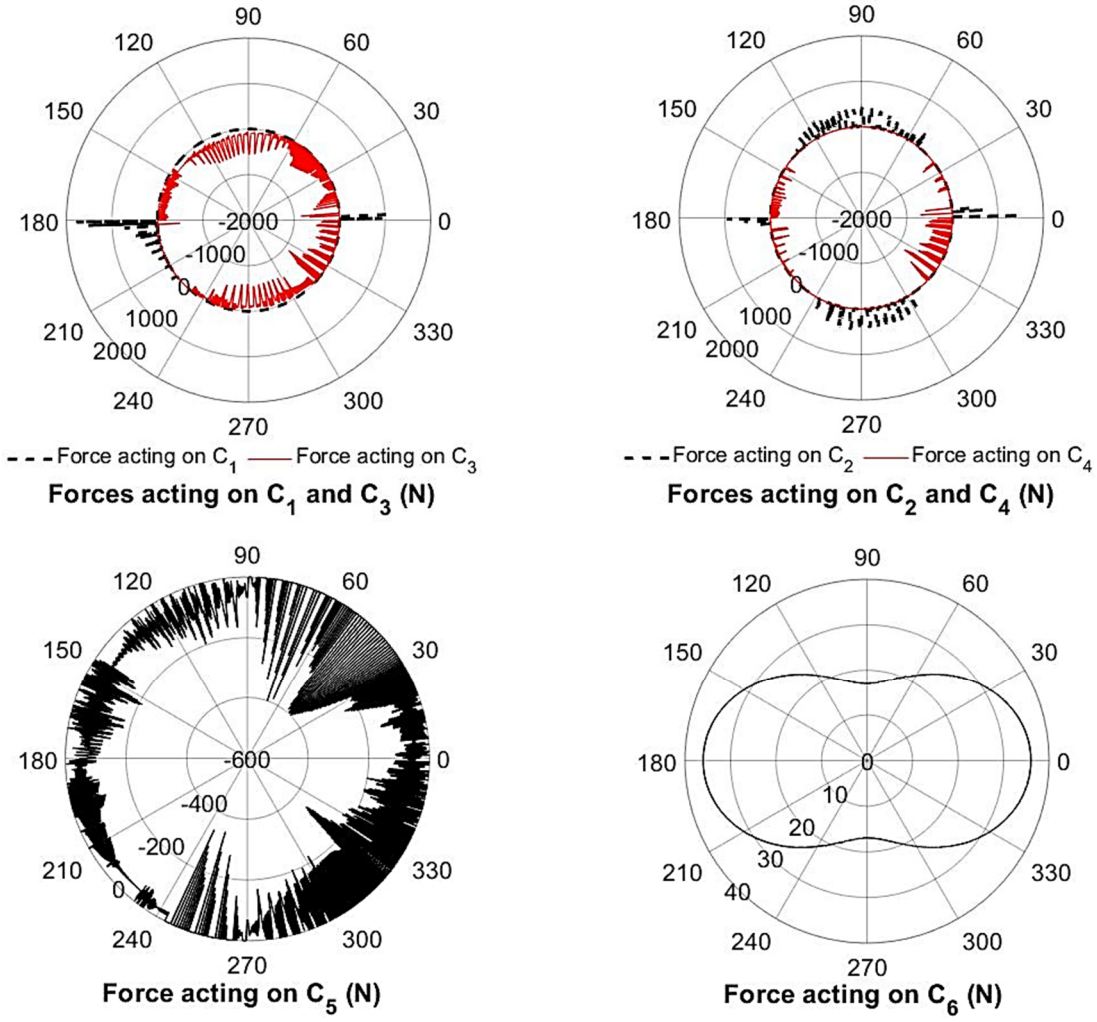

Fig. 4-12. Forces acting on different points of the apex seal.

4.6.2. Comparison of machine performance

Fig. 4-13 and Fig. 4-14 show the comparison of the volumetric and isentropic efficiencies of the two machines under different pressure ratios and operating speeds. To obtain the volumetric and isentropic efficiencies of the L2L-type compressor, the seal dynamic model presented in the work of Phung et al. (2018) is utilised. The dimensions used to produce Fig. 4-13 and Fig. 4-14 are listed in Table 4-1. Based on Fig. 4-13, the circolimaçon compressor exhibits better volumetric efficiency than that of the L2L-type compressor, but the largest difference is found less than 8%. The highest volumetric efficiency for the circolimaçon and L2L-type compressors are 88.58% and 86.89%, respectively. Additionally, the volumetric efficiency for both embodiments increases with the operating speed,

which is due to the significant reduction of leakage past the apex seal. However, the volumetric efficiency shows an opposite trend when the pressure ratio rises. This is mainly attributed to the increase in the amount of high-pressure fluid flowing back to the chamber as a result of the high pressure ratio, which can be explained by the sudden increase (occurred at around $180°$ to $220°$) in fluid mass in the working chamber, as shown in Fig. 4-15. It is also observed that the L2L compressor has more fluid mass remaining in the chamber as indicated in Fig. 4-15, and this also deteriorates the volumetric efficiency as the amount of fresh charge will be reduced. The isentropic efficiency of the L2L-type device, as depicted in Fig. 4-14, is higher than the circolimaçon compressor, but the largest difference is less than 3%. These results suggest that the circolimaçon embodiment has comparable performance to the L2L-type machines when used for fluid-compression tasks.

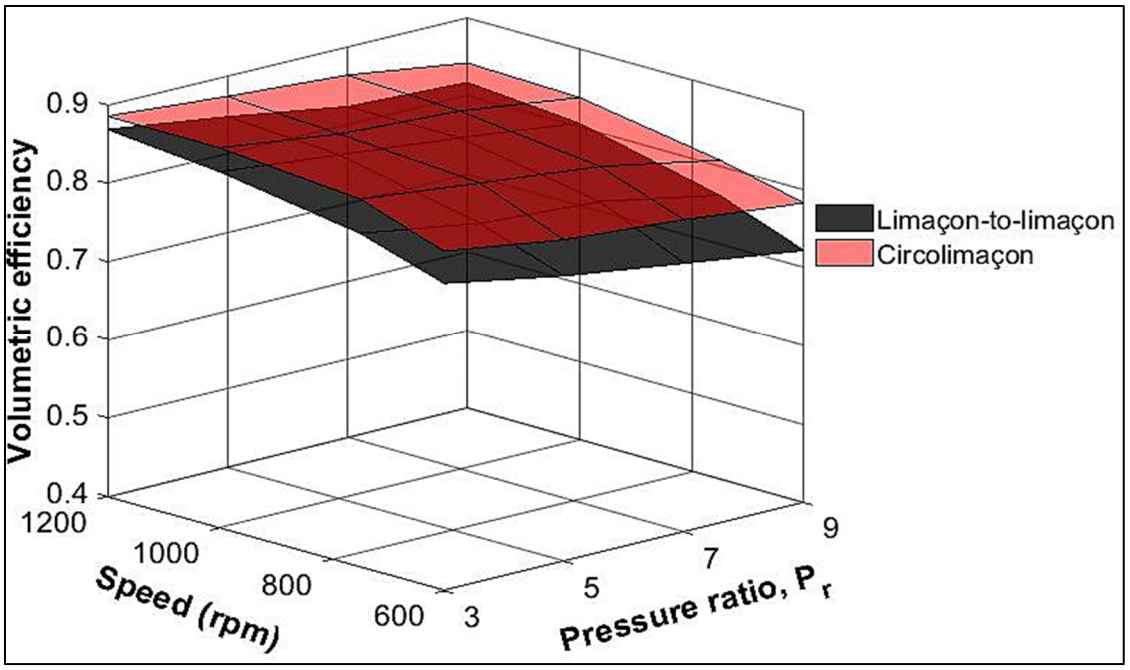

Fig. 4-13. Volumetric efficiency under different pressure ratios and operating speeds.

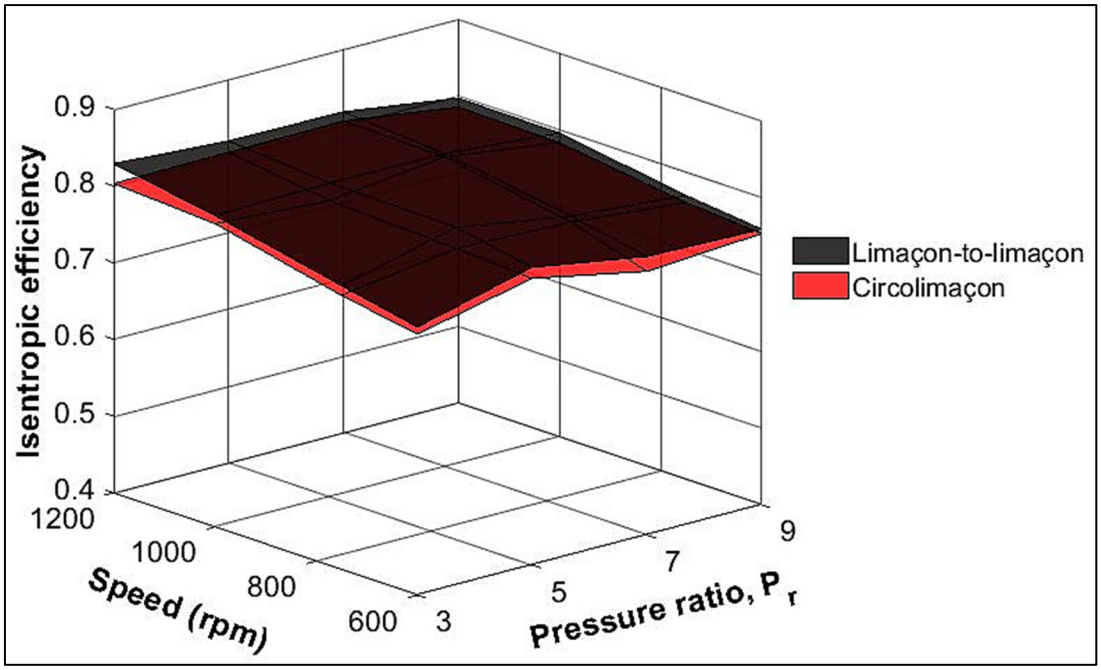

Fig. 4-14. Isentropic efficiency under different pressure ratios and operating speeds.

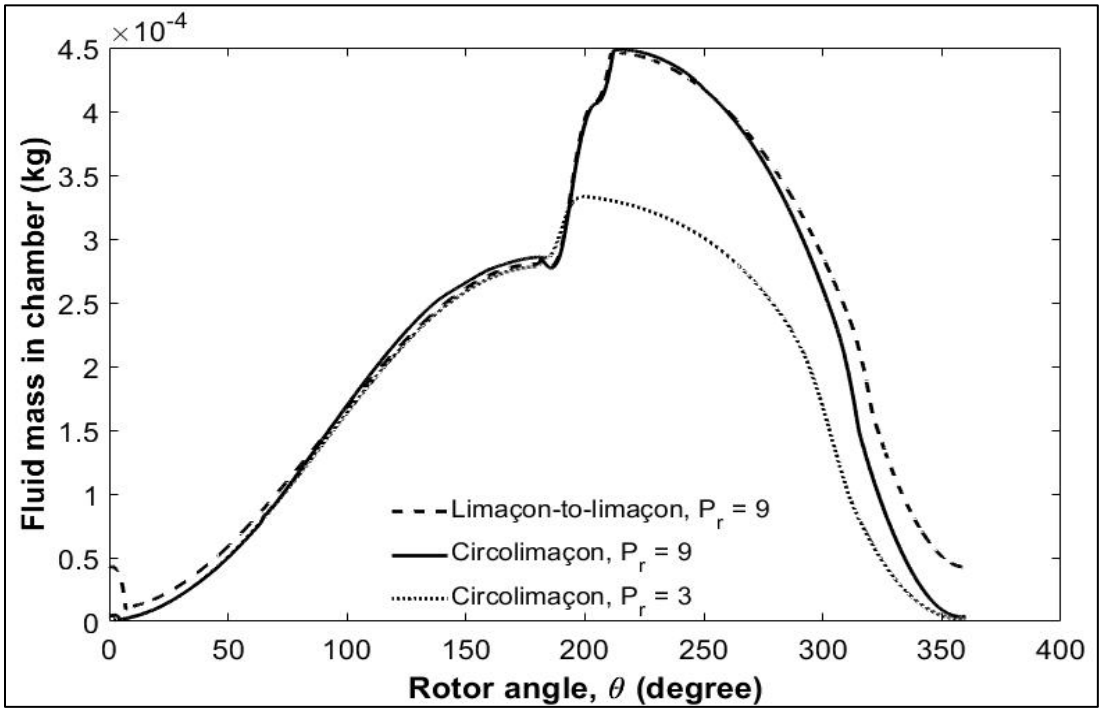

Fig. 4-15. Fluid mass inside the working chamber.

4.6.3. Effects of limaçon aspect ratio on seal dynamics

With the same machine size (as determined by H and L), the seal dynamics of the circolimaçon compressor under different limaçon aspect ratios, as depicted in Fig. 4-16. It is noticed that the level of seal vibrations becomes relatively lower when the aspect ratio,

β, decreases from 0.18 to 0.1. The reason for the reduced seal vibrations is due to the fact that the apex gap becomes smaller when β is reduced. Additionally, the maximum forces acting on the seal, as shown in Table 4-2, are also found to be smaller when β is reduced. In fact, the machine capacity is also reduced with the value of β, as indicated by equation (4-13). Therefore, these results suggest that the circolimaçon compressor with a relatively small capacity is subjected to less seal dynamics, and as a result, machine components would undergo less rubbing and impact at the contact surfaces between the seal, seal groove, and machine housing, which is beneficial for the machine reliability.

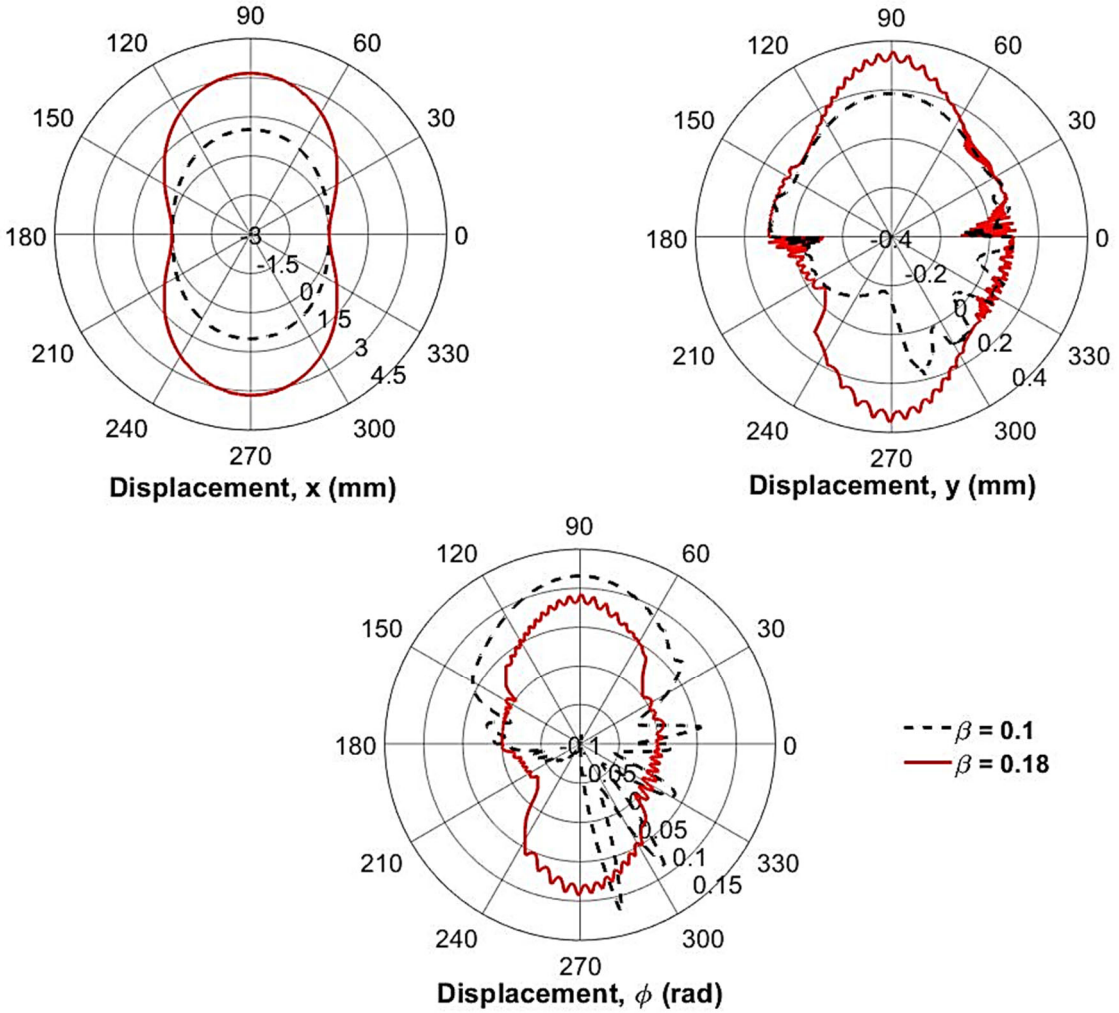

Fig. 4-16. Comparison of seal vibrations under different limaçon aspect ratios.

Table 4-2. Maximum magnitudes of each force under different limaçon aspect ratios

	Maximum magnitude of force (N)	
Location on seal	$\boldsymbol{\beta = 0.18}$	$\boldsymbol{\beta = 0.1}$
c_1	1779.32	1110.38
c_2	1475.63	897.67
c_3	896.26	760.97
c_4	825.38	304.51
c_5	400.23	229.84
c_6	36	36

4.7. Conclusion

The circolimaçon embodiment of the limaçon compressor features using circular arcs to construct profiles of the housing and the rotor. This paper investigates the feasibility of the circolimaçon embodiment from the thermodynamic aspect. A numerical example is presented to compare the circolimaçon compressor and the L2L-type machine in terms of apex seal performance. Based on the results, the following observations are made:

(1). Compared to the L2L-type compressor, the seal vibration of the circolimaçon compressor is exacerbated, especially in X direction. This is because the apex gap of the circolimaçon compressor changes with the rotor angle.

(2). Based on the numerical illustration, the circolimaçon compressor presents better volumetric efficiency than that of the L2L-type compressor, while the difference in the isentropic efficiency between the two machines is not significant, thus confirming the feasibility of the circolimaçon embodiment when used for fluid-compression tasks.

(3). Additionally, it is found that the decrease in the volumetric efficiency at high pressure ratios is due to the high-pressure backflows and residual fluid, which affects the amount of fresh charge drawn into the chamber during the suction stroke. In the current case study, the highest volumetric efficiency for the circolimaçon and L2L-type compressors are found to be 88.58% and 86.89%, respectively.

(4). When the limaçon aspect ratio is reduced from 0.18 to 0.1, the circolimaçon compressor is found to have a lower level of seal vibrations and smaller contact forces. This indicates that the machine with a small capacity can present relatively better reliability.

This paper demonstrates the potential of the circolimaçon embodiment of the limaçon compressor, and the information presented in the comparative analysis will benefit the design process of these machines.

4.8. References

Grand View Research. (2021). Market Analysis Report. Retrieved from https://www.grandviewresearch.com/industry-analysis/air-compressor-market

Ooi, K. T. (2005). Design optimisation of a rolling piston compressor for refrigerators. Applied thermal engineering, 25(5-6), 813-829.

Blunier, B., Cirrincione, G., Hervé, Y., & Miraoui, A. (2009). A new analytical and dynamical model of a scroll compressor with experimental validation. International Journal of Refrigeration, 32(5), 874-891.

Liu, Y., Hung, C., & Chang, Y. (2010). Design optimisation of scroll compressor applied for frictional losses evaluation. international journal of refrigeration, 33(3), 615-624.

Stosic, N. (2015). On heat transfer in screw compressors. International journal of heat and fluid flow, 51, 285-297.

Noh, K. Y., Min, B. C., Song, S. J., Yang, J. S., Choi, G. M., & Kim, D. J. (2016). Compressor efficiency with cylinder slenderness ratio of rotary compressor at various compression ratios. International journal of refrigeration, 70, 42-56.

Cavazzini, G., Giacomel, F., Ardizzon, G., Casari, N., Fadiga, E., Pinelli, M., Suman, A., Montomoli, F. (2020). CFD-based optimization of scroll compressor design and uncertainty quantification of the performance under geometrical variations. Energy, 209, 118382.

Shin, M., Na, S., Lee, J., Min, B., & Choi, G. (2019). Model analysis of a novel compressor with a dual chamber for high-efficiency systems. Applied Thermal Engineering, 158, 113717.

Gu, H., Zhou, X., Chen, Y., Wu, J., Wu, Z., Jiang, Y., & Sundén, B. (2021). Analysis, modeling and simulations of an innovative sliding vane rotary compressor with a rotating cylinder. Energy Conversion and Management, 230, 113822.

Lu, K., Phung, T. H., & Sultan, I. A. (2021). On the Design of a Class of Rotary Compressors Using Bayesian Optimization. Machines, 9(10), 219.

Lu, K., Sultan, I. A., & Phung, T. H. (2022). Mathematical modeling and parametric study of the limaçon rotary compressor. International Journal of Refrigeration, 134, 219-231.

Sultan, I. A. (2005). The Limaçon of Pascal: Mechanical Generation and Utilisation for Fluid Processing. Proceedings of the Institution of Mechanical Engineers, Part C: Journal of Mechanical Engineering Science, 219(8), 813-822. doi: 10.1243/095440605x31698

Sultan, I. A., & Schaller, C. G. (2011). Optimum positioning of ports in the limaçon gas expanders. Journal of engineering for gas turbines and power, 133(10).

Phung, T. H., Sultan, I. A., & Appuhamillage, G. K. (2018). On the apex seal analysis of limaçon positive displacement machines. Mechanism and Machine Theory, 127, 126-145.

Sultan, I. A. (2008). A geometric design model for the circolimaçon positive displacement machine. Journal of Mechanical Design, 130(6).

Phung, T. H., Sultan, I. A. (2018). Characterisation of Limaçon Gas Expanders with Consideration to the Dynamics of Apex Seals and Inlet Control Valve. Journal of Engineering for Gas Turbines and Power, 140(12).

Phung, T. H., & Sultan, I. A. (2021). Geometric Design of the Limaçon-to-Circular Fluid Processing Machine. Journal of Mechanical Design, 143(10). doi:10.1115/1.4050383

Sultan, I. (2007). A surrogate model for interference prevention in the limaçon-to-limaçon machines. Engineering Computations, 24(5), 437-449. doi: 10.1108/02644400710755852

Sultan, I. A. (2006). Profiling Rotors for Limaçon-to-Limaçon Compression-Expansion Machines. Journal of Mechanical Design, 128(4), 787-793. doi: 10.1115/1.2202877 %J Journal of Mechanical Design

Yuan, X., Chen, Z., Fan, Z. (1992). Calculating model and experimental investigation of gas leakage. In: 1992 International Compressor Engineering Conference at Purdue University.

Lemmon, E.W., Huber, M.L., McLinden, M.O. (2010). NIST Reference Fluid Thermodynamic and Transport Properties—REFPROP Version 10.0. U.S. Department of Commerce Technology Administration - National Institute of Standards and Technology, Gaithersburg, Maryland, p. 20899.

Chapter 5. Conclusion and recommendations for future work

In this thesis, a thorough study has been conducted to assert the suitability of the limaçon technology for use as a positive displacement compressor. Such an assertion could be achieved by ensuring the design is geometrically capable of delivering suction and compression strokes, ports can be arranged to support the working of these strokes, several parameters can be identified as impacting compressor performance and it is possible to calculate a set of parameters which optimise this performance.

Chapter 1 in the thesis offered a broad account of the published literature in the field of positive displacement compressors with a focus on the models proposed by various researchers to describe the workings of these compressors. Chapter 2 presented a comprehensive mathematical model, which includes kinematics, fluid dynamics, characteristics of the port flow, internal leakage, dynamics of the discharge valve, and thermodynamics, to theoretically study the workings of the limaçon rotary compressor. Furthermore, the effect of various parameters, including the operating speed, pressure ratio, and valve diameter, on the volumetric and isentropic efficiencies has also been investigated. The findings in Chapter 2 demonstrated the suitability of the limaçon technology in positive displacement compressors. However, the study in Chapter 2 is based on reasonable assumptions made for working conditions, i.e., the operating speed, working fluid, and certain machine dimensions. As such, the results obtained from the analysis correspond to the conditions assumed.

Subsequently, the mathematical model was used for optimisation purposes in Chapter 3, and an optimisation procedure has been developed by using a Bayesian optimisation

algorithm. The optimisation procedure is a two-stage one, in which the first stage optimises the machine dimensions based on certain design requirements, and the second stage aims to find the optimum port locations to improve machine performance. A numerical illustration, presented in this chapter, showed that the isentropic and volumetric efficiencies of the optimised design could significantly increase. This highlights the considerable potential of the limaçon rotary compressor as compared with other compressor technologies in terms of machine performance. Additionally, the robustness consideration suggests that the optimised design can maintain relatively stable performance when working conditions vary by a small percentage, which confirms the validity of the proposed optimisation approach. However, due to the complexity of the compressor model used for the analysis, the size of training data used for the optimisation procedure had to be limited in order to manage the computational cost involved. For a compressor which will actually be manufactured for performance testing, a larger size training data would be recommended.

In Chapter 4, the viability of the circolimaçon embodiment has been evaluated by comparing its performance with that of the limaçon-to-limaçon (L2L) machine based on apex seal performance. A nonlinear three-degree of freedom model has been proposed to describe the vibration of apex seals, and the leakage through the seal-housing gap is formulated by considering the inertia and viscous effects on the flow. The mathematical model developed in Chapter 2 was used to calculate the machine performance of the two machines. The comparison of the seal dynamics suggests that the vibration of apex seals of the circolimaçon embodiment is more noticeable than that of the L2L machine, especially along the rotor chord. This is mainly attributed to the fact that the clearance between the rotor apices and machine housing in the circolimaçon machine varies with the rotation of

the rotor, which exacerbates the vibration of the seal. In terms of machine performance, the differences in the volumetric and isentropic efficiencies between the two machines are found within 8% and 3%, respectively, which suggests that the circolimaçon embodiment is comparable to the L2L type machine. Additionally, it was also found that the circolimaçon embodiment with a smaller capacity would have a lower level of seal vibrations and smaller contact forces, indicating that the machine could present relatively better reliability. Nevertheless, the comparative analysis in Chapter 4 was conducted under a specific range of operating speed (600 to $1200\ rpm$) and pressure ratio (3 to 9) based on suitable assumptions about component properties and flow conditions. Therefore, the performance of the two embodiments outside the tested conditions might need further investigation and the results obtained in this study might serve as a reference. Moreover, the seal-housing and the seal-rotor interactions were modelled using a mass-spring-damper model where the damping and spring coefficients were assumed from material properties. Whilst these assumptions are widely accepted in modelling, more reliable figures can be obtained by experimental or finite element methods. In modelling the leakage flow, assumptions and simplifications were made to the Navier-Stokes equations in order to obtain a closed form solution for the leakage model. This may influence the leakage value obtained only in a minor fashion.

Through the work presented in this thesis, the research questions related to the development of the limaçon rotary compressor have been successfully answered. However, some aspects are still waiting to be studied, which provides directions for future work. To name a few, the complex multi-physical mathematical modelling proposed in this thesis to describe the working of limaçon compressors will be verified by experimental investigations on a prototype machine. Another research topic will be the sealing scheme at the

side clearance to prevent leakage to the rotor cavity, and it can be expected that the performance of the limaçon compressor will be further improved with a proper side sealing scheme. In addition to that, the heat transfer that occurs between the working fluid and solid components needs to be studied. Future work on this aspect could start by developing the Nusselt number correlation, which has not been proposed specifically for any rotary positive displacement compressors. Also, there are opportunities for interdisciplinary collaboration where lubrication and cooling schemes can be proposed and investigated. These are some examples of future research on the limaçon compressor, and it is hoped that this thesis could provide a useful reference for future work.

References

Stouffs, P., Tazerout, M., & Wauters, P. (2001). Thermodynamic analysis of reciprocating compressors. *International Journal of Thermal Sciences, 40*(1), 52-66.

Sultan, I. A., & Phung, T. H. (Eds.). (2019). Positive Displacement Machines: Modern Design Innovations and Tools. Academic Press.

Spark, I. J., & Lu, K. (2019). The orbital displacer: Implications and applications. In I. A. Sultan & T. H. Phung (Eds.), *Positive Displacement Machines* (pp. 3-34): Academic Press.

Li, J., Jia, X., Wu, Z., & Peng, X. (2014). The cavity profile of a diaphragm compressor for a hydrogen refueling station. *International journal of hydrogen energy*, *39*(8), 3926-3935.

Liang, K. (2017). A review of linear compressors for refrigeration. *International Journal of Refrigeration*, *84*, 253-273.

Yanagisawa, T., Shimizu, T., Chu, I., & Ishijima, K. (1982). Motion analysis of rolling piston in rotary compressor. In *International Compressor Engineering Conference*; Purdue e-Pubs: West Lafayette, IN, USA.

Stosic, N., Smith, I. K., & Kovacevic, A. (2011). Numerical and experimental research in heat transfer to screw compressor rotors. In *ASME/JSME Thermal Engineering Joint Conference* (Vol. 38921, p. T20050).

Chen, Y., Halm, N. P., Groll, E. A., & Braun, J. E. (2002). Mathematical modeling of scroll compressors—part I: compression process modeling. *International Journal of Refrigeration*, *25*(6), 731-750.

Prescient & Strategic Intelligence. (2020). *Compressor market research report (2020-2030).* Retrieved from https://www.psmarketresearch.com/market-analysis/compressor-market

Silva, W. L. V., Souza, L. C. O., Bortolaia, L. A., Paula, M. R. D., & Leal, E. M. (2017). Study of the electricity consumption reduction of a compressed air system: the case of a steelmaking company. *REM-International Engineering Journal*, *70*(4), 421-428.

Vittorini, D., & Cipollone, R. (2016). Energy saving potential in existing industrial compressors. *Energy*, *102*, 502-515.

Saidur, R., Rahim, N. A., & Hasanuzzaman, M. (2010). A review on compressed-air energy use and energy savings. *Renewable and sustainable energy reviews*, *14*(4), 1135-1153.

Sultan, I. A. (2005). The limaçon of Pascal: mechanical generation and utilization for fluid processing. *Proceedings of the Institution of Mechanical Engineers, Part C: Journal of Mechanical Engineering Science*, *219*(8), 813-822.

Heidari, M., Mortazavi, M., & Rufer, A. (2017). Design, modeling and experimental validation of a novel finned reciprocating compressor for Isothermal Compressed Air Energy Storage applications. *Energy*, *140*, 1252-1266.

Hu, Y. S., Wei, H. J., Xu, J., Du, Z. C., Yang, S., & Ren, L. P. (2019). The Theoretical and Experimental Research of a Novel Rotary Cylinder Compressor. In *IOP Conference Series: Materials Science and Engineering* (Vol. 604, No. 1, p. 012073). IOP Publishing.

Shin, M., Na, S., Lee, J., Min, B., & Choi, G. (2019). Model analysis of a novel compressor with a dual chamber for high-efficiency systems. *Applied Thermal Engineering*, *158*, 113717.

Shakya, P., & Ooi, K. T. (2020). Introduction to Coupled Vane compressor: Mathematical modelling with validation. *International Journal of Refrigeration*, *117*, 23-32.

Gao, X., & Liu, Y. (2021). Design, modeling and characteristics research of a novel self-air-cooling reciprocating compressor. *International Journal of Refrigeration*, *128*, 62-70.

Lu, K., Sultan, I. A., & Phung, T. H. (2021). Mathematical modeling and parametric study of the limaçon rotary compressor. *International Journal of Refrigeration*.

Ueno, K., Bye, R.E., Hunter, K.S. (2003) *Compressor Efficiency Definitions*. Retrieved from http://vairex.com/resources/VAIREX_Compressor_Efficiency_Def_12May03.pdf

Cho, N. K., Youn, Y., Lee, B. C., & Min, M. K. (2000). The characteristics of tangential leakage in scroll compressors for air-conditioners. In *International Compressor Engineering Conference*; Purdue e-Pubs: West Lafayette, IN, USA.

Yuan, X., Chen, Z., & Fan, Z. (1992). Calculating model and experimental investigation of gas leakage. In *International Compressor Engineering Conference*; Purdue e-Pubs: West Lafayette, IN, USA.

Kim, G., Min, B., Na, S., Choi, G., & Kim, D. (2017). Estimation of leakage through radial clearance during compression process of a rolling piston rotary compressor. *Journal of Mechanical Science and Technology*, *31*(12), 6033-6040.

Pereira, E. L., & Deschamps, C. J. (2020). Numerical analysis and correlations for radial and tangential leakage of gas in scroll compressors. *International Journal of Refrigeration*, *110*, 239-247.

Yanagisawa, T., & Shimizu, T. (1985a). Leakage losses with a rolling piston type rotary compressor. I. Radical clearance on the rolling piston. *International Journal of Refrigeration*, 8(2), 75-84.

Yanagisawa, T., & Shimizu, T. (1985b). Leakage losses with a rolling piston type rotary compressor. II. Leakage losses through clearances on rolling piston faces. *International journal of refrigeration*, 8(3), 152-158.

Rodgers, R. J., & Nieter, J. J. (1996). Comprehensive analysis of leakage in rotary compressors. In *International Compressor Engineering Conference*; Purdue e-Pubs: West Lafayette, IN, USA.

Kang, D. J., Kim, J. W., & Sohn, C. B. (2002). Effects of leakage flow model on the thermodynamic performance of a scroll compressor. In *International Compressor Engineering Conference*; Purdue e-Pubs: West Lafayette, IN, USA.

Teh, Y. L., & Ooi, K. T. (2009). Theoretical study of a novel refrigeration compressor-Part III: Leakage loss of the revolving vane (RV) compressor and a comparison with that of the rolling piston type. *International journal of refrigeration*, *32*(5), 945-952.

Silva, L. R., & Deschamps, C. J. (2015). Modeling of gas leakage through compressor valves. *International journal of refrigeration*, *53*, 195-205.

AW, K. T., & Ooi, K. T. (2020). Leakage study of a Lubricant-free Revolving Vane Compressor. *International Journal of Refrigeration*. doi: https://doi.org/10.1016/j.ijrefrig.2020.12.017

Ferreira, R. T. S., & Lilie, D. E. B. (1984). Evaluation of the leakage through the clearance between piston and cylinder in hermetic compressors. In *International Compressor Engineering Conference*; Purdue e-Pubs: West Lafayette, IN, USA.

Ishii, N., Bird, K., Sano, K., Oono, M., Iwamura, S., & Otokura, T. (1996). Refrigerant leakage flow evaluation for scroll compressors. In *International Compressor Engineering Conference*; Purdue e-Pubs: West Lafayette, IN, USA.

Lohn, S. K., & Pereira, E. L. L. (2014). Numerical investigation of the gas leakage through the piston-cylinder clearance of reciprocating compressors. In *International Compressor Engineering Conference*; Purdue e-Pubs: West Lafayette, IN, USA.

Annand, W. J. D., & Thermodynamics and Fluid Mechanics Group (1963). Heat transfer in the cylinders of reciprocating internal combustion engines. *Proceedings of the Institution of Mechanical Engineers*, *177*(1), 973-996.

Adair, R. P., Qvale, E. B., & Pearson, J. T. (1972). Instantaneous heat transfer to the cylinder wall in reciprocating compressors. In *International Compressor Engineering Conference*; Purdue e-Pubs: West Lafayette, IN, USA.

Liu, R., & Zhou, Z. (1984). Heat transfer between gas and cylinder wall of refrigerating reciprocating compressor. In *International Compressor Engineering Conference*; Purdue e-Pubs: West Lafayette, IN, USA.

Tan, K. M., & Ooi, K. T. (2011). Heat transfer in compression chamber of a revolving vane (RV) compressor. *Applied thermal engineering*, *31*(8-9), 1519-1526.

Hsieh, W. H., & Wu, T. T. (1996). Experimental investigation of heat transfer in a high-pressure reciprocating gas compressor. *Experimental thermal and fluid science*, *13*(1), 44-54.

Disconzi, F. P., Deschamps, C. J., & Pereira, E. L. (2012). Development of an in-cylinder heat transfer correlation for reciprocating compressors. In *International Compressor Engineering Conference*; Purdue e-Pubs: West Lafayette, IN, USA.

Ooi, K. T., & Zhu, J. (2004). Convective heat transfer in a scroll compressor chamber: a 2-D simulation. *International Journal of Thermal Sciences*, *43*(7), 677-688.

Jang, K., & Jeong, S. (2006). Experimental investigation on convective heat transfer mechanism in a scroll compressor. *International Journal of Refrigeration*, *29*(5), 744-753.

Rak, J., & Pietrowicz, S. (2020). Internal flow field and heat transfer investigation inside the working chamber of a scroll compressor. *Energy*, *202*, 117700.

Padhy, S. K., & Dwivedi, S. N. (1994). Heat transfer analysis of a rolling-piston rotary compressor. *International journal of refrigeration*, *17*(6), 400-410.

Ooi, K. T. (2003). Heat transfer study of a hermetic refrigeration compressor. *Applied thermal engineering*, *23*(15), 1931-1945.

Sanvezzo Jr, J., & Deschamps, C. J. (2012). A heat transfer model combining differential and integral formulations for thermal analysis of reciprocating compressors. In *International Compressor Engineering Conference*; Purdue e-Pubs: West Lafayette, IN, USA.

Dutra, T., & Deschamps, C. J. (2013). Experimental characterization of heat transfer in the components of a small hermetic reciprocating compressor. *Applied thermal engineering*, *58*(1-2), 499-510.

Patil, V. C., Acharya, P., & Ro, P. I. (2019). Experimental investigation of heat transfer in liquid piston compressor. *Applied Thermal Engineering*, *146*, 169-179.

Stosic, N. (2015). On heat transfer in screw compressors. *International journal of heat and fluid flow*, *51*, 285-297.

Yanagisawa, T., & Shimizu, T. (1985c). Friction losses in rolling piston type rotary compressors. III. *International journal of refrigeration*, *8*(3), 159-165.

Ooi, K. T. (2005). Design optimization of a rolling piston compressor for refrigerators. *Applied thermal engineering*, *25*(5-6), 813-829.

Teh, Y. L., & Ooi, K. T. (2009b). Theoretical study of a novel refrigeration compressor–Part I: Design of the revolving vane (RV) compressor and its frictional losses. *International journal of refrigeration*, *32*(5), 1092-1102.

Liu, Y., Hung, C., & Chang, Y. (2010). Design optimization of scroll compressor applied for frictional losses evaluation. *International journal of refrigeration*, *33*(3), 615-624.

Yang, B., Bradshaw, C. R., & Groll, E. A. (2013). Modeling of a semi-hermetic CO2 reciprocating compressor including lubrication submodels for piston rings and bearings. *International journal of refrigeration*, *36*(7), 1925-1937.

Bianchi, G., & Cipollone, R. (2015). Friction power modeling and measurements in sliding vane rotary compressors. *Applied Thermal Engineering*, *84*, 276-285.

Gu, H., Zhou, X., Chen, Y., Wu, J., Wu, Z., Jiang, Y., & Sundén, B. (2021). Analysis, modeling and simulations of an innovative sliding vane rotary compressor with a rotating cylinder. *Energy Conversion and Management*, *230*, 113822.

Kim, H. J., & Lancey, T. W. (2003). Numerical study on the lubrication oil distribution in a refrigeration rotary compressor. *International journal of refrigeration*, *26*(7), 800-808.

Afshari, F., Comakli, O., Lesani, A., & Karagoz, S. (2017). Characterization of lubricating oil effects on the performance of reciprocating compressors in air–water heat pumps. *International Journal of Refrigeration*, *74*, 505-516.

Wu, X., Xing, Z., He, Z., Wang, X., & Chen, W. (2017). Effects of lubricating oil on the performance of a semi-hermetic twin screw refrigeration compressor. *Applied thermal engineering*, *112*, 340-351.

Ozsipahi, M., Kose, H. A., Cadirci, S., Kerpicci, H., & Gunes, H. (2019). Experimental and numerical investigation of lubrication system for reciprocating compressor. *International Journal of Refrigeration*, *108*, 224-233.

Valenti, G., Colombo, L., Murgia, S., Lucchini, A., Sampietro, A., Capoferri, A., & Araneo, L. (2013). Thermal effect of lubricating oil in positive-displacement air compressors. *Applied Thermal Engineering*, *51*(1-2), 1055-1066.

Pizarro-Recabarren, R. A., & Barbosa, J. R. (2016). The effect of the lubricating oil on heat transfer in a hermetic reciprocating compressor. *Journal of the Brazilian Society of Mechanical Sciences and Engineering*, *38*(1), 189-208.

Nagata, S., Nozaki, T., & Akizawa, T. (2010). Analysis of dynamic behavior of suction valve using strain gauge in reciprocating compressor. In *International Compressor Engineering Conference*; Purdue e-Pubs: West Lafayette, IN, USA.

Ma, Y., He, Z., Peng, X., & Xing, Z. (2012). Experimental investigation of the discharge valve dynamics in a reciprocating compressor for trans-critical CO2 refrigeration cycle. *Applied Thermal Engineering*, *32*, 13-21.

Wang, Y., Xue, C., Feng, J., & Peng, X. (2013). Experimental investigation on valve impact velocity and inclining motion of a reciprocating compressor. *Applied Thermal Engineering*, *61*(2), 149-156.

Mu, G., Wang, F., Mi, X., & Gao, G. (2019). Dynamic modeling and analysis of compressor reed valve based on movement characteristics. *Applied Thermal Engineering*, *150*, 522-531.

Egger, A., Almbauer, R., Dür, L., Hopfgartner, J., & Lang, M. (2020). Multi-Response optimization applied to a mechanically assisted reed valve of a hermetic reciprocating compressor. *International Journal of Refrigeration*, *119*, 119-130.

Huang, B., & Xie, F. (2008). Dynamic analysis of the discharge valve of the rotary compressor. In *International Compressor Engineering Conference*; Purdue e-Pubs: West Lafayette, IN, USA.

Teh, Y. L., Ooi, K. T., & Djamari, D. W. (2009). Theoretical study of a novel refrigeration compressor–Part II: Performance of a rotating discharge valve in the revolving vane (RV) compressor. *International Journal of Refrigeration*, *32*(5), 1103-1111.

Yu, X., Ren, Y., Tan, Q., Lu, Z., Jia, X., & Wang, X. (2018). Study on the torsional movement of a reed valve in a rotary compressor. *Advances in Mechanical Engineering*, *10*(6), 1687814018778402.

Min, B., Na, S., Yang, J., & Choi, G. (2018). Geometric correlation of discharge coefficients for discharge valve system in rolling piston rotary compressor. *Journal of Mechanical Science and Technology*, *32*(8), 3943-3954.

Kim, H. J., Ahn, J. M., Hwang, S. W., & Kiem, M. K. (2004). Performance analysis of a twin rotary compressor. In *International Compressor Engineering Conference*; Purdue e-Pubs: West Lafayette, IN, USA.

Mujic, E., Kovacevic, A., Stosic, N., & Smith, I. K. (2008). The influence of port shape on gas pulsations in a screw compressor discharge chamber. *Proceedings of the*

Institution of Mechanical Engineers, Part E: Journal of Process Mechanical Engineering, *222*(4), 211-223.

Sultan, I. A., & Schaller, C. G. (2011). Optimum positioning of ports in the limaçon gas expanders. *Journal of engineering for gas turbines and power*, *133*(10).

Lim, Y. D., Lin, M., & Ooi, K. T. (2017). Simulation study of multi-chamber rotary compressor. In *IOP Conference Series: Materials Science and Engineering* (Vol. 232, No. 1, p. 012064). IOP Publishing.

Zhao, R., Li, W., & Zhuge, W. (2020). Unsteady characteristic and flow mechanism of a scroll compressor with novel discharge port for electric vehicle air conditioning. *International Journal of Refrigeration*, *118*, 403-414.

Gu, H., Chen, Y., Wu, J., Jiang, Y., & Sundén, B. (2021). Impact of discharge port configurations on the performance of sliding vane rotary compressors with a rotating cylinder. *Applied Thermal Engineering*, *186*, 116526.

Hong, W., Jin, J., Wu, R., & Zhang, B. (2009). Theoretical analysis and realization of stepless capacity regulation for reciprocating compressors. *Proceedings of the Institution of Mechanical Engineers, Part E: Journal of Process Mechanical Engineering*, *223*(4), 205-213.

Tuymer, W. J. (1974). Stepless variable capacity control. In *International Compressor Engineering Conference*; Purdue e-Pubs: West Lafayette, IN, USA.

Bin, T., Yuanyang, Z., Liansheng, L., Guangbin, L., Le, W., Qichao, Y., Haiping, X., Feng, Z., & Wenhui, M. (2013). Thermal performance analysis of reciprocating compressor with stepless capacity control system. *Applied thermal engineering*, *54*(2), 380-386.

Wang, Y., Jiang, Z., Zhang, J., Zhou, C., & Liu, W. (2018). Performance analysis and optimization of reciprocating compressor with stepless capacity control system under variable load conditions. *International Journal of Refrigeration*, *94*, 174-185.

Jin, J., & Hong, W. (2012). Valve dynamic and thermal cycle model in stepless capacity regulation for reciprocating compressor. *Chinese journal of mechanical engineering*, *25*(6), 1151-1160.

Tang, B., Zhao, Y., Li, L., Wang, L., Liu, G., Yang, Q., Xu, H., Zhu, F., & Meng, W. (2014). Dynamic characteristics of suction valves for reciprocating compressor with stepless capacity control system. *Proceedings of the Institution of Mechanical Engineers, Part E: Journal of Process Mechanical Engineering*, *228*(2), 104-114.

Liu, G., Zhao, Y., Tang, B., & Li, L. (2016). Dynamic performance of suction valve in stepless capacity regulation system for large-scale reciprocating compressor. *Applied Thermal Engineering*, *96*, 167-177.

Jiang, Z., Zhou, C., Wang, Y., Zhang, J., Liu, W., & Sun, X. (2020). Optimization Design of Actuator Parameters in Multistage Reciprocating Compressor Stepless Capacity Control System Based on NSGA-II. *Mathematical Problems in Engineering*, *2020*.

Zhang, J., Zhou, C., Jiang, Z., Wang, Y., & Sun, X. (2020). Optimization Design of Actuator Parameters with Stepless Capacity Control System Considering the Effect of Backflow Clearance. *Applied Sciences*, *10*(8), 2703.

Sun, X., Zhang, J., Wang, Y., Wang, J., & Qi, Z. (2021). Optimization of capacity control of reciprocating compressor using multi-system coupling model. *Applied Thermal Engineering*, *195*, 117175.

Li, W. (2013). Simplified steady-state modeling for variable speed compressor. *Applied thermal engineering*, *50*(1), 318-326.

Qureshi, T. Q., & Tassou, S. A. (1996). Variable-speed capacity control in refrigeration systems. *Applied Thermal Engineering*, *16*(2), 103-113.

Aprea, C., Mastrullo, R., & Renno, C. (2006). Experimental analysis of the scroll compressor performances varying its speed. *Applied thermal engineering*, *26*(10), 983-992.

Wang, Z., Wang, Z., Wang, J., Jiang, W., & Feng, Q. (2017). Research of thermal dynamic characteristics for variable load single screw refrigeration compressor with different capacity control mechanism. *Applied Thermal Engineering*, *110*, 1172-1182.

Yaqub, M., & Zubair, S. M. (2000). Performance evaluation of hot-gas by-pass capacity control schemes for refrigeration and air-conditioning systems. *Energy*, *25*(6), 543-561.

Jeong, S. K., Lee, D. B., & Hong, K. H. (2014). Comparison of system performance on hot-gas bypass and variable speed compressor in an oil cooler for machine tools. *Journal of Mechanical Science and Technology*, *28*(2), 721-727.

Wang, B., Han, L., Shi, W., & Li, X. (2012). Modulation method of scroll compressor based on suction gas bypass. *Applied Thermal Engineering*, *37*, 183-189.

Hollingsworth, J., Phillippi, G., Hinchliff, M., Kulhanek, C., Rimpel, A. M., & Maywald, F. (2019). Reciprocating Compressors. In *Compression Machinery for Oil and Gas* (pp. 167-252). Gulf Professional Publishing.

Wang, L., Liu, G. B., Zhao, Y. Y., & Li, L. L. (2015). Performance comparison of capacity control methods for reciprocating compressors. In *IOP Conference Series: Materials Science and Engineering* (Vol. 90, No. 1, p. 012029). IOP Publishing.

Yaqub, M., & Zubair, S. M. (1996). Thermodynamic analysis of capacity-control schemes for refrigeration and air-conditioning systems. *Energy*, *21*(6), 463-472.

Holdack-Janssen, H., & Kruse, H. (1984). Continuous and discontinuous capacity control for high speed refrigeration compressors. In *International Compressor Engineering Conference*; Purdue e-Pubs: West Lafayette, IN, USA.

Ooi, K. T., & Wong, T. N. (1997). A computer simulation of a rotary compressor for household refrigerators. *Applied thermal engineering*, *17*(1), 65-78.

Sultan, I. A. (2007). A surrogate model for interference prevention in the limaçon-to-limaçon machines. *Engineering Computations*.

Jain, A. K., Mao, J., & Mohiuddin, K. M. (1996). Artificial neural networks: A tutorial. *Computer*, *29*(3), 31-44.

Sanaye, S., Dehghandokht, M., Mohammadbeigi, H., & Bahrami, S. (2011). Modeling of rotary vane compressor applying artificial neural network. *International journal of refrigeration*, *34*(3), 764-772.

Namdeo, R., Manepatil, S., & Saraswat, S. (2008). Detection of valve leakage in reciprocating compressor using artificial neural network (ANN). In International Compressor Engineering Conference; Purdue e-Pubs: West Lafayette, IN, USA.

Belman-Flores, J. M., Ledesma, S., Barroso-Maldonado, J. M., & Navarro-Esbrí, J. (2015). A comparison between the modeling of a reciprocating compressor using artificial neural network and physical model. *International Journal of Refrigeration*, *59*, 144-156.

Tian, Z., Gu, B., Yang, L., & Lu, Y. (2015). Hybrid ANN–PLS approach to scroll compressor thermodynamic performance prediction. *Applied Thermal Engineering*, *77*, 113-120.

Zendehboudi, A., Li, X., & Wang, B. (2017). Utilization of ANN and ANFIS models to predict variable speed scroll compressor with vapor injection. *International journal of refrigeration*, *74*, 475-487.

Whitley, D. (1994). A genetic algorithm tutorial. *Statistics and computing*, *4*(2), 65-85.

Huang, Y. M., & Tsay, S. N. (2009). Mechanical efficiency optimization of a sliding vane rotary compressor. *Journal of pressure vessel technology*, *131*(6).

Chen, Q. J., & Ooi, K. T. (2021). Geometric Optimisation of a Coupled Vane Compressor. In *IOP Conference Series: Materials Science and Engineering* (Vol. 1180, No. 1, p. 012028). IOP Publishing.

Silva, E., & Dutra, T. (2021). Piston trajectory optimization of a reciprocating compressor. *International Journal of Refrigeration*, *121*, 159-167.

Lu, K., Phung, T. H., & Sultan, I. A. (2021). On the Design of a Class of Rotary Compressors Using Bayesian Optimization. Machines, 9(10), 219.

Sultan, I. A., & Kalim, A. (2011). Improving reciprocating compressor performance using a hybrid two-level optimisation approach. *Engineering Computations*.

Phung, T. H., & Sultan, I. A. (2021). Geometric design of the limaçon-to-circular fluid processing machine. *Journal of Mechanical Design,* 143(10).

Qi, G., Zhu, Z., Erqinhu, K., Chen, Y., Chai, Y., & Sun, J. (2018). Fault-diagnosis for reciprocating compressors using big data and machine learning. *Simulation Modelling Practice and Theory*, 80, 104-127.

Lu, K., Sultan, I. A., & Phung, T. H. (2021). A study on the use of machine learning methods to improve reciprocating compressor reliability via torque tailoring. In *2021 International Conference on Maintenance and Intelligent Asset Management (ICMIAM)* (pp. 1-6). IEEE.

Ma, J., Ding, X., Horton, W. T., & Ziviani, D. (2020). Development of an automated compressor performance mapping using artificial neural network and multiple compressor technologies. *International Journal of Refrigeration*, *120*, 66-80.

AHRI (2020). *2020 Standard for Performance Rating of Positive Displacement Refrigerant compressors*.

Afshari, F., Comakli, O., Adiguzel, N., & Ghasemi Zavaragh, H. (2016). Influence of refrigerant properties and charge amount on performance of reciprocating compressor in air source heat pump. *J. Energy Eng*, *10*.

Karnaz, J., Seeton, C., & Dixon, L. (2017). Identifying lubricant options for compressor bearing designs. In *IOP Conference Series: Materials Science and Engineering* (Vol. 232, No. 1, p. 012092). IOP PubAfshari, F., Comakli, O., Adiguzel, N., & Ghasemi Zavaragh, H. (2016). Influence of refrigerant properties and charge amount on performance of reciprocating compressor in air source heat pump. *J. Energy Eng*, 10.

Chen, Y., Halm, N. P., Groll, E. A., Braun, J. E. (2002a). Mathematical modeling of scroll compressors—part I: compression process modeling. *International Journal of Refrigeration, 25*(6), 731-750. doi: https://doi.org/10.1016/S0140-7007(01)00071-8

Chen, Y., Halm, N. P., Braun, J. E., Groll, E. A. (2002b). Mathematical modeling of scroll compressors — part II: overall scroll compressor modeling. *International Journal of Refrigeration, 25*(6), 751-764. doi:https://doi.org/10.1016/S0140-7007(01)00072-X

Cuevas, C., Lebrun, J., Lemort, V., & Winandy, E. (2010). Characterization of a scroll compressor under extended operating conditions. *Applied thermal engineering*, *30*(6-7), 605-615.

Lemmon, E. W., Huber, M. L., McLinden, M. O. (2010). NIST Reference Fluid Thermodynamic and Transport Properties—REFPROP Version 10.0. Gaithersburg, Maryland 20899: U.S. Department of Commerce - Technology Administration - National Institute of Standards and Technology.

Phung, T., Sultan, I., Boretti, A. (2016). Design of Limaçon Gas Expanders. In R. N. Jazar & L. Dai (Eds.), *Nonlinear Approaches in Engineering Applications: Advanced Analysis of Vehicle Related Technologies* (pp. 91-119). Cham: Springer International Publishing.

Phung, T. H., Sultan, I. A., & Appuhamillage, G. K. (2018). On the apex seal analysis of limaçon positive displacement machines. *Mechanism and Machine Theory*, *127*, 126-145.

Stosic, N., Smith, I., Kovacevic, A. (2003). Opportunities for innovation with screw compressors. *Proceedings of the Institution of Mechanical Engineers, Part E: Journal of Process Mechanical Engineering, 217*, 157-170. doi: 10.1177/095440890321700301

Subiantoro, A., Ooi, K. T. (2009). Introduction of the Revolving Vane Expander. *HVAC&R Research, 15*(4), 801-816. doi:10.1080/10789669.2009.10390865

Subiantoro, A., Ooi, K. T. (2011). Analytical study of the endface friction of the revolving vane mechanism. *International Journal of Refrigeration, 34*(5), 1276-1285. doi:https://doi.org/10.1016/j.ijrefrig.2011.01.019

Subiantoro, A., Ooi, K. T. (2012a). Analysis of the revolving vane (RV-0) expander, Part 1: Experimental investigations. *International Journal of Refrigeration, 35*(6), 1734-1743. doi:https://doi.org/10.1016/j.ijrefrig.2012.04.015

Subiantoro, A., Ooi, K. T. (2012b). Analysis of the Revolving Vane (RV-0) expander, part 2: Verifications of theoretical models. *International Journal of Refrigeration*, 35(6), 1744-1756. doi:https://doi.org/10.1016/j.ijrefrig.2012.04.014

Sultan, I. A. (2006). Profiling Rotors for Limaçon-to-Limaçon Compression-Expansion Machines. *Journal of Mechanical Design, 128*(4), 787-793. doi: 10.1115/1.2202877 %J Journal of Mechanical Design

Sultan, I. A. (2008a). Inverse geometric design for a class of rotary positive displacement machines. *Inverse Problems in Science and Engineering, 16*(2), 127-139. doi: 10.1080/17415970601162164

Sultan, I. A. (2008b). A geometric design model for the circolimaçon positive displacement machine. *Journal of Mechanical* Design*, 130*(6).

Sultan, I. A. (2012). Optimum design of limaçon gas expanders based on thermodynamic performance. *Applied Thermal Engineering, 39*, 188-197. doi: https://doi.org/10.1016/j.applthermaleng.2012.01.039

Tuymer, W. J., Machu, E. H., & Hanlon, P. C. (2001). Compressor valves. *Compressor handbook*, 20-1.

Wheildon, W. M. (1896). *U.S. Patent No. 553,086.* Washington, DC: U.S. Patent and Trademark Office.

Zhang, H., Wu, J., Xie, F., Chen, A., & Li, Y. (2014). Dynamic behaviors of the crankshafts in single-cylinder and twin-cylinder rotary compressors. *International journal of refrigeration, 47*, 36-45.

Ooi, K. (2005). Design optimization of a rolling piston compressor for refrigerators. Applied Thermal Engineering, 25(5-6), 813-829. doi: 10.1016/j.applthermaleng.2004.07.017

Cavazzini, G., Giacomel, F., Ardizzon, G., Casari, N., Fadiga, E., Suman, A. & Pinelli, M. (2020). CFD-based optimization of scroll compressor design and uncertainty quantification of the performance under geometrical variations. *Energy*, *209*, 118382. doi: 10.1016/j.energy.2020.118382

Aw, K. T., & Ooi, K. T. (2021). A Review on Sliding Vane and Rolling Piston Compressors. Machines, 9(6), 125. doi:10.3390/machines9060125.

Pelikan, M., Goldberg, D. E., & Cantú-Paz, E. (1999). BOA: The Bayesian optimization algorithm. In Proceedings of the Genetic and Evolutionary Computation Conference GECCO-99 (Vol. 1, pp. 525-532).

Snoek, J., Larochelle, H., & Adams, R. P. (2012). Practical Bayesian optimization of machine learning algorithms. In Proceedings of the Advances in neural information processing systems, 2951-2959.

Frazier, P. I. and Wang, J. (2016). Bayesian optimization for materials design. In Lookman, T., Alexander, F. J., and Rajan, K. (eds.), *Information Science for Materials Discovery and Design*, pages 45–75. Springer.

Torun, H., Swaminathan, M., Kavungal Davis, A., & Bellaredj, M. (2018). A Global Bayesian Optimization Algorithm and Its Application to Integrated System Design. *IEEE Transactions on Very Large Scale Integration (VLSI) Systems*, *26*(4), 792-802. doi: 10.1109/tvlsi.2017.2784783

Griffiths, R. R., & Hernández-Lobato, J. M. (2017). Constrained Bayesian optimization for automatic chemical design. arXiv preprint arXiv:1709.05501.

Letham, B., Karrer, B., Ottoni, G., & Bakshy, E. (2019). Constrained Bayesian Optimization with Noisy Experiments. *Bayesian Analysis*, *14*(2). doi: 10.1214/18-ba1110

Hickish, B., Fletcher, D., & Harrison, R. (2019). Investigating Bayesian Optimization for rail network optimization. *International Journal of Rail Transportation*, *8*(4), 307-323. doi: 10.1080/23248378.2019.1669500

Rasmussen, C. E. and Williams, C. K. I. (2006) Gaussian Processes for Machine Learning. MIT Press, Cambridge, Massachusetts.

Noè, U., & Husmeier, D. (2018). On a new improvement-based acquisition function for bayesian optimization. arXiv preprint arXiv:1808.06918.

Pan, X., Tian, C., Wu, S., Xing, Z., & Pan, S. (2019). Experimental study of the swing compressor with no valves. *Applied Thermal Engineering*, *163*, 114274. doi: 10.1016/j.applthermaleng.2019.114274

Wang, J., Liu, Y., Chen, Z., & Tan, Q. (2021). Geometric model and pressurization analysis on a novel sliding vane compressor with an asymmetrical cylinder profile. *International Journal of Refrigeration*, *129*, 175-183. doi: 10.1016/j.ijre

Grand View Research. (2021). *Market Analysis Report.* Retrieved from https://www.grandviewresearch.com/industry-analysis/air-compressor-market

Blunier, B., Cirrincione, G., Hervé, Y., & Miraoui, A. (2009). A new analytical and dynamical model of a scroll compressor with experimental validation. *International Journal of Refrigeration*, *32*(5), 874-891.

Noh, K. Y., Min, B. C., Song, S. J., Yang, J. S., Choi, G. M., & Kim, D. J. (2016). Compressor efficiency with cylinder slenderness ratio of rotary compressor at various compression ratios. *International journal of refrigeration*, *70*, 42-56.

Lu, K., Phung, T. H., & Sultan, I. A. (2021). On the Design of a Class of Rotary Compressors Using Bayesian Optimization. *Machines*, *9*(10), 219.

Lu, K., Sultan, I. A., & Phung, T. H. (2022). Mathematical modeling and parametric study of the limaçon rotary compressor. *International Journal of Refrigeration*, *134*, 219-231.

Yuan, X., Chen, Z., Fan, Z. (1992). Calculating model and experimental investigation of gas leakage. In: 1992 International Compressor Engineering Conference at Purdue University.